# INVESTIGATING MECHANISMS OF MITOTIC SPINDLE POSITIONING

Jennifer Kathryn Heppert

A dissertation submitted to the faculty of the University of North Carolina at Chapel Hill in fulfillment of the requirements for the degree of Doctor of Philosophy in the Department of Biology in the College of Arts and Sciences.

Chapel Hill
2017

Approved by:

Robert P. Goldstein

Victoria L. Bautch

Paul S. Maddox

Michael B. Major

Stephen L. Rogers

## ABSTRACT

Jennifer Kathryn Heppert: INVESTIGATING MECHANISMS OF MITOTIC SPINDLE POSITIONING
(Under the direction of Bob Goldstein)

The direction, or orientation, of cell division is important because it determines the fate and positions of cells within a tissue. The position of the mitotic spindle, the molecular machine that separates the chromosomes during mitosis, determines the plane of cell division. Cells sometimes use intercellular signals as spatial cues to position the mitotic spindle, but how mitotic spindles are positioned within cells in response to external cues remains unclear. To approach this question, I used the EMS cell in the early *C. elegans* embryo, an established model for studying cell interactions and miotic spindle orientation during development. I used contemporary genome editing strategies such as CRISPR, confocal live imaging, and classic embryological techniques, to address how proteins are deployed within cells to position mitotic spindles.

The second chapter of this work is an *in vivo* comparison of fluorescent proteins in *C. elegans.* This study was a valuable technical advance and revealed which fluorescent proteins to use for *in vivo* live imaging.

In the third chapter, using fluorescent proteins, I created tools to visualize our proteins of interest, and determined whether they were cortically enriched by cell-cell signaling mechanisms to direct mitotic spindle positioning. I found surprisingly, that

APC and Dishevelled are enriched asymmetrically at the EMS cortex, but NuMA and dyenin are not. These findings have implications for better understanding how signaling pathway proteins might function as positional cues for spindle orientation, independent of the asymmetric enrichment of the canonical Gα/LGN/NuMA complex.

For Tyler.
Thank you for always believing in me, and at times, enough for both of us.

## ACKNOWLEDGEMENTS

First, I'd like to thank my advisor, Bob Goldstein. Thank you for the opportunity to join your lab and for treating me like a scientist from day one. I have grown so much as a person and a biologist and much of my progress is due to your mentorship and encouragement. I cannot sufficiently express my appreciation for the time I have spent in your lab. Among your many talents is your amazing ability to put together a fantastic team. Thank you for the fabulous humans you have brought into my life as fellow lab members, colleagues, and friends. I have been privileged to be among you all.

I'd like to thank my committee: Steve Rogers, Paul Maddox, Vicki Bautch, and Ben Major (and in the beginning, Dave Reiner). Thank you for your questions, concerns and care for my present projects, as well as my future. Along with giving me helpful and critical feedback, you always encouraged me to reach for more. Also, I've used equipment and reagents in each of your labs at some point, so thank you for that additional generosity.

I would like to thank the Goldstein lab postdocs who I have had the privilege to work with: Jessica Sullivan-Brown, Jenny Tenlen, Dan Dickinson, Frank Smith, Thomas Boothby, Ari Pani, and Mark Slabodnick. You all were a dream team, a second committee, and a mentor to me in different ways. I have benefitted so much from learning from your unique perspectives and approaches to science.

There is no one I would have rather been on this journey with than the grad students I overlapped with in my time in the lab. Adam Werts and Jacob Sawyer, you guys were a big reason I joined the lab, and I still miss you . Chris Higgins, Sophie Tintori, and Tim Cupp: you all were a joy to be around and I'm lucky to have gone through this experience with you. Allyson Roberts and Kira Glynn, it has been fun getting to know you over the last few months – you'll do great.

Terrance Wong and Alicia Chen, thank you for all of your hard work making plates, solutions, and ordering reagents– this definitely wouldn't have been possible without you. I'd also like to thank all the past Goldstein lab members whom I never overlapped with in the lab, and yet somehow have managed to have delightful and meaningful interactions with over the years. You all are truly a kind of family.

To my friends near and far: thank you for all the fun we've had along the way. Our adventures have been some of the most necessary and sustaining times for me during this process. I look forward to many more.

Finally, I'd like to thank my family. Extended family: thank you for your love, support, and understanding. My sister Joanne: your talent, creativity, generosity and kindness far surpass mine. I love you and miss you terribly. My parents, Kathy and Joe: thank you for all the opportunities you gave me, and for your support and encouragement throughout this process. Tyler: you are my greatest inspiration. I love you and admire you, and thank you for everything you do for me every day. And finally, Gio (our dog). You came into our lives at one of my lowest points in this process, and I am not at all sure that I would have made it to the end without you. Thank you.

## PREFACE

When I was a kid I told a lot of people I didn't want to be a scientist. My parents are chemists, and growing up, I was frequently asked if I was going to be a chemist like them. At the time, I wasn't very interested in that possibility. The lab was where my sister and I went on days off of school, holidays, and lots of weekends. It was fun in some ways: there were vast numbers of chalkboards and eventually, computers we could play on.

Even though I didn't want to be a scientist, I always liked science. In grade school I was obsessed with marine biology. My mom even helped me decorate my room in an elaborate under-the-sea theme with nets, seashells, and sponge-painted blue walls. But, marine biology was a pretty unfortunate passion for a kid growing up in Kansas. At one time, millions of years ago, Kansas was at the bottom of a giant ocean, and as kids, we did get to go look for marine fossils, which was cool. But rocks will never be dolphins, and it just wasn't the same. Needless to say, my early passion for marine biology did not survive my land-locked upbringing.

Geography wasn't the only way growing up in Kansas shaped my interest in biology. I loved going to the natural history museum on the campus of the University of Kansas. There I could spend hours pointing out animals in the enormous two-story diorama full of taxidermy animals displayed in natural settings, complete with an electronic prairie dog that would pop its head up at regular intervals. There was also an entire floor of the museum filled with tanks containing every snake species

indigenous to the state. That floor was always really quiet, like a library of snakes. In the summers, I went to camp at the museum where we would do “field work” projects, poke around in the collections, and hang out in the museum. We also spent a lot of time outdoors. I loved being in nature, exploring wetlands, prairies, ponds and fields, finding wildlife, and being out in the fresh air. The landscape was vast and beautiful.

In 1999, when I was in seventh grade, the Kansas Board of Education voted to remove all references to evolution from the state science standards. I was struck by the impassioned response from the scientists at the state universities and many teachers, defending the importance of teaching these basic principles. The conflict became national news. At the time, it felt like the public backlash against science was something that could only happen in a place like Kansas. However, recent efforts on a national scale to discredit and deny the science behind vaccination and climate change suggest that this struggle is more ubiquitous and contemporary than I could have imagined.

It is generally understood that trying to suppress an idea often has the opposite effect. If “they” don’t want you to know about something, it must be pretty cool, right? I think this is pretty standard teenage logic, and the controversy over evolution certainly made me curious about biology and what all the fuss was about. Thankfully, my teachers were wonderful, and taught evolution in our biology classes (with probably even more gusto than they might have otherwise). I especially loved the biology class I took my senior year of high school with Mr. Reber. In his class I

became fascinated by all the aspects of biology you can't see with the naked eye, including the inner workings of cells.

I went to college to play volleyball, at the University of Central Florida without much idea about what I wanted to do for a career. I liked biology, so I thought maybe I'd study to be a medical doctor. Although I enjoyed the subject matter, I was never excited about gaining experience in a hospital or doctor's office. My advisor, Dr. Parkinson, recommended that I try doing some research. I joined Dr. Jeanette Nadeau's lab and studied leaf development. I learned that cells "talk" to each other to coordinate the development of a leaf, and that they use protein signaling molecules to communicate. I wanted to understand how these signaling pathways were different in plants with broad leaves, like a maple leaf, versus plants with strap shaped leaves, like a blade of grass. I also learned that you could spy on cells and see what was happening inside them if you used a special microscope with lasers called a confocal microscope.

After I graduated, I had the opportunity to work as a technician at the University of Kansas working on a really interesting, interdisciplinary project. I got to spend time in Dr. Blake Peterson's lab mostly listening to synthetic chemists describe how they made new fluorescent probes, and in Dr. Brian Ackley's lab learning how to work with *C. elegans* – the animal model system where we were testing the probes. Although I was working with adult *C. elegans*, one day Dr. Martin Hudson cut open one of the animals we were working with and showed me what its embryos looked like. At the time, I was applying to grad school, and I remember

thinking to myself “that’s what I want to work on.” So, at the places I applied, I requested meetings with everyone working on *C. elegans* embryogenesis.

Once I decided to go to graduate school at the University of North Carolina, I was sure I wanted to rotate in Dr. Bob Goldstein’s lab. At some point during my rotation, Bob showed me an image of a dividing cell with its microtubules lit up with GFP. I was immediately hooked on mitosis and wanted to understand how that amazing molecular machine, the mitotic spindle, found its proper orientation within cells. I worked for several years testing whether purified signaling proteins alone were sufficient to induce mitotic spindle positioning. Everyone I told about this project said it would be difficult, and it was! I really didn’t want to give up (I’m not sure I knew how), but eventually, I decided I needed to try a new approach.

Around that time, biologists were getting excited about a new bacterial immune system that had just been discovered called CRIPSR. The promise of CRIPSR was that it could harnessed and used to edit the genome of any organism. I was lucky that my lab mate Dr. Dan Dickinson, along with others in the field, adapted this new genome editing technology for *C. elegans.* We were suddenly able to alter the genome at any locus we wanted, including adding genes like fluorescent proteins to our proteins of interest.

I started applying this new technology to my favorite problem: How do cells know what direction to divide? By tagging the genes involved in asymmetric spindle positioning and examining their localization *in vivo,* I hoped to identify those that were asymmetric in dividing cells. I hypothesized that these proteins might be important for providing spatial information to the mitotic spindle. I was surprised to

find that some of our top candidates did not lead the way for mitotic spindle positioning through their asymmetric localization, as they do in many other systems. However, other proteins were asymmetric in our dividing cell and provide a foothold for furthering the understanding of this how spindles are oriented in response to signals. The results of this work are in Chapter 3 of this dissertation.

I am very grateful to all of the people who have given me opportunities and encouraged me to take up this path. I have grown enormously as a person and a scholar through this experience.

## TABLE OF CONTENTS

## LIST OF FIGURES

## LIST OF ABBREVIATIONS

| | |
|---|---|
| AB | Anterior blastomere |
| C | Carboxy terminus |
| CI | Confidence interval |
| CRISPR | Clustered, Regularly Interspersed, Short Palindromic Repeats |
| DNA | Deoxyribonucleic acid |
| dsRNA | Double stranded ribonucleic acid |
| E | Endodermal precursor |
| EMS | Endomesodermal precursor cell |
| FP | Fluorescent Protein |
| GSC | Germline stem cells |
| GFP | Green Fluorescent Protein |
| mNG | monomeric Neon Green |
| MS | Mesodermal precursor cell |
| mYPet | monomeric Yellow Fluorescent Protein for energy Transfer |
| mRNA | messenger RNA |
| N | N (amino) terminus |
| NCC | Nucleus centrosome complex |
| nm | nanometer |
| ns | not of statistical significance |
| $P_2$ | Posterior blastomere |
| PCP | Planar cell polarity |
| PCR | Polymerase chain reaction |

| | |
|---|---|
| pN | piconewton |
| RNA | Ribonucleic acid |
| RNAi | RNA interference |
| S | second |
| SOP | Sensory organ precursor |
| $t_{1/2}$ | half-life |
| ts | Temperature sensitive |
| TIRF | Total Internal Reflection Fluorescence Micrscopy |
| UTR | untranslated region |

# CHAPTER 1: INTRODUCTION

## 1.1 Introduction to mitosis and the mitotic spindle

Mitosis is the process by which a cell physically divides its duplicated genome into two new cells. Biologists have been studying mitosis since the late nineteenth century when advances in microscopy facilitated the resolution of features within cells and staining allowed the observation of chromosomes, named for their ready uptake of colored dyes (khroma = colored, soma = body) (McIntosh and Hays, 2016). In 1878, Walter Flemming described and illustrated chromosome behaviors during cell division and gave the process its name. The mitotic spindle is the molecular machine responsible for the movement and separation of the duplicated chromosomes during cell division. Although the mitotic spindle was observed and described in fixed samples by early microscopists and embryologists, it wasn't until the late 1940s that Shinya Inoue made real-time observations of the mitotic spindle possible using polarized light microscopy (Inoué, 1953; Inoué and Sato, 1967). Inoue showed that the mitotic spindle was made up of dynamic fibers, and that the growth and shrinkage of these fibers could move the chromosomes within the cell. These historic experiments and many others laid the foundation for our current understanding of the process of cell division.

We now know that mitoses are tightly controlled in time and space, and multiple regulatory mechanisms exist to ensure that the duplicated genome is segregated intact. Errors in cell division and separation of genetic material increase

the likelihood of developmental failure, cell death, and tumorigenic events (Potapova and Gorbsky, 2017). The regulation of mitosis extends to the direction, or orientation, of cell divisions in space. During division, the position of mitotic spindle within a cell establishes the location of the cytokinetic furrow, and thus the plane of cell division (Rappaport, 1961). Oriented cell divisions occur when the mitotic spindle is aligned relative to a given axis of polarization within a diving cell or tissue (Lu and Johnston, 2013). Errors in oriented cell division are thought to contribute to a number of human pathologies, including microcephaly and possibly tumorigenesis (Pease and Tirnauer, 2011). In this introduction, I will focus on the significance of oriented cell divisions and what is known about how they are achieved in diverse biological systems.

## 1.2 Oriented cell divisions position cells and establish cell fates

### *Tissue architecture*

Oriented cell divisions are a critical part of both development and homeostasis because they often play a role in establishing the fates and positions of cells within a tissue (Williams and Fuchs, 2013; Chen *et al.*, 2016a; Smith *et al.*, 2017). Oriented cell divisions contribute to tissue architecture, by determining where new cells are installed within an existing tissue. In order to maintain the two-dimensional shape of an epithelial monolayer, cells must divide within the plane of the epithelium. These planar, epithelial cell divisions are actively oriented by the localization of key proteins at the cell cortex (Zheng *et al.*, 2010; Morin and Bellaïche, 2011), See below for more about these complexes). If these divisions are biased in a given direction, they can also contribute to tissue lengthening (Aigouy *et al.*, 2010). In the developing

murine skin, the balance between progenitor divisions within the basal epithelial layer and differentiating divisions perpendicular to the basal layer, are critical for forming a stratified epithelium that functions as an effective barrier (Williams *et al.*, 2011). Thus, the orientation of cell divisions is an important factor in generating and maintaining the shapes of tissues.

***Positioning cells relative to extracellular cues***

Cell division orientation can also determine the local signaling microenvironment of the resulting daughter cells, influencing for example, whether one or both daughter cells are installed in proximity to mitogenic cues that might induce them to undergo further divisions or alter their developmental potential (Yadlapalli and Yamashita, 2012). Oriented cell divisions are known to play such a role in the maintenance of stem cell niches, such as the *Drosophila* male germline stem cell niche. *Drosophila* male germline stem cells (GSCs) divide perpendicular to a cluster of cells called the Hub, which signal to their GSC neighbors to maintain their pluripotent, stem cell identity (Kiger *et al.*, 2001; Tulina and Matunis, 2001). The perpendicular orientation of the GSC division ensures that one daughter remains in contact with the Hub and retains its stem cell fate (Yamashita, 2003). The second daughter cell is positioned so that it no longer contacts the Hub, and therefore, differentiates, eventually becoming a gamete. Proximity to basement membranes is emerging as an important factor in the maintenance of stem cell populations in the mammalian skin, muscle, and developing neuronal cortex (Williams and Fuchs, 2013; Smith *et al.*, 2017). Oriented divisions play a role in determining cell fate by the placement of daughters with respect to these extracellular cues.

### *Differential segregation of fate determinants*

Oriented cell divisions also control cell identities through the differential segregation of fate determinants, such as developmentally potent RNAs and/or proteins. In the one-cell stage *C. elegans* embryo, the plane of division is established such that fate determinants, known as germ granules or P-granules, are inherited by only one of the resulting daughter cells (Rose and Gönczy, 2005). Domains of fate determining proteins also form at the cell cortex and can be segregated to a single daughter cell. For example, *Drosophila* neuroblast divisions are oriented such that the Notch-signaling antagonist, Numb, is inherited by only one of the resulting daughter cells, causing it to differentiate (Rhyu *et al.*, 1994; Wu *et al.*, 2008; Knoblich, 2010; Williams and Fuchs, 2013). In order for division to result in two cells with different fates, mitotic spindles must be oriented such that these fate determinants are segregated into only one of the daughter cells.

## 1.2 Orienting the mitotic spindle within a cell

### *Introduction to the mitotic spindle*

The mitotic spindle is composed of polar polymers called microtubules that grow and shrink, in a process known as dynamic instability (Mitchison and Kirschner, 1984a; 1984b). Centrosomes are the cellular organelles that nucleate and organize microtubules during mitosis, anchoring the minus-ends of the microtubule arrays and forming the two spindle poles. Dynamic microtubule plus-ends grow out from the centrosomes and are stabilized at key sites in cells. During the mitotic phase of the cell cycle, a population of microtubules is stabilized at kinetochores, protein scaffolds that associate with regions of centromeric DNA on the chromosomes (Maddox *et al.*,

2003). In many cell types, a different population of spindle microtubules called astral microtubules reaches from the spindle poles to the cell cortex. Interactions between astral microtubules, the cell cortex, and cortically localized protein complexes are central to how mitotic spindles are positioned within cells (Grill, 2003; Grill and Hyman, 2005).

***Astral microtubules and the cell cortex***

The astral microtubules that reach out from spindle poles to the cell cortex play an important role in mitotic spindle positioning. Single microtubule asters in a cell-free system can position themselves in the geometric center of a glass chamber through polymerization and length dependent buckling of microtubules (Holy *et al.*, 1997). This suggests that a microtubule aster and dynamic instability of microtubules is sufficient to center an aster in a defined space. Oscar Hertwig observed that the geometry of cells could affect their plane of division, and that cells tend to divide along their long axis (Hertwig, 1884). These experiments suggest that microtubules probe the cell cortex and exert pushing and/or pulling forces on the mitotic spindle that allow the spindle to sense and respond to the shape of the of cell.

Evidence that key sites at the cell cortex are important for mitotic spindle positioning came from experiments performed using *Chaetopterus* oocytes (Lutz *et al.*, 1988). Meiotic spindles were pulled away from a site at the cortex to the center of the cell using a glass microneedle. When released, the spindles quickly returned to their original position on the cortex, suggesting that region of the cortex was specialized for positioning the spindle. We now know that some astral microtubules interact with force generating complexes at the plasma membrane to pull on the

mitotic spindle (Grill *et al.*, 2001; Labbe, 2004). The distribution of these pulling, force-generating complexes at the cell cortex often dictates the position of the mitotic spindle within a cell.

***Key cortical proteins***

The force-generating complex consisting of the proteins consiting of Gα (Gαi), LGN, and NuMA (Nuclear Mitotic Apparatus), is highly conserved across metazoans and has been demonstrated to play a role in mitotic spindle positioning in diverse organisms (di Pietro *et al.*, 2016). The role of this complex is to recruit and tether the motor protein dynein to cell cortex. Gαi is a myristolated protein that serves as the complex's physical link to the plasma membrane (Gotta and Ahringer, 2001). LGN binds to Gαi through its GoLoco protein domain, and to NuMA through its TPR repeat domain (Couwenbergs *et al.*, 2007; Yuzawa *et al.*, 2011). NuMA mediates the complex's interaction with the dynein motor protein (Merdes *et al.*, 1996). Often during asymmetric spindle positioning, this complex is restricted to one side or domain of the cell cortex through the regulation of a least one of its members. NuMA has been shown to have other cortical adapters besides Gαi and LGN, including Dishevelled and Band4.1 (Segalen *et al.*, 2010; Kiyomitsu and Cheeseman, 2013; Seldin *et al.*, 2013). NuMA has also been shown to regulate microtubule dynamics at both their plus and minus ends (Elting *et al.*, 2014; Seldin *et al.*, 2016). NuMA may regulate plus end microtubule activity at the cortex as part of its role in mitotic spindle positioning (Seldin *et al.*, 2016).

Astral microtubules are thought to form end-on attachments with dynein motor proteins tethered by these complexes at the cell cortex. This is supported by cortical

and TIRF microscopy data from multiple systems, including *C. elegans* (Labbe and Kozlowski). Microtubule depolymerization is thought to generate more force (~70pN) than motor domain stepping (~5pN) (Grishchuk *et al.*, 2005; Laan *et al.*, 2012). However, it is unclear whether force on astral microtubules is generated by dynein processivity toward minus ends, or if dyneins simply tether depolymerizing microtubules to drive force generation (McNally, 2013). *In vitro* experiments where dynein is tethered to a passive substrate suggest that dynein-microtubule end-on interactions induce microtubule depolymerization, but at a slower rate, allowing for longer interactions (Laan *et al.*, 2012). The dynactin complex, a key regulator of dynein motor activity, and other dynein regulators may play a role in determining the efficiency of dynein motor proteins in generating force on astral microtubules (Kardon and Vale, 2009).

Dynein and its cortical adaptor complex play a central in mitotic spindle positioning in most well characterized, oriented cell divisions. However, there appears to be substantial variation in the regulation of the proteins involved. This regulation is a key part of how members of this complex become localized to specific cortical domains.

***Mechanisms of mitotic spindle positioning***

Oriented cell divisions typically fall into two categories: symmetric or asymmetric cell divisions depending on the sizes and/or fates of the resulting daughter cells. Cell divisions that result in daughter cells of two different sizes are considered asymmetric, and usually result from positioning the mitotic spindle closer to one side of the cell than the other. Asymmetric cell divisions also may result in

differential segregation of fate determinants. Oriented cell divisions that result in equal sized daughters are considered symmetric cell divisions and result from mitotic spindles that are centered within a cell.

Both asymmetric and symmetric cell divisions can be oriented with respect to polarity axes. Symmetric cell divisions have been shown to use intrinsic cues from the spindle poles through Ran-GTP and Plk4 to regulate cortical proteins, and center the mitotic spindle (Kiyomitsu and Cheeseman, 2012). Asymmetric cell divisions can also be directed intrinsically, by existing polarity complexes, such as Par3/Par6/aPKC, within a cell (Knoblich, 2008; Wu *et al.*, 2008; Morin and Bellaïche, 2011). Cell contacts, cell shape, adhesions, and the axis of tension in a tissue are all extrinsic cues known to orient symmetric and asymmetric cell divisions.

Intracellular signaling can also serve as an extrinsic cue for mitotic spindle positioning. How do cells interpret signaling ligands as spatial cues and position the mitotic spindle in response to receiving them? This is the key question that underlies the work in this thesis. In the next section, I will discus what is know about how cell-cell signaling can control mitotic spindle positioning.

**1.4 Cell-cell signaling induced mitotic spindle positioning**

Conserved cell-cell signaling pathways are required for patterning tissues, directional cell migrations, and in a few known cases, mitotic spindle positioning (Werts and Goldstein, 2011; Bergstralh *et al.*, 2017). Although loss of function for secreted protein signaling molecules often leads to phenotypes that suggest a loss of spatial organization within or among cells, in many cases it is not clear how extracellular signals are interpreted as spatial cues by the cells that receive them. In

fact, successful rescue experiments where protein signaling molecules are provided back ubiquitously, instead of in a directional manner, suggest that mechanisms of providing spatial information to cells are more complex than previously appreciated (Whangbo and Kenyon, 1999).

One possibility is that the same signals that induce cells to divide and regulate the fates of the resulting cells, might also regulate how those divisions are executed in space, as this would be one way to coordinate these processes. There is a growing list of cases for which signals between cells are known or suspected to be important spatial cues for asymmetric cell division and mitotic spindle positioning (Werts and Goldstein, 2011; di Pietro *et al.*, 2016; Bergstralh *et al.*, 2017). However, for surprisingly few cases do we understand the molecular details of how an extracellular ligand received on the surface of a cell is interpreted by the mitotic apparatus. Below, some examples from recent literature are discussed, organized by signaling pathway.

### *1.4.1 Wnt signaling*

Wnt signaling is a major cell-cell communication pathway with diverse roles in animal development. Genes in the Wnt pathway have been implicated in human diseases, acting as oncogenes or tumor suppressors in cancer (Logan and Nusse, 2004; Clevers and Nusse, 2012; Krausova and Korinek, 2014). Wnt ligands are secreted, lipid-modified signaling molecules that can activate a variety of receptors and co-receptors on the cell surface, including Frizzleds (Fz) (Willert *et al.*, 2003; Takada *et al.*, 2006; Angers and Moon, 2009; Niehrs, 2012). Multiple non-canonical Wnt signaling pathways have also been described, with the Planar Cell Polarity

(PCP) pathway being particularly well characterized. Although alternative Wnt signaling pathways generally involve some of the same core proteins as the canonical pathways, they do not revolve around the activation of transcriptional target genes. Instead, these pathways modulate cellular processes such as the organization of protein domains at the cell cortex, cytoskeletal elements, and protein stabilization (Acebron *et al.*, 2014; Butler and Wallingford, 2017).

PCP signaling coordinates cell polarity and cell movements across tissues and in some cases, PCP signaling has been shown to play a role in asymmetric cell division (Smith *et al.*, 2017). In satellite stem cells of regenerating muscle tissue, PCP signaling via WNT7A, Fzd7, and Vangl2 regulates the balance between asymmetric, differentiating divisions, and symmetric, proliferative, cell divisions (Le Grand *et al.*, 2009). These PCP components are required to stimulate symmetric cell divisions, by controlling the axis of cell division such that both stem cell daughters remain in contact with the underlying basal lamina. In the developing mammalian neuronal cortex, a change in the level of PCP signaling, again, regulates the switch between symmetric and asymmetric cell divisions (Delaunay *et al.*, 2014). In this case however, PCP signaling regulates spindle asymmetry instead of the orientation of division. Later in development when PCP signaling in the cortex drops, the mitotic spindles become asymmetric, leading to daughter cell size asymmetry. The larger daughter cell often adopts a neuronal cell fate, whereas the smaller daughter remains a precursor cell. These examples provide evidence that non-canonical Wnt signaling might be a common extracellular signaling mechanism for controlling asymmetric cell divisions in both developmental and stem cell divisions. However, in

neither context is it clear how PCP signaling or Wnt pathway members might regulate the mitotic spindle directly to achieve the outcomes described. In the following sections I will describe the mechanistic links that have been made between Wnt signaling pathway components and the mitotic spindle in other systems.

***Drosophila sensory organ precursors***

One of the best-understood examples of how signaling pathways position mitotic spindles comes from *Drosophila* sensory organ precursor (SOP) cell divisions. SOPs are clusters of neural precursors that undergo asymmetric cell divisions to produce mechanosensory bristles (Gho *et al.*, 1999; Fichelson and Gho, 2003). PCP signaling through the Frizzled receptor establishes an anterior-posterior polarity axis in these cells, where both Frizzled (Fzd) and Dishevelled (Dsh) are localized to the posterior end of the dividing cell. Mud/NuMA, a cortical adaptor of the motor protein dynein, colocalizes with Fzd/Dsh at the cell cortex, and Dsh is required for this localization (Segalen *et al.*, 2010). Dsh and Mud/NuMA can bind in *Drosophila* S2 cells, through the DEP domain of Dsh and the C-terminus of NuMA. Further, Mud/NuMA was demonstrated to be required for proper segregation of fate determinants (PON, Partner of Numb) in SOPs. This work was the first to demonstrate a functional and biochemical link between a cell-cell signaling protein, Dsh and a protein known to function in mitotic spindle rotation Mud/NuMA (Segalen *et al.*, 2010).

*Zebrafish epidermis*

In the same work, Segalan et al. 2010, the authors demonstrate that this mechanism is functionally conserved in vertebrate development. Gastrulating

zebrafish epiblast cells undergo symmetric divisions that are polarized along the animal-vegetal axis in response to Wnt11 induced PCP signaling (Gong *et al.*, 2004). Dvl3::GFP (Dishevelled) expression in these cells induced NuMA enrichment at the cell cortex. Both knockdown of Dishevelled (MO Dvl1, Dvl2, and Dvl3 in combination) and expression of a dominant negative form of Dishevelled (Xdd1) led to a loss of polarized cell divisions (Segalen *et al.*, 2010). Partial depletion of NuMA also resulted in fewer polarized cell divisions. Taken together these results suggest that PCP signaling through Dvl localizes NuMA to the cell cortex to orient divisions in the zebrafish epiblast. This was the first work to implicate NuMA in mitotic spindle orientation in vertebrate development *in vivo* (Segalen *et al.*, 2010).

***Drosophila male germline stem cell niche***

As mentioned previously, *Drosophila* hub cells in the male germline signal to neighboring GSCs to maintain their pluripotency (Kiger *et al.*, 2001). GSCs undergo oriented, asymmetric cell divisions, with one daughter remaining in contact with the hub cell niche, and the other daughter differentiating into a gamete precursor. Mitotic spindle alignment in GSCs is achieved through cell-cell interactions at the hub-GSC interface that position GSC centrosomes. E-cadherin is a transmembrane protein that interacts with other E-cadherin proteins on neighboring cells to form cell-cell junctions. In the *Drosophila* male germline, disruption of E-cadherin signaling in GSCs causes mis-positioning of centrosomes that are normally anchored at the hub-GSC contact (Inaba *et al.*, 2010).

A homolog of mammalian APC (Adenomatous polyposis coli), Apc2, is also required for proper centrosome positioning (Yamashita, 2003). Apc2 is localized

within GSCs to the hub-GSC cell-cell contact, and is required to anchor one centrosome, more often the mother centrosome, at the contact while the other centrosome migrates to the opposite pole of the GSC (Yamashita *et al.*, 2007). The asymmetric localization of Apc2 is disrupted upon loss of E-cadherin signaling in GSCs, suggesting that cell-cell interactions through E-cadherin induce Apc2 localization (possibly involving beta-catenin) and centrosome anchoring to orient GSC divisions relative to the hub.

Until recently almost nothing was known about the mechanism that retains the mother centrosome at the GSC contact. Klp10A, a member of the kinesin-13 family, that act as microtubule depolymerases, was recently shown to be enriched at the mother centrosome, and to modulate the size of the mother centrosome in GSCs (Chen *et al.*, 2016b). Failure to control mother centrosome size resulted in divisions where the mother centrosome overgrew, mitotic spindles were larger on the side of the mother centrosome, and the resulting cells were asymmetric in size. This suggests that there is a specific mechanism in GSCs to regulate mother centrosome size that facilitates centrosome anchoring and spindle orientation, but restricts size via Klp10A to maintain spindle and cell size symmetry (Chen *et al.*, 2016b). It is interesting that this mechanism for spindle positioning involves a Wnt signaling pathway member, Apc2, but appears to have unique upstream inputs, E-cadherin, and has not been shown to involve dynein or its cortical adaptors.

***Mouse embryonic stem cells***

Although experiments *in vivo* in diverse model systems have suggested that Wnt ligands and their downstream effectors may be important for mitotic spindle

orientation, Habib et al. 2013 demonstrated for the first time that a purified Wnt ligand could instruct mitotic spindle positioning. By chemically anchoring purified Wnt3a protein to microbeads, the ligand was provided as a local, immobile signal to one side of mouse embryonic stem cells. Two Wnt receptors, LRP6 and Frizzled1, and APC, a member of the beta-catenin destruction complex, were localized proximal to the Wnt3a signaling bead (Habib *et al.*, 2013). However, the overall mechanism of spindle positioning in response to Wnt3a remains poorly understood.

***Mammalian intestinal cells***

Cells found at the base of crypts from the small intestines and colons of humans and mice were found to undergo oriented divisions. Cell divisions in the stem cell compartment of the crypts are oriented perpendicular relative to the apical surface of these cells (Quyn *et al.*, 2010). APC (Adendomatus polyposis coli) has been shown to be crucial for maintenance of the stem cell compartment, and both humans and mice heterozygous for mutations in the Apc gene locus are prone to colorectal cancers (Barker *et al.*, 2009). Oriented cell divisions in the stem cell compartment were disrupted in $Apc^{min/+}$ mice, suggesting that even tissue in a precancerous, heterozygous state might be prone to cell division errors (Quyn *et al.*, 2010). How APC is involved in orienting cell divisions in the mammalian intestine, and whether intercellular signaling plays a role in this process remains largely unclear.

### *1.4.2 Cell-cell junction and cell adhesion proteins*

Other extrinsic cues besides secreted signals have been shown to impact mitotic spindle orientation. Although not typically thought of as “signaling proteins,”

proteins involved in the formation of cell-cell junctions and cell adhesion to substrates have also been shown to act as instructive cues for mitotic spindle orientation. In these contexts cell junction and adhesion proteins not only play a structural role, but also provide spatial information for positioning the mitotic spindle.

***E-cadherin***

As previously discussed, *Drosophila* male GSCs use E-cadherin as a spatial cue for centrosome anchoring and mitotic spindle positioning through Apc2 (see above (Yamashita, 2010)). Recently, E-cadherin has also been shown to act instructively for LGN recruitment and for mitotic spindle orientation in MDCK cells (Gloerich *et al.*, 2017). The authors demonstrate that E-cadherin and LGN form a biochemical complex in cells through the interaction of the E-cadherin cytosolic tail and the TPR-repeat domain of LGN, and mitotic spindle orientation in these cells is dependent on this interaction. NuMA also colocalizes with E-cadherin/LGN during mitotic spindle positioning, however, it appears that LGN binding to E-cadherin and NuMA is mutually exclusive. The authors propose that the LGN/NuMA complexes form sequentially and independently, but that E-cadherin recruitment of LGN is an initial important step. JAM-A, another junctional protein, has been shown to regulate spindle positioning in MDCK cells, and may also be important for this process (Tuncay *et al.*, 2015).

***Integrins***

Cultured cells plated on extracellular matrix (ECM) typically orient their mitotic spindles parallel to the substrate. Micropatterned substrates made of the ECM components fibronectin and collagen, engage integrins to adhere to the substrate.

Micropatterns of different shapes cause mitotic spindles to be differentially oriented in the X and Y orientation relative to the micropatterned surface (Théry and Bornens, 2006), and in some cases integrins are required for this response (Toyoshima and Nishida, 2007). Recent work has also suggested that in at least one context, integrins can directly recruit a member of the Dynactin complex, p50, a key regulator of the dynein motor protein (Morris *et al.*, 2015). Mammalian skin cells also require integrins for proper mitotic spindle orientation, however it is unclear whether the adhesion proteins provide a spatial cue for mitotic spindle positioning.

### *1.4.3 Other signaling pathways*

#### *GPCR-G protein signaling*

Drosophila neuroblasts are a primary model system for informing our understanding of how mitotic spindles are positioned during asymmetric cell division (Wodarz, 2005). The divisions of these neuronal precursors are highly polarized with an apical and basal side of the cell that correspond with domains of cortical fate determinants. The mitotic spindle in these cells is highly asymmetric, and aligned such that fate determinants are segregated into the much larger self-renewed neuroblast or the smaller, differentiating, ganglion mother cell (GMC). The central nervous system tissue in which these cells reside is highly ordered, and *in vivo* the neuroblast divisions are polarized relative to an underlying layer of epithelial cells called the neural ectoderm (Schmid *et al.*, 1999).

Siegrist and Doe 2006 demonstrated that mitotic spindle orientation in dividing neuroblasts requires contact with epithelial cells to first, induce a polarized domain of Par proteins and Pins/LGN and second, to anchor one of the centrosomes

of the dividing cell (Siegrist, 2006). They hypothesized that these epithelial cells were providing an extrisinic cue, however the nature of the extrinsic cue remained mysterious. Yoshiura et al. 2012, discovered that the GPCR Tre1 is required in neuroblasts for mitotic spindle positioning and tissue polarity (Yoshiura *et al.*, 2012). The authors demonstrate that Pins/LGN preferentially binds activated Gαo (Gαo-GTP) over Gαi. This suggests a model in which a ligand from the epithelial cells binds the GPCR Tre1, activates Gαo and recruits Pins/LGN to the apical side of the cell where Tre1 is activated. The identity of the ligand remains unknown, and it is also unknown if mammalian LGN exhibits the same preferential binding to activated forms of Gαos. However, it is enticing to imagine that GPCR-G protein signaling might be a common mechanism for LGN polarization in other oriented divisions instructed by cell-cell signaling.

***Semaphorin Signaling***

Recently, cell-cell signaling via semaphorins has been shown to direct mitotic spindle orientation in two different mammalian cell types. In kidney cells, both renal tubular epithelial cells and MDCK cyst cells in culture, the transmembrane receptor protein Plexin-B2 and transmembrane ligands, Semaphorins, are required for proper mitotic spindle positioning (Xia *et al.*, 2015). The Plexin-B2 receptor GAP domain is essential for this function, and active Cdc42 levels dropped when Plexin-B2 was depleted. Expression of constitutively active Cdc42 (CA-Cdc42) could rescue spindle orientation defects in Plexin-B2 depleted cysts, suggesting that Plexin-B2's role in mitotic spindle positioning involves activation of Cdc42. However, it is interesting to consider how spindle orientation is rescued by global CA-Cdc42 in the absence of a

local Plexin-B2 signal. It is possible that either another pathway restricts Cdc-42 activity to specific cortical domains, or a second Cdc-42 dependent pathway exists for mitotic spindle positioning in these cells.

Semaphorin signaling has also been shown to be critical for the orientation of neuroepithelial progenitor divisions in the mouse spinal cord (Arbeille *et al.*, 1AD). Sema3B protein binds specifically to the apical surface of the mitotic progenitors and is required for oriented division. GSK3 and the microtubule stabilizing protein $CRMP_2$ seem to have some involvement in this process, however it is unclear whether spindle orientation is achieved through microtubule regulation by these proteins alone, or if they work in parallel with LGN/NuMA and dynein motor proteins.

***The Hippo pathway***

The Hippo signaling pathway is involved in regulating organ size by mediating cell proliferation, cell death and differentiation. In *Drosophila,* members of the hippo signaling pathway, Hippo, Salvador, and Warts, have been implicated in Pins/LGN mediated mitotic spindle positioning (Dewey *et al.*, 2015). Warts was shown to regulate Pins/LGN – Mud/NuMA binding at the cell cortex through phosphorylation of the Mud coiled-coil domain. Depletion of Warts in the *Drosophila* imaginal disc epithelium resulted in spindle orientation defects and a reduction of Mud/NuMA at the cell cortex. Although an upstream, intercellular signaling component of this pathway has not been identified, it is clear that Hippo signaling can unmask polarity cues, and may play a role in spindle orientation in diverse contexts.

***MES-1 (Receptor tyrosine kinase-like) protein signaling***

In the four-cell stage *C. elegans* embryo cell-cell signaling is known to be necessary for mitotic spindle positioning in both the $P_2$ and EMS cells. $P_2$ and EMS interact via two cell-cell signaling pathways, the Wnt pathway and a tyrosine kinase signaling cascade. This tyrosine kinase signaling cascade is initiated at the contact between $P_2$ and EMS through the transmembrane receptor, MES-1(Bei *et al.*, 2002). MES-1 is a *C. elegans* specific receptor tyrosine kinase-like protein that is predicted to have no catalytic activity. Signaling through MES-1/Src is required for mitotic spindle orientation in $P_2$. GPR-1/LGN is asymmetrically localized to the $P_2$:EMS contact in the $P_2$ cell in response to MES-1/Src signaling (Werts *et al.*, 2011). When MES-1 or SRC-1 is depleted, GPR-1/LGN is no longer enriched at the cell cortex, and the $P_2$ mitotic spindle fails to orient properly. This study represents the first highly time-resolved imaging of GPR-1/LGN localization, and revealed that excess GPR-1 is removed from the cell cortex by a microtubule dependent mechanism.

In the aforementioned cases, there are some patterns to be found, but no protein or mechanism appears universal. For example, Wnt signaling seems to be involved in orienting mitotic spindles in several systems. However, it is clear that other signaling pathways such as junctional proteins, Semaphorins, and GPCRs can serve as extrinsic cues as well. In many cases, signaling pathways seem to “plug in” to the Gα/LGN/NuMA force-generating complex by recruiting various members to a specific cortical domain, but in other cases, no role for this complex has been identified, and signaling pathway proteins may play a more direct role. Are mechanisms of signaling induced mitotic spindle positioning conserved among

diverse systems? How universal is the asymmetric recruitment of Gα/LGN/NuMA force-generating complex? Can members of signaling pathways interact directly with spindle components to direct orientation? Are signaling pathways commonly used to link differentiation events with division orientation? I decided to take advantage of a simple model system, the early *C. elegans* embryo, to better understand how Wnt signaling serves as an extrinsic cue for mitotic spindle positioning.

### 1.5 Investigating mechanisms of Wnt dependent mitotic spindle orientation in the *C. elegans* embryo

The *C. elegans* embryo has been used extensively to study oriented cell divisions during development (Cowan and Hyman, 2004; Galli and van den Heuvel, 2008; Gönczy, 2008; Segalen and Bellaïche, 2009; Sawa, 2012). At the four-cell stage in the *C. elegans* embryo, interaction between the $P_2$ and EMS cells is required for accurate mitotic spindle positioning in EMS and for the proper fate of EMS daughter cells (Goldstein, 1992; 1993; 1995) (Fig.1). When EMS divides, its spindle is aligned along the anterior-posterior axis of the embryo (Fig.1). The posterior EMS daughter cell becomes the endoderm, and the anterior daughter cell becomes mesoderm which gives rise to muscle and the pharyngeal tissue (Priess and Thomson, 1987). Genes in the Wnt signaling pathway are critical for endoderm production and spindle orientation in EMS (Rocheleau and Priess, 1997; Thorpe *et al.*, 1997; Schlesinger *et al.*, 1999; Walston *et al.*, 2004).

*Wnt signaling is required for spindle orientation and fate of the C. elegans EMS cell*

Wnt signaling plays a transcriptional role in endoderm specification in the EMS cell (Phillips and Kimble, 2009). In contrast, spindle orientation in EMS requires Wnt signaling, but does not require new transcription (Schlesinger *et al.*, 1999).

Therefore, Wnt pathway proteins likely participate in non-canonical regulation of cell division machinery in EMS. However, how Wnt pathway proteins interface with the mitotic spindle or the proteins that regulate spindle microtubules is only beginning to be understood. Does Wnt signaling recruit a member of the Gα/LGN/NuMA force-generating complex to one side of EMS? Do members of the Wnt signaling pathway have a more direct role in regulating spindle microtubules? Are there other yet to be identified proteins involved in mitotic spindle positioning? I use the four-cell stage *C. elegans* embryo as a model system to explore these questions in Chapter 3. The four-cell stage embryo is a good model system to study oriented cell divisions for a number of reasons: divisions in the early *C. elegans* embryo are highly stereotyped, it is a simple 2 cell system ($P_2$ and EMS), we can move the signals to new positions using direct cell manipulations, and we can modify the genome using CRISPR-Cas9 triggered homologous recombination to create fluorescent protein fusions.

***A Wnt signaling cell acts as a positional cue for spindle orientation in EMS***

In Wnt mutant *C. elegans* embryos, spindle rotation in EMS is compromised and metaphase spindles are often mis-aligned (Thorpe *et al.*, 1997; Schlesinger *et al.*, 1999; Walston *et al.*, 2004). During wild type spindle orientation the centrosomes migrate to opposite sides of the nucleus, ending in the left-right axis of the embryo (Fig.1) (Hyman and White, 1987). Next, the nucleus-centrosome complex (NCC) rotates 90 degrees, aligning the centrosomes with the anterior-posterior axis of the embryo (Hyman, 1989). NCC rotation is a critical process for spindle positioning in EMS because its final position establishes metaphase spindle orientation. I will refer to the rotation of the NCC as “spindle rotation” throughout this thesis. In Wnt

signaling mutants, spindle rotation fails, and instead of an anterior-posterior orientation, spindles form in left-right and dorsal-ventral orientations (Thorpe *et al.*, 1997; Schlesinger *et al.*, 1999; Walston *et al.*, 2004). The receptor tyrosine kinase-like protein MES-1, and the Src tyrosine kinase, SRC-1, are necessary for spindle orientation in EMS, and are redundant with members of the Wnt pathway for endoderm specification (Bei *et al.*, 2002).

Previous experiments have indicated that a Wnt signaling $P_2$ cell acts as a positional cue for spindle orientation in EMS (Goldstein *et al.*, 2006). In isolated $P_2$:EMS cell pairs, wild type EMS spindles align perpendicular to the $P_2$:EMS cell contact. In *mom-2*/Wnt and *mes-1* mutant cell pairs, EMS spindles are randomized with respect to $P_2$ (Fig.2) (Schlesinger *et al.*, 1999; Goldstein *et al.*, 2006). When $P_2$ cells isolated from both *mom-2*/Wnt and *mes-1* mutant embryos are placed on an EMS cell, the EMS cell spindle orients towards the mes-1 mutant MOM-2/WNT+ signaling cell. The *mom-2*/Wnt mutant MES-1+ signaling cell is necessary, but does not act as a positional cue (Fig.2) (Goldstein *et al.*, 2006). Because Wnt signaling cells act as positional cues for spindle orientation, it is likely that Wnt signaling regulates proteins associated with spindle positioning in EMS. However, an understanding of the mechanism of spindle orientation downstream of Wnt signaling is lacking in any system.

### *Motor proteins may facilitate microtubule-cortex interactions for spindle rotation in EMS*

A predominant hypothesis for the mechanism of spindle positioning in EMS is that during rotation, microtubules are captured at a site on the EMS cortex, and that cortical capture at the $P_2$:EMS cell contact facilitates spindle rotation into the

anterior-posterior axis (Goldstein, 1995; Zhang *et al.*, 2008). There is evidence to support this hypothesis: 1) the position of the $P_2$:EMS contact determines position of the mitotic spindle even when the contact is randomized prior to rotation, 2) spindle rotation does not occur when EMS is cultured in isolation, 3) when two $P_2$ cells are placed on a single EMS cell, each can attract a spindle pole, and 4) rotation fails when cells are treated with nocodazole, a microtubule-destabilizing drug, indicating that spindle rotation requires dynamic microtubules (Goldstein, 1995). A cortical capture mechanism requires that spindle microtubules interact with distinct sites on the cell cortex. Motor proteins are good candidates to facilitate such interactions because they are members of complexes that connect microtubules and the cortex (Siller and Doe, 2009; Morin and Bellaïche, 2011; Kotak and Gönczy, 2013; Williams and Fuchs, 2013). Dynein plays roles in spindle positioning in early divisions in the C. elegans embryo, although dynein has not directly been shown to regulate microtubules during spindle positioning in EMS (Schmidt *et al.*, 2005).

Loss of function of proteins involved in dynein regulation, GPA-16, LET-99, DNC-1, and LIN-5/NuMA cause defects in EMS spindle rotation (Tsou, 2003; Zhang *et al.*, 2008; Liro and Rose, 2016). GPA-16/Gα is membrane-anchored protein that interacts with GPR-1/2 (LGN/Pins) and LIN-5 (NuMA) to form a ternary complex. This complex regulates spindle positioning through its interactions with dynein (See above, (Srinivasan, 2003; Werts *et al.*, 2011)). LET-99 is an antagonist of the ternary complex in C. elegans (Tsou, 2003). GPR-1/2 (Pins, LGN) often regulates asymmetric activity of the ternary complex, gpa-16 (Gα) GPR-1/2 (LGN/Pins), LIN-5 (NuMA), through its asymmetric localization (Werts *et al.*, 2011). GPR-1/2 is

enriched at the $P_2$:EMS border, and thus was hypothesized to work in combination with GPA-16 and LET-99, to asymmetrically position the EMS spindle (Tsou, 2003). Surprisingly however, it was demonstrated that GPR-1/2 enrichment is specific to the $P_2$ cell and is not enriched in EMS (Werts *et al.*, 2011). Therefore, spindle positioning in EMS is not achieved through asymmetric localization of GPR-1/2, as previously expected. *dnc-1*/Dynactin (p150-glued) is a member of a complex of proteins that regulate the function and localization of dynein. DNC-1 is enriched at the $P_2$:EMS border (Zhang *et al.*, 2008). Enrichment of DNC-1/Dynactin at the $P_2$:EMS border depends on Wnt signaling and does not require GPA-16/Gα (Zhang *et al.*, 2008). This suggests that DNC-1 localization is independent of the ternary complex and may be a target of the Wnt signaling pathway. However, it is not known whether DNC-1 is enriched in the EMS cell, or the EMS neighbor $P_2$.

In addition to dyneins, kinesins are a diverse family of microtubule motor proteins that also have roles in oriented cell division. In Drosophila neuroblasts, Khc-73, a plus-end directed kinesin, is involved in linking microtubule plus-ends to the cortex through its interactions with Discs large and polarized LGN/Pins/GPR-1/2 (Siegrist, 2006). Furthermore, kinesins have been shown to be involved in specifying cell fate in EMS and stabilizing microtubules in the anterior of EMS during telophase of mitosis (Sugioka *et al.*, 2011).

Although much has been learned about the proteins required for mitotic spindle positioning in the EMS cell from the above-mentioned genetic studies, questions remain about which of these molecules act as positional cues for mitotic spindle orientation. Understanding mechanisms of extrinsic control of mitotic spindle

positioning requires knowledge of not simply which proteins are required for this process, but which proteins provide positional information to the mitotic spindle and how. In this work, using the $P_2$ and EMS cells as a model system, I examine how extrinsic cues, in this case Wnt signaling, results in mitotic spindle positioning. To do this I generate endogenously tagged versions of many of the gene products known to be required for spindle positioning in EMS, and some candidate proteins additionally. Using live imaging, RNAi depletions, and classical embryology, I discover that neither LIN-5/NuMA nor DHC-1/Dynein is asymmetrically enriched in EMS. This surprising result led me to investigate the roles of Wnt pathway members Dishevelled and APC in directly regulating mitotic spindle positioning.

The first of the two chapters that follow (Chapter 2) is my study characterizing genetically encoded fluorescent protein performance *in vivo*. This work was published in 2016 in *Molecular Biology of the Cell.* The next chapter (Chapter 3) is my work on mitotic spindle positioning that I plan to submit for publication this summer.

## 1.6 Chapter 1 Figures

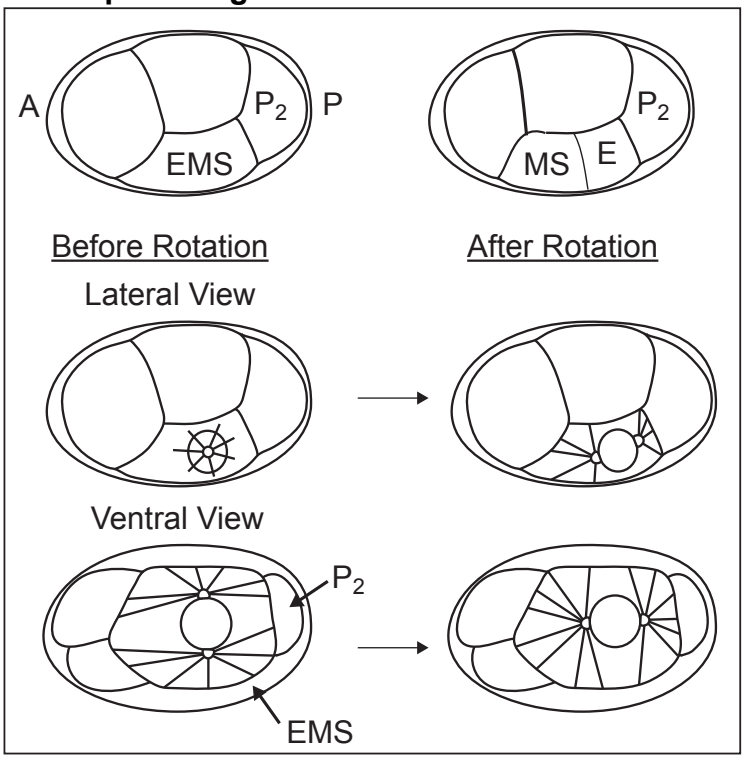


**Figure 1.1** Spindle rotation in the four-cell stage *C. elegans* embryo Top panel: embryos before and after EMS division Box: Spindle rotation from lateral and ventral view

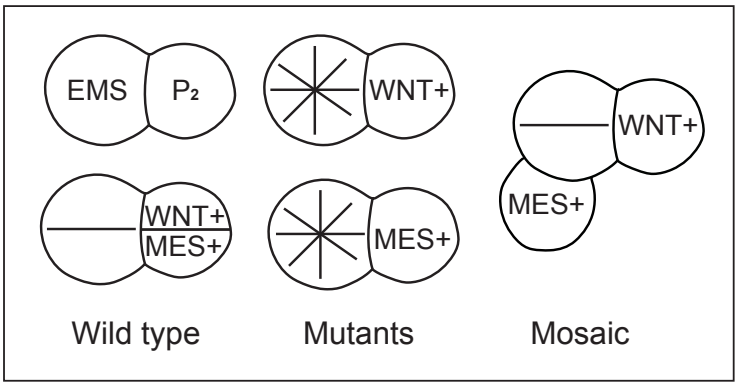


**Figure 1.2** Spindle rotation in isolated $P_2$:EMS cell pairs: lines indicated mitotic spindle alignment. Spindles align with wild type $P_2$ cell. Spindle alignment is random in response to *mom-2*/Wnt(MES+) or *mes-1*(WNT+) mutant $P_2$ cells. In cases where an EMS cell is in contact with two $P_2$ cells of different genotypes, the EMS spindle aligns with the *mes-1*(WNT+) $P_2$ cell (Goldstein, 2006).

## REFERENCES


Acebron, S. P., Karaulanov, E., Berger, B. S., Huang, Y.-L., and Niehrs, C. (2014). Mitotic Wnt Signaling Promotes Protein Stabilization and Regulates Cell Size. Molecular Cell *54*, 663–674.

Aigouy, B., Farhadifar, R., Staple, D. B., Sagner, A., Röper, J.-C., Jülicher, F., and Eaton, S. (2010). Cell flow reorients the axis of planar polarity in the wing epithelium of Drosophila. Cell *142*, 773–786.

Angers, S., and Moon, R. T. (2009). Proximal events in Wnt signal transduction. Nat Rev Mol Cell Biol.

Arbeille, E., Reynaud, F., Sanyas, I., Bozon, M., Kindbeiter, K., Causeret, F. E. D. E. R., Pierani, A., Falk, J., Moret, F. E. D. E. R., and Castellani, V. E. R. (1AD). Cerebrospinal fluid-derived Semaphorin3B orients neuroepithelial cell divisions in the apicobasal axis. Nature Communications *6*, 1–14.

Barker, N., Ridgway, R. A., van Es, J. H., van de Wetering, M., Begthel, H., van den Born, M., Danenberg, E., Clarke, A. R., Sansom, O. J., and Clevers, H. (2009). Crypt stem cells as the cells-of-origin of intestinal cancer. Nature *457*, 608–611.

Bei, Y., Hogan, J., Berkowitz, L. A., Soto, M. C., Rocheleau, C. E., Collins, J., and Mello, C. C. (2002). SRC-1 and Wnt Signaling Act Together to Specify Endoderm and to Control Cleavage Orientation in Early *C. elegans* Embryos. Developmental Cell *3*, 113–125.

Bergstralh, D. T., Dawney, N. S., and St Johnston, D. (2017). Spindle orientation: a question of complex positioning. Development *144*, 1137–1145.

Butler, M. T., and Wallingford, J. B. (2017). Planar cell polarity in development and disease. Nat Rev Mol Cell Biol.

Chen, C., Fingerhut, J. M., and Yamashita, Y. M. (2016a). The ins(ide) and outs(ide) of asymmetric stemcell division. Current Opinion in Cell Biology *43*, 1–6.

Chen, C., Inaba, M., Venkei, Z. G., and Yamashita, Y. M. (2016b). Klp10A, a stem cell centrosome-enriched kinesin, balances asymmetries in Drosophila male germline stem cell division. Elife.

Clevers, H., and Nusse, R. (2012). Wnt/β-Catenin Signaling and Disease. Cell *149*, 1192–1205.

Couwenbergs, C., Labbe, J. C., Goulding, M., Marty, T., Bowerman, B., and Gotta, M. (2007). Heterotrimeric G protein signaling functions with dynein to promote spindle positioning in C. elegans. The Journal of Cell Biology *179*, 15–22.

Cowan, C. R., and Hyman, A. A. (2004). Asymmetric cell division in C. elegans: Cortical Polarity and Spindle Positioning. Annu. Rev. Cell Dev. Biol. *20*, 427–453.

Delaunay, D., Cortay, V., Patti, D., Knoblauch, K., and Dehay, C. (2014). Mitotic spindle asymmetry: a Wnt/PCP-regulated mechanism generating asymmetrical division in cortical precursors. CellReports *6*, 400–414.

Dewey, E. B., Sanchez, D., and Johnston, C. A. (2015). Warts Phosphorylates Mud to Promote Pins-Mediated Mitotic Spindle Orientation in Drosophila, Independent of Yorkie. Current Biology *25*, 2751–2762.

di Pietro, F., Echard, A., and Morin, X. (2016). Regulation of mitotic spindle orientation: an integrated view. EMBO Reports *17*, 1106–1130.

Elting, M. W., Hueschen, C. L., Udy, D. B., and Dumont, S. (2014). Force on spindle microtubule minus ends moves chromosomes. The Journal of Cell Biology *206*, 245–256.

Fichelson, P., and Gho, M. (2003). The glial cell undergoes apoptosis in the microchaete lineage of Drosophila. Development *130*, 123–133.

Galli, M., and van den Heuvel, S. (2008). Determination of the Cleavage Plane in Early C. elegansEmbryos. Annu. Rev. Genet. *42*, 389–411.

Gho, M., Bellaïche, Y., and Schweisguth, F. (1999). Revisiting the Drosophila microchaete lineage: a novel intrinsically asymmetric cell division generates a glial cell. Development *126*, 3573–3584.

Gloerich, M., Bianchini, J. M., Siemers, K. A., Cohen, D. J., and Nelson, W. J. (2017). Cell division orientation is coupled to cell-cell adhesion by the E-cadherin/LGN complex. Nature Communications *8*, 13996.

Goldstein, B. (1992). Induction of Gut in *Caenorhabditis Elegans* Embryos. Nature, 255–257.

Goldstein, B. (1993). Establishment of gut fate in the E lineage of C. elegans: the roles of lineage-dependent mechanisms and cell interactions. Development *118*, 1267–1277.

Goldstein, B. (1995). Cell Contacts Orient Some Cell Division Axes in the C. elegans Embryo. The Journal of Cell Biology *129*, 1071–1080.

Goldstein, B., Takeshita, H., Mizumoto, K., and Sawa, H. (2006). Wnt Signals Can Function as Positional Cues in Establishing Cell Polarity. Developmental Cell *10*, 391–396.

Gong, Y., Mo, C., and Fraser, S. E. (2004). Planar cell polarity signalling controls cell

division orientation during zebrafish gastrulation. Nature *430*, 689–693.

Gotta, M., and Ahringer, J. (2001). Distinct roles for Galpha and Gbetagamma in regulating spindle position and orientation in Caenorhabditis elegans embryos. Nature Cell Biology *3*, 297–300.

Gönczy, P. (2008). Mechanisms of asymmetric cell division: flies and worms pave the way. Nat Rev Mol Cell Biol *9*, 355–366.

Grill, S. W., and Hyman, A. A. (2005). Spindle Positioning by Cortical Pulling Forces. Developmental Cell *8*, 461–465.

Grill, S. W., Gonczy, P., Stelzer, E. H. K., and Hyman, A. A. (2001). Polarity controls forces governing asymmetric spindle positioning in the Caenorhabditis elegans embryo. Nature *409*, 630–633.

Grill, S. W., Howard, J., Schäffer, E., Stelzer, E. H. K., and Hyman, A. A. (2003). The distribution of active force generators controls mitotic spindle position. Science *301*, 518–521.

Grishchuk, E. L., Molodtsov, M. I., Ataullakhanov, F. I., and McIntosh, J. R. (2005). Force production by disassembling microtubules. Nature *438*, 384–388.

Habib, S. J., Chen, B. C., Tsai, F. C., Anastassiadis, K., Meyer, T., Betzig, E., and Nusse, R. (2013). A Localized Wnt Signal Orients Asymmetric Stem Cell Division in Vitro. Science *339*, 1445–1448.

Hertwig, O. (1884). Untersuchungen zur Morphologie und Physiologie der Zelle: Welchen Einfluss übt die Schwerkraft auf die Theilung der Zellen?

Holy, T. E., Dogterom, M., Yurke, B., and Leibler, S. (1997). Assembly and positioning of microtubule asters in microfabricated chambers.

Hyman, A. A. (1989). Caenorhabditis elegans: A Cortical Site Determining Centrosome Position. The Journal of Cell Biology *109*, 1185–1193.

Hyman, A. A., and White, J. G. (1987). Determination of Cell Division Axes in the Early Embryogenesis of *Caenorhabditis elegans*. The Journal of Cell Biology *105*, 2123–2135.

Inaba, M., Yuan, H., Salzmann, V., Fuller, M. T., and Yamashita, Y. M. (2010). E-Cadherin Is Required for Centrosome and Spindle Orientation in Drosophila Male Germline Stem Cells. PLoS ONE *5*, e12473.

Inoué, S. (1953). Polarization Optical Studies of the Mitotic Spindle. Chromosoma (Berl) *5*, 487–500.

Inoué, S., and Sato, H. (1967). Cell motility by labile association of molecules. The nature of mitotic spindle fibers and their role in chromosome movement. J. Gen. Physiol. *50*, Suppl:259–Suppl:292.

Kardon, J. R., and Vale, R. D. (2009). Regulators of the cytoplasmic dynein motor. Nat Rev Mol Cell Biol *10*, 854–865.

Kiger, A. A., Jones, D. L., Schulz, C., Rogers, M. B., and Fuller, M. T. (2001). Stem cell self-renewal specified by JAK-STAT activation in response to a support cell cue. Science *294*, 2542–2545.

Kiyomitsu, T., and Cheeseman, I. M. (2012). Chromosome- and spindle-pole-derived signals generate an intrinsic code for spindle position and orientation. Nature Cell Biology *14*, 311–317.

Kiyomitsu, T., and Cheeseman, I. M. (2013). Cortical Dynein and Asymmetric Membrane Elongation Coordinately Position the Spindle in Anaphase. Cell *154*, 391–402.

Knoblich, J. A. (2008). Mechanisms of Asymmetric Stem Cell Division. Cell *132*, 583–597.

Knoblich, J. A. (2010). Asymmetric cell division: recent developments and their implications for tumour biology. Nat Rev Mol Cell Biol *11*, 849–860.

Kotak, S., and Gönczy, P. (2013). Mechanisms of spindle positioning: cortical force generators in the limelight. Current Opinion in Cell Biology *25*, 741–748.

Krausova, M., and Korinek, V. (2014). Cellular Signalling. Cellular Signalling *26*, 570–579.

Laan, L., Pavin, N., Husson, J., Romet-Lemonne, G., van Duijn, M., López, M. P., Vale, R. D., Jülicher, F., Reck-Peterson, S. L., and Dogterom, M. (2012). Cortical Dynein Controls Microtubule Dynamics to Generate Pulling Forces that Position Microtubule Asters. Cell *148*, 502–514.

Labbé, J.-C., McCarthy, E. K., and Goldstein, B. (2004). The forces that position a mitotic spindle asymmetrically are tethered until after the time of spindle assembly. The Journal of Cell Biology *167*, 245–256.

Le Grand, F., Jones, A. E., Seale, V., Scimè, A., and Rudnicki, M. A. (2009). Wnt7a activates the planar cell polarity pathway to drive the symmetric expansion of satellite stem cells. Cell Stem Cell *4*, 535–547.

Liro, M. J., and Rose, L. S. (2016). Mitotic Spindle Positioning in the EMS Cell of Caenorhabditis elegans Requires LET-99 and LIN-5/NuMA. Genetics *204*, 1177–1189.

Logan, C. Y., and Nusse, R. (2004). The Wnt signaling pathway in development and disease. Annu. Rev. Cell Dev. Biol. *20*, 781–810.

Lu, M. S., and Johnston, C. A. (2013). Molecular pathways regulating mitotic spindle orientation in animal cells. Development *140*, 1843–1856.

Lutz, D. A., Hamaguchi, Y., and Inoué, S. (1988). Micromanipulation studies of the asymmetric positioning of the maturation spindle in Chaetopterus sp. oocytes: I. Anchorage of the spindle to the cortex and migration of a displaced spindle. Cell Motil. Cytoskeleton *11*, 83–96.

Maddox, P., Straight, A., Coughlin, P., Mitchison, T. J., and Salmon, E. D. (2003). Direct observation of microtubule dynamics at kinetochores in Xenopus extract spindles: implications for spindle mechanics. The Journal of Cell Biology *162*, 377–382.

McIntosh, J., and Hays, T. (2016). A Brief History of Research on Mitotic Mechanisms. Biology *5*, 55.

McNally, F. J. (2013). Mechanisms of spindle positioning. The Journal of Cell Biology *200*, 131–140.

Merdes, A., Ramyar, K., Vechio, J. D., and Cleveland, D. W. (1996). A complex of NuMA and cytoplasmic dynein is essential for mitotic spindle assembly. Cell *87*, 447–458.

Mitchison, T., and Kirschner, M. (1984a). Dynamic instability of microtubule growth. Nature.

Mitchison, T., and Kirschner, M. (1984b). Microtubule assembly nucleated by isolated centrosomes. Nature.

Morin, X., and Bellaïche, Y. (2011). Mitotic Spindle Orientation in Asymmetric and Symmetric Cell Divisions during Animal Development. Developmental Cell *21*, 102–119.

Morris, E. J., Assi, K., Salh, B., and Dedhar, S. (2015). Integrin-Linked Kinase links Dynactin-1/Dynactin-2 with cortical Integrin receptors to orient the mitotic spindle relative to the substratum. Sci. Rep. *5*, 8389.

Niehrs, C. (2012). The complex world of WNT receptor signalling. Nat Rev Mol Cell Biol *13*, 767–779.

Pease, J. C., and Tirnauer, J. S. (2011). Mitotic spindle misorientation in cancer--out of alignment and into the fire. Journal of Cell Biology *124*, 1007–1016.

Phillips, B. T., and Kimble, J. (2009). A New Look at TCF and β-Catenin

through the Lens of a Divergent C. elegans Wnt Pathway. Developmental Cell *17*, 27–34.

Potapova, T., and Gorbsky, G. (2017). The Consequences of Chromosome Segregation Errors in Mitosis and Meiosis. Biology *6*, 12.

Priess, J., and Thomson, J. N. (1987). Cellular Interactions in Early C. elegans Embryos. Cell *48*, 241–250.

Quyn, A. J., Appleton, P. L., Carey, F. A., Steele, R. J. C., Barker, N., Clevers, H., Ridgway, R. A., Sansom, O. J., and NAthke, I. S. (2010). Spindle Orientation Bias in Gut Epithelial Stem Cell Compartments Is Lost in Precancerous Tissue. Stem Cell *6*, 175–181.

Rappaport, R. (1961). Experiments concerning the cleavage stimulus in sand dollar eggs. The Journal of Experimental Zoology *148*, 81–89.

Rhyu, M. S., Jan, L. Y., and Jan, Y. N. (1994). Asymmetric distribution of numb protein during division of the sensory organ precursor cell confers distinct fates to daughter cells. Cell.

Rocheleau, C. E., and Priess, J. R. (1997). Wnt Signaling and an APC-Related Gene Specify Endoderm in Early C. Elegans Embryos. 1–10.

Rose, L., and Gönczy, P. (2005). Polarity establishment, asymmetric division and segregation of fate determinants in early C. elegans embryos.

Sawa, H. (2012). Control of Cell Polarity and Asymmetric Division in C. elegans, Elsevier Inc.

Schlesinger, A., Shelton, C. A., Maloof, J. N., Meneghini, M., and Bowerman, B. (1999). Wnt pathway components orient a mitotic spindle in the early Caenorhabditis elegans embryo without requiring gene transcription in the responding cell. Genes & Development *13*, 2028–2038.

Schmid, A., Chiba, A., and doe, C. Q. (1999). Clonal analysis of Drosophila embryonic neuroblasts: neural cell types, axon projections and muscle targets. Development *126*, 4653–4689.

Schmidt, D. J., Rose, D. J., Saxton, W. M., and Strome, S. (2005). Functional Analysis of Cytoplasmic Dynein Heavy Chain in *Caenorhabditis elegans* with Fast-acting Temperature- sensitive Mutations. Molecular Biology of the Cell *16*, 1200–1212.

Segalen, M., and Bellaïche, Y. (2009). Cell division orientation and planar cell polarity pathways. Seminars in Cell & Developmental Biology *20*, 972–977.

Segalen, M., Johnston, C. A., Martin, C. A., Dumortier, J. G., Prehoda, K. E., David, N. B., Doe, C. Q., and Bellaïche, Y. (2010). The Fz-Dsh Planar Cell Polarity Pathway Induces Oriented Cell Division via Mud/NuMA in Drosophila and Zebrafish. Developmental Cell *19*, 740–752.

Seldin, L., Muroyama, A., and Lechler, T. (2016). NuMA-microtubule interactions are critical for spindle orientation and the morphogenesis of diverse epidermal structures. Elife *5*.

Seldin, L., Poulson, N. D., Foote, H. P., and Lechler, T. (2013). NuMA localization, stability, and function in spindle orientation involve 4.1 and Cdk1 interactions. Molecular Biology of the Cell *24*, 3651–3662.

Siegrist, S. E., and Doe, C. Q. (2006). Extrinsic cues orient the cell division axis in Drosophila embryonic neuroblasts. Development *133*, 529–536.

Siller, K. H., and Doe, C. Q. (2009). Spindle orientation during asymmetric cell division. Nature Cell Biology *11*, 365–374.

Smith, P., Azzam, M., and Hinck, L. (2017). Extracellular Regulation of the Mitotic Spindle and Fate Determinants Driving Asymmetric Cell Division. In: Results and Problems in Cell Differentiation, Cham: Springer International Publishing, 351–373.

Srinivasan, D. G., Fisk, R. M., Xu, H., and van den Heuvel, S. (2003). A complex of LIN-5 and GPR proteins regulates G protein signaling and spindle function in C elegans. Genes & Development *17*, 1225–1239.

Sugioka, K., Mizumoto, K., and Sawa, H. (2011). Wnt Regulates Spindle Asymmetry to Generate Asymmetric Nuclear β-Catenin in C. elegans. Cell *146*, 942–954.

Takada, R., Satomi, Y., Kurata, T., Ueno, N., Norioka, S., Kondoh, H., Takao, T., and Takada, S. (2006). Monounsaturated Fatty Acid Modification of Wnt Protein: Its Role in Wnt Secretion. Developmental Cell *11*, 791–801.

Théry, M., and Bornens, M. (2006). Cell shape and cell division. Current Opinion in Cell Biology *18*, 648–657.

Thorpe, C. J., Schlesinger, A., Carter, J. C., and Bowerman, B. (1997). Wnt Signaling Polarizes an Early C. Elegans Blastomere to Distinguish Endoderm From Mesoderm. 1–11.

Toyoshima, F., and Nishida, E. (2007). Integrin-mediated adhesion orients the spindle parallel to the substratum in an EB1-and myosin X-dependent manner. The EMBO Journal.

Tsou, M. F. B. (2003). LET-99 opposes G /GPR signaling to generate asymmetry for

spindle positioning in response to PAR and MES-1/SRC-1 signaling. Development *130*, 5717–5730.

Tulina, N., and Matunis, E. (2001). Control of stem cell self-renewal in Drosophila spermatogenesis by JAK-STAT signaling. Science *294*, 2546–2549.

Tuncay, H. U. S., Brinkmann, B. F., Steinbacher, T., rmann, A. S. U., Gerke, V., Iden, S., and Ebnet, K. (2015). JAM-A regulates cortical dynein localizationthrough Cdc42 to control planar spindleorientation during mitosis. Nature Communications *6*, 1–12.

Walston, T., Tuskey, C., Edgar, L., Hawkins, N., Ellis, G., Bowerman, B., Wood, W., and Hardin, J. (2004). Multiple Wnt Signaling Pathways Converge to Orient the Mitotic Spindle in Early C. elegans Embryos. Developmental Cell *7*, 831–841.

Werts, A. D., and Goldstein, B. (2011). How signaling between cells can orient a mitotic spindle. Seminars in Cell & Developmental Biology *22*, 842–849.

Werts, A. D., Roh-Johnson, M., and Goldstein, B. (2011). Dynamic localization of C. elegans TPR-GoLoco proteins mediates mitotic spindle orientation by extrinsic signaling. Development *138*, 4411–4422.

Whangbo, J., and Kenyon, C. (1999). A Wnt signaling system that specifies two patterns of cell migration in C. elegans. Molecular Cell *4*, 851–858.

Willert, K., Brown, J. D., Danenberg, E., Duncan, A. W., Weissman, I. L., Reya, T., Yates, J. R., III, and Nusse, R. (2003). Wnt proteins are lipid-modified and can act as stem cell growth factors. Nature *423*, 448–452.

Williams, S. E., and Fuchs, E. (2013). Oriented divisions, fate decisions. Current Opinion in Cell Biology *25*, 749–758.

Williams, S. E., Beronja, S., Pasolli, H. A., and Fuchs, E. (2011). nature09793. Nature *470*, 353–358.

Wodarz, A. (2005). Molecular control of cell polarity and asymmetric cell division in Drosophila neuroblasts. Current Opinion in Cell Biology *17*, 475–481.

Wu, P.-S., Egger, B., and Brand, A. H. (2008). Asymmetric stem cell division: Lessons from Drosophila. Seminars in Cell & Developmental Biology *19*, 283–293.

Xia, J. *et al.* (2015). Semaphorin-Plexin Signaling Controls Mitotic Spindle Orientation during Epithelial Morphogenesis and Repair. Developmental Cell *33*, 299–313.

Yadlapalli, S., and Yamashita, Y. M. (2012). Spindle positioning in the stem cell niche. Wiley Interdiscip Rev Dev Biol *1*, 215–230.

Yamashita, Y. M. (2010). Cell adhesion in regulation of asymmetric stem cell division. Current Opinion in Cell Biology *22*, 605–610.

Yamashita, Y. M., Jones, D. L., and Fuller, M. T. (2003). Orientation of asymmetric stem cell division by the APC tumor suppressor and centrosome. Science *301*, 1547–1550.

Yamashita, Y. M., Mahowald, A. P., Perlin, J. R., and Fuller, M. T. (2007). Asymmetric Inheritance of Mother Versus Daughter Centrosome in Stem Cell Division. Science *315*, 518–521.

Yoshiura, S., Ohta, N., and Matsuzaki, F. (2012). Tre1 GPCR Signaling Orients Stem Cell Divisions in the Drosophila Central Nervous System. Developmental Cell *22*, 79–91.

Yuzawa, S., Kamakura, S., Iwakiri, Y., Hayase, J., and Sumimoto, H. (2011). Structural basis for interaction between the conserved cell polarity proteins Inscuteable and Leu-Gly-Asn repeat-enriched protein (LGN). Proceedings of the National Academy of Sciences *108*, 19210–19215.

Zhang, H., Skop, A. R., and White, J. G. (2008). Src and Wnt signaling regulate dynactin accumulation to the P2-EMS cell border in C. elegans embryos. Journal of Cell Biology *121*, 155–161.

Zheng, Z., Zhu, H., Wan, Q., Liu, J., Xiao, Z., Siderovski, D. P., and Du, Q. (2010). LGN regulates mitotic spindle orientation during epithelial morphogenesis. The Journal of Cell Biology *189*, 275–288.

## CHAPTER 2: COMPARATIVE ASSESSMENT OF FLUORESCENT PROTEINS FOR IN VIVO IMAGING IN AN ANIMAL MODEL SYSTEM

*The following was published in 2016, in Molecular Biology of the Cell's Quantitative Biology Special Issue (Heppert et. al., 2016).*

Fluorescent protein tags are fundamental tools used to visualize gene products and analyze their dynamics *in vivo*. Recent advances in genome editing have expedited the precise insertion of fluorescent protein tags into the genomes of diverse organisms. These advances expand the potential of *in vivo* imaging experiments, and they facilitate experimentation with new, bright, photostable fluorescent proteins. Most quantitative comparisons of the brightness and photostability of different fluorescent proteins have been made *in vitro*, removed from biological variables that govern their performance in cells or organisms. To address the gap, we quantitatively assessed fluorescent protein properties *in vivo* in an animal model system. We generated transgenic *C. elegans* strains expressing green, yellow, or red fluorescent proteins in embryos, and we imaged embryos expressing different fluorescent proteins under the same conditions for direct comparison. We found that mNeonGreen was not as bright *in vivo* as predicted based on *in vitro* data, but that mNeonGreen is a better tag than GFP for specific kinds of experiments, and we report on optimal red fluorescent proteins. These results identify ideal fluorescent proteins for imaging *in vivo* in *C. elegans* embryos,

and they suggest good candidate fluorescent proteins to test in other animal model systems for *in vivo* imaging experiments.

## 2.1 Introduction

For more than two decades, cell and developmental biologists have used genetically-encoded fluorescent protein fusion tags to visualize proteins in living cells and organisms. Efforts to engineer and discover superior fluorescent proteins have resulted in variants with diverse emission wavelengths and photophysical properties (Tsien, 1998; Matz *et al.*, 1999; Shaner *et al.*, 2004; 2007; Shcherbo *et al.*, 2009; Shaner *et al.*, 2013; Shaner, 2014). The color, brightness, and photostability of a fluorescent protein are critical parameters to consider for experiments in which proteins will be imaged *in vivo* (Shaner *et al.*, 2005; Davidson and Campbell, 2009; Shaner, 2014). However, most brightness and photostability measurements are made with purified fluorescent proteins *in vitro* (Shaner *et al.*, 2005). While this approach provides information about the intrinsic optical properties of each fluorescent protein, it does not replicate many of the conditions of an *in vivo,* biological system.

Historically, many methods used to express fluorescently tagged proteins resulted in non-physiological levels of proteins of interest, limiting the interpretation of some experiments (Huang *et al.*, 2000; Krestel *et al.*, 2004; Doyon *et al.*, 2011). However, genome engineering techniques based on the CRISPR/Cas9 system have recently made it possible to more precisely edit the genomes of diverse cell types and organisms (Doudna and Charpentier, 2014; Gilles and Averof, 2014; Harrison *et al.*, 2014; Hsu *et al.*, 2014; Peng *et al.*, 2014) and to routinely insert fluorescent

protein tags into endogenous genomic loci in some organisms, as has long been standard in yeast (Dickinson *et al.*, 2013; Auer *et al.*, 2014; Bassett *et al.*, 2014; Ma *et al.*, 2014; Paix *et al.*, 2014; Xue *et al.*, 2014; Aida *et al.*, 2015; Dickinson *et al.*, 2015; Perry and Henry, 2015; Ratz *et al.*, 2015). With this technological advance comes an increase in need for information about the best fluorescent proteins to use for *in vivo* imaging studies. Fortunately, advances in genome editing techniques have also created an opportunity to close this gap in knowledge by facilitating the comparison of fluorescent proteins *in vivo*.

Our goal in this study was to make a systematic comparison of some of the brightest known fluorescent proteins that would answer the question: What fluorescent protein should one use *in vivo* for a given experiment? A previous systematic analysis of fluorescent proteins performed in *Saccharomyces cerevisiae* revealed clear information about which tags to use *in vivo* in yeast (Lee *et al.*, 2013). Since that study, new fluorescent proteins have been characterized, including some reported to be brighter than GFP (Shaner *et al.*, 2013). Here we report direct comparisons of monomeric green (GFP, mNeonGreen - mNG), yellow (mYPet, mNG), and red (TagRFP-T, mRuby2, mCherry, mKate2) fluorescent proteins *in vivo,* in a multicellular animal model organism. We used CRISPR/Cas9-triggered homologous recombination in *C. elegans* to express the same transgene tagged with optimized versions of various fluorescent proteins from the same genomic locus. This allowed us to quantitatively compare the brightness and photostability of these fluorescent proteins in embryos imaged under typical experimental conditions. Because we made observations *in vivo,* encapsulated in our measurements are the

variables that govern a given fluorescent protein's performance including intrinsic brightness, transcript or protein stability, and maturation rate, all of which contribute to practical use in live imaging experiments.

Our findings provide quantitative data that are useful for choosing which fluorescent proteins to use for *in vivo* experiments in *C. elegans*. The results suggest a set of candidate fluorescent proteins for testing in other model systems, and more generally, they demonstrate the value of testing fluorescent protein performance *in vivo*. We also contribute novel tools for the field including constructs containing optimized fluorescent proteins and an Excel based tool to assist investigators in choosing the best fluorescent proteins to use with their imaging resources.

## 2.2 Results and Discussion

### *Predictions of Fluorescent Protein Brightness*

Before making *in vivo* measurements, we made quantitative predictions about which fluorescent proteins were expected to be brightest. We calculated the predicted brightness of each fluorescent protein by the product of the quantum yield and extinction coefficient as reported in the literature (Figure 2.1A)(Yang *et al.*, 1996; Shaner *et al.*, 2004; Nguyen and Daugherty, 2005; Shaner *et al.*, 2008; Shcherbo *et al.*, 2009; Lam *et al.*, 2012; Lee *et al.*, 2013; Shaner *et al.*, 2013). Because imaging conditions such as excitation wavelength and emission filter sets used impact the observed brightness of a fluorescent protein, we sought to use these values to make more useful predictions of fluorescent protein brightness for directly comparing with our results.

To facilitate the visual and quantitative evaluation of fluorescent protein spectra with the specific laser lines and filter sets that are used by us and others, we

developed a simple and customizable Microsoft Excel-based tool that we call the Spectrum Viewer. Using this tool, we calculated a predicted brightness for each fluorescent protein by integrating the portion of the fluorescent protein emission peak under our emission filter and multiplying by the quantum yield (Figure 2.1B). We then used the Spectrum Viewer to plot the normalized absorbance and emission spectra for the fluorescent proteins in our comparisons with the excitation wavelength and emission filter sets we used for imaging (Figure 2.2 A-D, third column).

***Measuring C. elegans embryo autofluorescence at different wavelengths***

Because single-copy fluorescent transgenes sometimes produce weak fluorescent signal *in vivo*, we quantitatively assessed the endogenous autofluorescence levels of *C. elegans* embryos. We measured autofluorescence using two different techniques. In one case we used a spectral detector to measure autofluorescence at various emission wavelengths. In the other we used a spinning disk confocal microscope with standard lasers and filter sets and an EM-CCD camera. The results of both experiments were consistent (Figure 2.1C), and are likely to be similar on other comparable imaging systems. We found autofluorescence to be most prominent under 488nm excitation, across a broad range of emission wavelengths (Figure 2.1C). Thus, when expressed at low levels, fluorescent proteins excited by 488nm light, including GFP, will have significant background noise in *C. elegans* embryos. Embryos had considerably less autofluorescent background with 514nm excitation (Figure 2.1C). This suggests that when imaging proteins expressed at low levels in embryos, using 514nm excitation

and yellow fluorescent proteins, such as mNeonGreen or mYPet, may be superior to GFP and 488nm illumination. We found autofluorescence to be lowest using 405nm and 442nm excitation, but we generally avoid live imaging in these wavelengths due to increased phototoxicity.

***Generating single-copy transgene knock-ins***

To directly compare fluorescent proteins *in vivo*, we used CRIPSR/Cas-9 to generate single-copy transgene knock-in strains expressing distinct fluorescent proteins. Constructs used to create these strains were identical except for the fluorescent protein sequences encoded in each case, and each transgene was inserted into the same locus in the *C. elegans* genome (Figure 2.2, see *Materials and Methods*). We confirmed the knock-ins by observation of the predicted fluorescence localization pattern at the plasma membrane, and we confirmed that knock-ins were single copy by PCR genotyping and by sequencing (Figure 2.3).

***In vivo fluorescent protein brightness***

To assess the brightness of this set of fluorescent protein transgenes *in vivo*, we imaged staged *C. elegans* embryos, in some cases mounted side-by-side for direct comparisons, by spinning disk confocal microscopy. We first compared GFP and mNG by quantifying the fluorescence from embryos illuminated with 488nm excitation. Although mNG was predicted to be brighter than GFP based on *in vitro* data (Figure 2.1A and B), we found that the GFP signal was nearly twice as bright as the mNG signal *in vivo* (Figure 2.2A). Mean values within each comparison are significantly different ($p<0.05$) except where indicated with ns: not significantly

different (determined by Student's t-test with Welch's correction), and all significance values (P-values) are reported in Figure 2.4, B.

Using 514nm illumination, mYPet was also brighter than mNG (Figure 2.2B). Though our calculations predicted that mYPet would be almost twice as bright as mNG (Figure 2.1B), we observed mYPet to be about four times as bright as mNG on average (Figure 2.2B). The data from the comparisons of mNG with GFP and mYpet suggest that mNG is not as bright *in vivo* as we predicted based on the published extinction coefficient and quantum yield (Shaner *et. al.,* 2013) (Figure 2.1B, Figure 2.2A and B).

Next we examined the brightness of four red fluorescent proteins (TagRFP-T, mRuby2, mCherry and mKate2). We performed experiments with two different emission filter sets, 561LP and 630/75BP, which are well matched to some or all of these red fluorescent proteins. The 561LP emission filter is optimal because it collects the majority of the emission peak emission for each fluorescent protein (Figure 2.2C). A band pass filter, such as the 630/75BP, is less optimal (compare right column Figure 2.2C and D), however, it may be useful for decreasing spectral overlap for two or three-color imaging.

Using 561nm illumination we measured the brightness of the four red fluorescent proteins. We found that TagRFP-T was the brightest using the 561LP filter set (Figure 2.2C). Using the 630/75BP filter set, the average fluorescence intensity of TagRFP-T was indistinguishable from that of mCherry (Figure 2.2D). These results are consistent with the orange-shifted emission spectra of TagRFP-T and with our calculated predictions for these fluorescent proteins (Figure 2.1B, 2.2C

and D). mRuby2, which was predicted to be the brightest of the four red fluorescent proteins (Figure 2.1B), was the least bright regardless of the emission filter set we used (Figure 2.2C and D). Taken together, these data reveal fluorescent protein brightnesses *in vivo*, which did not always match predictions made using parameters measured *in vitro*.

***Variation in fluorescent protein brightness between single-copy transgenes***

Because we predicted that mNG would be ~1.8 times brighter than GFP, we were surprised to find that the GFP embryos were significantly brighter than mNG embryos (Figure 2.1B, 2.2A). Germline silencing in *C. elegans* can have heterogeneous effects on certain single-copy transgenes (Shirayama *et al.*, 2012). Consequently, fluorescent protein transgenes that are in every other way identical could be expressed at different levels, causing discrepancies between predicted and observed brightness. To ask whether differences in fluorescent protein abundance could account for the differences in fluorescence intensity we observed, we analyzed protein levels in each of our single-copy transgenic strains by western blot (Figure 2.3). We observed approximately 2-fold higher levels of *mex-5* driven GFP::PH protein compared with mNG::PH protein (Figure 2.3, C, paired t-test, p=0.0408), which may be due to partial transgene silencing or post-transcriptional regulation of these transgenes.

To further investigate the discrepancy between our predictions and observations, we compared a second set of identical GFP and mNG single-copy transgene knock-in strains. These fluorescent proteins were fused to the C-terminus of a histone gene (*his-58)*. As expected, the resulting fluorescence was brightest in

nuclei (Figure 2.5A). To control for effects of cell cycle timing on histone protein abundance, we staged embryos to within 3 minutes of one another. We measured the fluorescence intensity in the nucleus of one embryonic cell (the EMS cell) in each embryo and found that the average fluorescence intensity of the GFP-histone expressing embryos and the mNG-histone embryos were not significantly different (Figure 2.5A). Although in our initial comparison of membrane localized transgenes we found that GFP-expressing embryos were significantly brighter than those expressing mNG (Figure 2.2A), both results suggest that in early *C. elegans* embryos mNG is not as bright when compared with GFP as we had predicted (Figure 2.1B).

Because protein levels in the *C. elegans* germline and early embryo can be affected by silencing mechanisms (Shirayama *et al.*, 2012), we compared GFP and mNG in a *C. elegans* tissue that has not been reported to exhibit the silencing. We replaced the germline promoter in our original GFP and mNG::PH repair template constructs with the *myo-2* promoter, which drives expression in the pharynx (Okkema *et al.*, 1993) and generated single-copy transgene knock-ins at the same genomic locus used for our initial comparison. We imaged staged worms and quantified GFP and mNG fluorescence and again found no significant difference between average GFP and mNG intensities (Figure 2.5B). These data are consistent with our findings in early embryos, and are consistent with the possibility that factors outside of germline silencing may also play a role in determining the observed fluorescence from single-copy transgenes.

### *Comparing green fluorescent proteins as endogenous tags*

We next set out to compare GFP and mNG inserted into existing genes at their endogenous loci. We picked three genomic loci for which N-terminal mNG knock-ins already exist, *gex-3, rap-1, and nmy-2* (Dickinson *et. al.,* 2015), and we generated identical GFP knock-ins at those loci by the same method used to create the original mNG strains. We imaged embryos from the paired strains side-by-side at the same developmental stage as in our previous comparisons (Figure 2.5C-E). Using 488nm illumination, we found no consensus in our comparisons: mNG::GEX-3 was brighter than GFP:GEX-3, mNG and GFP::RAP-1 were equally bright, and GFP::NMY-2 was brighter than mNG::NMY-2 (Figure 2.5C-E).

Because background embryo autofluorescence is higher at 488nm illumination (Figure 2.1C), we also imaged these embryos using 514nm illumination. Background autofluorescence is most prevalent when fluorescent protein signal levels are low. Therefore, we were most interested, in this comparison, in *gex-3* knock-in embryos because we had observed that it has the lowest expression of the three genes we tagged (Figure 2.5C-E). Although we could not quantitatively compare fluorescence intensity of embryos illuminated with 488nm vs. 514nm wavelengths due to differences in image acquisition set-up (e.g. laser power, filter sets, etc.), we observed that mNG::GEX-3 imaged with 514 nm illumination gave qualitatively the best results under these imaging conditions (Figure 2.5C). The wild-type embryos in each image show the level of autofluorescent background contributed under the given imaging conditions.

### *Photostability of fluorescent proteins in vivo*

The brightness of a fluorescent protein together with its photobleaching rate determine how useful a fluorescent protein is for time-lapse imaging (Shaner *et. al.,* 2005; Davidson and Campbell, 2009; Shaner, 2014). To test the rate of photobleaching of the fluorescent proteins used in our initial comparison in Figure 2.2, we imaged embryos over time under continuous illumination (Figure 2.6 A-C). Fluorescence intensities were normalized to initial brightness measured for each embryo, and averages were plotted for each strain over time (Figure 2.6 A-C; left). Each photobleaching curve was fit to a one-phase exponential decay and the half-life was calculated (Figure 2.7). To estimate a photon budget (Lee *et. al.,* 2013), or the amount of signal emitted by each fluorescent protein over time, we integrated the fluorescence intensity measured for each embryo up to 50% of its initial intensity (Figure 2.6 A-C; right).

GFP and mNG displayed similar photobleaching half-life, with mNG being slightly more photostable (Figure 2.6A, Figure 2.7B). However, because the GFP embryos are brighter, on average, the integrated intensity, or photon budget of the GFP embryos was slightly higher than that of mNG (Figure 2.6A). mYPet was observed to photobleach far faster than mNG, as expected (Figure 2.7B) (Shaner *et. al.,* 2013). Because mYPet is significantly brighter than mNG, its photon budget is only slightly less than that of mNG (Figure 2.6B). Of the red fluorescent proteins we tested, mKate2 had the slowest average photo bleaching rate and about the same photon budget as mCherry (Figure 2.6C). The photobleaching profile of mKate2 suggests that it exhibits kindling (photoactivation) in the first few frames of

illumination (Figure 2.5C and Figure 2.7). Photoactivation was not reported in the initial characterization of mKate2, but had been observed for its precursor protein mKate (Shcherbo *et al.*, 2009). We conclude that mRuby2 and mYPet exhibited relatively poor photostability *in vivo*, and that GFP, mNG and mKate2 were the most photostable.

### 2.3 Summary and Recommendations

Our results suggest specific recommendations for fluorescent proteins to use in *in vivo* experiments in *C. elegans* embryos, forming a baseline for comparisons in other *in vivo* systems. In general, we observed a lower-than-expected brightness for mNG. In some comparisons GFP and mNG performed similarly (Figure 2.2A and Figure 2.5), but surprisingly in some experiments, each was clearly brighter than the other. GFP was brighter than mNG in a germline transgene expressed at high levels and in an *nmy-2* endogenous tag (Figure 2.2A and Figure 2.5E). However, mNG was brighter than GFP in the more weakly expressed *gex-3* endogenous tag (Figure 2.5C). These results suggests that GFP and mNG may each be ideal in different contexts, and that testing may be required to identify the best green fluorescent protein for a specific experiment. mYPet was significantly brighter than mNG, but its high rate of photobleaching makes it an unattractive choice for long-term imaging (Figure 2.2B and Figure 2.6B). The four red fluorescent proteins we tested were only compared under one set of conditions, which is a limitation of this study. However, TagRFP-T, mCherry, and mKate2 performed similarly in terms of brightness, mKate2 had the superior photobleaching dynamics *in vivo* (Figure 2.2C, D and 4C).

Our measurements of autofluorescence in the early *C. elegans* embryo highlight the value of taking such measurements before designing *in vivo* imaging experiments. For *C. elegans* embryos, using 488nm illumination gave higher background than imaging using 514nm illumination (Figure 2.1C). Therefore, for genes with low expression levels, better signal-to-noise ratios may be achieved using a yellow fluorescent protein and exciting with 514nm illumination, rather than a green fluorescent protein and 488nm illumination (Figure 2.5C). Because of the rapid photobleaching we observed for mYPet (Figure 2.6B), we would choose mNG to tag proteins expressed at lower levels in *C. elegans* embryos for long-term, live-cell imaging. Although these measurements are informative for considering which fluorescent proteins to use *in vivo,* because of variability in detector sensitivity and emission light scattering at different wavelengths, they may not reflect the actual autofluorescent properties of *C. elegans* embryos.

We observed several differences between our predictions and our *in vivo* measurements of fluorescent protein brightness, most notably for mNeonGreen and for mRuby2 (Figure 2.1B and Figure 2.2). These results demonstrate the value of direct *in vivo* comparisons for selecting fluorescent proteins to use *in vivo*. Because we measured fluorescent protein performance head-to-head, *in vivo*, we expect that the differences in brightness we observed were due to the combination of intrinsic differences in fluorescent protein brightness and the cumulative effects of any regulatory mechanisms (at the mRNA or protein level) at play in the biological system that we used. Cases where our quantitative expectations based on the

intrinsic properties of fluorescent proteins were violated suggest that other regulatory mechanisms are indeed a factor in determining fluorescent protein performance.

Although identifying variables, other than intrinsic brightness, that might affect fluorescent protein brightness *in vivo* is outside the scope of this work, there are a variety of interesting possibilities to consider. One possibility is that coding sequence differences in fluorescent proteins result in differential silencing of the transgenes we compared. Germline silencing in *C. elegans* has been shown to have heterogeneous effects on certain single-copy transgenes (Shirayama *et al.*, 2012). Consequently, fluorescent protein transgenes that are in every other way identical could be expressed at different levels, causing discrepancies between predicted and observed brightness. Any effects of silencing on expression and observed brightness would likely differ in different model systems. Another possibility is that fluorescent proteins mature and decay at different rates *in vivo* than they do *in vitro*. Temperature could affect the performance of fluorescent proteins designed for expression in mammalian systems (37°C) as *C. elegans* are maintained and imaged near room temperature (20-25°C).

Identifying the cellular and organismal mechanisms underlying the context specific performance of fluorescent proteins is important for understanding how universal findings in any one system may be. At present, it is unknown how applicable the specific results of this study are in model systems beyond *C. elegans*. The fluorescent proteins we found to be optimal were not the same as another comprehensive *in vivo* comparison of fluorescent proteins in yeast (Lee *et. al,* 2013), suggesting some potential for organism-specific rules for governing fluorescent

protein performance *in vivo*. Future studies in diverse systems are needed to reveal whether there is a universally best set of fluorescent proteins. We used exclusively spinning disk confocal microscopy for our comparisons. However, differences in illumination source and detectors used in different light microscopy techniques (e.g. widefield, TIRF, lightsheet, etc.) may change the observed performance of fluorescent proteins in live imaging experiments.

This study contributes information of practical value about which fluorescent proteins to use for *in vivo* experiments, as well as a tool for researchers to use to evaluate the spectra of different fluorescent proteins relative to their own imaging resources. The findings are especially applicable for experiments in *C. elegans*, and they suggest the value of performing similar experiments in other model systems, as well as good candidate fluorescent proteins to test.

## 2.4 Materials and Methods

### *C. elegans Strains and Maintenance*

All *C. elegans* strains used in this study are listed in Figure 2.3 and were handled using standard techniques (Brenner, 1974). The strains were raised at 25°C, in incubators in the dark, and fed *E. coli* OP50 except where otherwise indicated. The HT1593 (*unc-119(ed3)* III) strain, used as the parent to the LP306, LP274, LP402, LP193, LP307, LP308, LP401, LP403, and LP404 strains generated in this study, was raised at 15°C and fed *E. coli* HB101 prior to injection (Hochbaum *et al.*, 2010; Dickinson *et al.*, 2013).

### *Fluorescent Protein Selection*

Because of their current widespread use, we chose to compare GFP and mCherry with newer green and red fluorescent proteins that are less commonly used but that have been described as having superior brightness and/or photostability. We used a GFP variant, GFP S65C, commonly used in *C. elegans,* which we refer to as GFP (Green *et al.*, 2008). S65C and S65T (eGFP) variants perform similarly (Heim and Tsien, 1996), and a previous *in vivo* study of fluorescent proteins in yeast reported that S65T outperformed certain green fluorescent protein variants (such as Clover and Emerald) in a direct comparison (Lee *et al.*, 2013). mNeonGreen (mNG), is a newer, monomeric green fluorescent protein (peak excitation ~506nm) that is reported to be up to three times as bright and more photostable than eGFP *in vitro* (Shaner *et al.*, 2013). We therefore compared mNG to GFP in our *in vivo* system. To assess the practical value of mNG's yellow-shifted excitation spectrum (Shaner *et al.*, 2013), we compared mNG with a yellow fluorescent protein, mYPet—the brightest reported yellow fluorescent protein reported to date (Nguyen and Daugherty, 2005). We chose three red fluorescent proteins to compare with mCherry: TagRFP-T, mKate2, and mRuby2. A direct comparison in yeast found that all three were brighter than mCherry *in vivo* (Lee *et al.*, 2013). These red fluorescent proteins range in peak emission from 584nm to 633nm (Shaner *et al.*, 2008; Shcherbo *et al.*, 2009; Lam *et al.*, 2012), making them useful in combination with different fluorescent proteins for two- or three-color imaging.

***Fluorescent protein optimization and repair template construction***

Single-copy transgenic knock-in strains (LP306, LP274, LP402, LP193, LP307, LP308, LP401, LP403, LP404) were generated using the method described in Dickinson *et. al.,* 2013. Fluorescent protein sequences were obtained from the following sources (Heim and Tsien, 1996; Shaner *et al.*, 2004; Nguyen and Daugherty, 2005; Shaner *et al.*, 2008; Shcherbo *et al.*, 2009; Lam *et al.*, 2012; Shaner *et al.*, 2013). mNeonGreen was licensed from Allele Biotechnology. To increase the monomeric character of YPet, we introduced a well-characterized mutation to the original YPet sequence (A206K) to generate mYPet (Zacharias *et al.*, 2002; Ohashi *et al.*, 2007).

Repair template constructs were identical, except for the sequences of the fluorescent proteins tested. Each transgene construct consisted of a germline promoter sequence (*Pmex-5*) driving the expression of a fluorescent protein fused to the N-terminus of the same polypeptide: the pleckstrin homology domain from phospholipase C-δ1 (PH domain) and a 2x Flag epitope tag. The PH domain localizes to the plasma membrane by binding phosphatidylinositol 4,5-bisphosphate ($PIP_2$) (Audhya *et. al.*, 2005). Because many of our source sequences are optimized for expression in mammalian systems, we sought to mitigate any effects that the presence of codons rarely used in *C. elegans* might have on translational efficiency. Therefore, the nucleotide sequences of the fluorescent proteins and PH domain were optimized for expression in *C. elegans* using the *C. elegans* Codon Adapter (CAI ~1) (Redemann *et al.*, 2011). Synthetic *C. elegans* introns were added to each fluorescent protein to facilitate expression of the transgenes (Fire *et.al.*, 1990). The

fluorescent protein genes were synthesized in ~500bp overlapping gBlock fragments (Integrated DNA Technologies), assembled using Gibson Assembly Master Mix (NEB), PCR amplified, and cloned using the Zero Blunt TOPO PCR cloning kit (Invitrogen).

All repair template constructs were made using a derivative of the pCFJ150 vector backbone modified for Cas9 mediated homologous recombination (Frøkjær-Jensen *et al.*, 2008; Dickinson *et al.*, 2013). The *mex-5* promoter, the *C. elegans* sequence-optimized mNeonGreen fluorescent protein and PH domain, and the *tbb-2* 3'UTR were added using Gibson Assembly (NEB) to create vector pAP006. To generate repair templates with different fluorescent protein sequences, pAP006 was amplified into a linear fragment using the forward primer 5' CACGGACTCCAAGACGAC (binds after the *mex-5* promoter) and reverse primer 5' TCTCTGTCTGAAACATTCAATTGATTATC (binds at the start of the *C. elegans* optimized PH domain). Fluorescent protein genes were amplified using gene-specific primers with minimum 30bp overlapping sequence to the parent vector fragment (Forward 5' CGATAATCAATTGAATGTTTCAGACAGAGA + FP sequence; Reverse 5' GCCGGCCACGGACTCCAAGACGACCCAGACCTCCAAG + FP sequence). The vector backbone fragment and fluorescent protein genes were assembled using Gibson Assembly (NEB). The repair templates for strains LP403 and LP404 were made using a similar strategy to exchange the *mex-5* promoter for the *myo-2* promoter sequence.

We have deposited constructs containing the optimized fluorescent proteins in Addgene. Addgene detected an error in our original mKate2 plasmid that we used

to generate the strain used in this study (LP307). The mutation causes a nonsynonmous change in the PH domain of this construct (A735T). Because the mutation was not in the fluorescent protein, and the construct localizes to the plasma membrane, we predicted the mutation would have no affect on observed fluorescence. The mutation was corrected, and the two strains were compared side-by-side; no different in fluorescence intensity was detected (Figure 2.5C).

***Insertion and confirmation of transgene knock-ins***

Single-copy transgenes were inserted into the *C. elegans* genome via Cas9 triggered homologous recombination, using the reagents and methods described in Dickinson *et. al.,* 2013. The transgenes were inserted near the *ttTi5605* MosI insertion site on *C. elegans* chromosome II. This site has been used for both CRISPR/Cas-9 and *Mos1* transposon-based transgene insertions and is known to permit the expression of transgenes in the germline (Frøkjær-Jensen *et al.*, 2008; Dickinson *et al.*, 2013). We used a guide RNA with the following target sequence: 5' - GATATCAGTCTGTTTCGTAA (Dickinson *et al.*, 2013). Single-copy knock-ins were confirmed by rescue of the HT1593 uncoordinated phenotype, observation of the predicted fluorescence localization pattern at the plasma membrane, and PCR genotyping (Figure 2.2 and Figure 2.3, B). PCR genotyping was performed on genomic DNA extracted from putative knock-in animals, using primers outside the insertion site (5' – AGGCAGAATGTGAACAAGACTCG and 5' – ATCGGGAGGCGAACCTAACTG) as described in Dickinson *et. al.,* 2013. We further confirmed the integrity of the inserts by sequencing the promoter, coding

regions, and 3'UTRs of each strain. All seven transgenes resulted in minimal embryonic lethality at 25°C (Figure 2.4, A).

JA1699 was made using standard MosSCI methods using pJA449 (*mtm-3* associated HOT core/*his-58*/mNeonGreen::*tbb-2* 3'UTR), which was constructed using triple gateway into pCFJ150 using *mtm-3* promoter in pDONRP4P1R, pJA273 (*his-58* coding in pDONR221) and pJA448 (*C. elegans* optimized mNeonGreen::*tbb-2* 3'UTR in pDONR P2R-P3) (Zeiser *et al.*, 2011; Dickinson *et al.*, 2013). The construction of strain JA1610 is described in Chen *et. al.,* 2014 (Chen *et al.*, 2014). LP431 (GFP::*gex-3*), LP574 (GFP::*rap-1*), LP572 (GFP::*nmy-2*) were made using the strategy described for LP362 (mNG::*gex-3*) in Dickinson *et. al.,* 2015. PCR genotyping was performed to confirm knock-ins.

***Predicted Brightness Calculation***

We calculated the predicted brightness of each fluorescent protein imaged with excitation and emission settings that match the settings we used for our comparisons. For each fluorescent protein at a given wavelength we quantified the fraction of the total emission peak covered by the emission filter and multiplied by the brightness at a given illumination wavelength. To determine the fraction of the total emission peak, we took the sum of the normalized emission values over the range of the emission filter used for imaging (the area under the emission peak within the shaded region, third column Figure 2.2) and divided by the sum of the total normalized emission values (the area under total emission peak, third column Figure 2.2). To determine the brightness at a given excitation wavelength (blue line, third column Figure 2.2) we took the product of the quantum yield (literature reported

value) and the extinction coefficient times the fraction of excitation peak at the imaging wavelength (Yang *et al.*, 1996; Shaner *et al.*, 2004; Nguyen and Daugherty, 2005; Shaner *et al.*, 2008; Shcherbo *et al.*, 2009; Lam *et al.*, 2012; Lee *et al.*, 2013; Shaner *et al.*, 2013).

### *Microscopy*

#### Imaging embryos

*C. elegans* embryos were dissected for imaging and mounted in egg buffer at the 2-3 cell stage on poly-L-lysine coated coverslips, with 2.5% agar pads. Embryos expressing different fluorescent proteins were initially imaged side-by-side, as shown in Figures 2 and 3 (n=3 pairs/groups per comparison). To increase the number of embryos imaged for quantification, multiple embryos from the same strain were mounted in groups and images were acquired using the same settings as the initial side-by-side comparisons. To minimize the effect of any unavoidable, minor, variation in imaging conditions, embryos from strains for a given comparison were imaged alternately using identical settings. HIS-58::GFP and mNG embryos were mounted at the three-cell stage, a short (~3min), identifiable stage between cell divisions. Fluorescence intensity was measured in the EMS cell nucleus. For the GFP and mNeonGreen endogenous knock-in strain comparisons, embryos from each strain plus an N2 wild-type embryo were imaged and compared in groups.

All embryos were imaged with a Nikon Eclipse Ti spinning disk confocal microscope (Yokogawa CSU-X1 spinning disk head) using a Hamamatsu ImagEM X2 EM-CCD camera (C9100-13) and a 60X/1.4 NA Plan Apo oil immersion objective (Nikon). Samples were illuminated using solid-state lasers of the following

wavelengths: 488nm, 514nm, and 561nm. The following emission filter sets were used for a given excitation wavelength: 488nm: ET525/50m (Chroma), 514nm: ET545/40m (Chroma), 561nm: ET630/75m (Chroma) and 561lp (Semrock).

**Imaging whole worms**

Whole worms were mounted at the L4 developmental stage and immobilized using nano-particles as previously described (Kim *et al.*, 2013). Worms were imaged using a Nikon Eclipse Ti spinning disk confocal microscope (Yokogawa CSU-X1 spinning disk head) using a Hamamatsu ImagEM X2 EM-CCD camera (C9100-13) and a 10X/0.30 NA Plan Fluor objective (Nikon) with 488nm excitation and ET525/50x emission filter.

***Image Quantification***

For membrane labeled strains, fluorescence intensity was quantified using Metamorph Software (Molecular Devices) by taking the average of a 3 pixel wide linescan perpendicular to the plasma membrane in the posterior-most embryonic cell (the $P_2$ cell). For each time point, the maximum intensity from this linescan was recorded and average off-embryo background was subtracted. GraphPad Prism software was used to plot the mean and 95% confidence intervals (CIs) for all initial brightness measurements, and at each time point for bleaching measurements. To determine the half-life of a given fluorescent protein, the individual photobleaching traces were fit to a standard one-phase decay curve, the 'half-life' for each curve was recorded, and the mean and 95% CIs were recorded for each fluorescent protein. The photon budget was determined by integrating the fluorescence intensity measured for each embryo until the intensity reached 50% of the initial intensity.

For histone fusion proteins and pharyngeal labeled strains, the images were thresholded and segmented using ImageJ to define a region for measurement (either the nucleus or pharynx). For GFP and mNeonGreen knock-in strains, a region was drawn around each embryo. The average fluorescence intensity of the given regions were calculated by measuring the average integrated intensity of the region and subtracting average off-embryo background for each image. Each embryo was displayed as an individual data point, and the mean and 95% CIs were plotted using GraphPad Prism software.

Unpaired, two-tailed t-tests with Welch's correction were used to compare means in all imaging experiments, and all statistical analyses were performed using GraphPad Prism software (GraphPad Software, Inc.). All comparisons are significantly different ($p<0.05$), unless otherwise indicated by 'ns'. Statistics for individual experiments can be found in Figure 2.4, B.

***Quantifying autofluorescence in C. elegans embryos***

We measured embryo autofluorescence in two separate experiments. For both, wild type (N2) embryos were mounted in egg buffer on poly-l-lysine coated coverslips, with 2.5% agar pads. In one experiment we used the same microscope, objective (60X), and camera described previously for imaging fluorescent embryos. We used a laser photodiode sensor (OPHIR Photonics #7Z02410 and filter #688657) to adjust the settings so that laser power for each wavelength was 1mW at the objective. We then imaged embryos under these conditions for each wavelength (445nm n=13, 488nm n=16 , 514nm n=16, 561nm n=14) with a common exposure time and the filter settings previously described. The emission filters used in this

experiment range in the breadth of wavelengths they transmit and will allow different amounts of light to pass through. In the second experiment, embryos were imaged using a Nikon A1R laser scanning confocal microscope. The excitation wavelengths used were 405nm, 442nm, 488nm, 515nm, and 561nm. The illumination settings for each wavelength were set to a common wattage in the Nikon elements software. Images of embryo autofluorescence were collected using a multispectral detector and emission fingerprinting for each of the given wavelengths.

For both experiments, image analysis was performed using ImageJ. Pixel intensity values were measured for three regions per embryo and averaged. Average off-embryo background was subtracted for each embryo, and the resulting fluorescence intensity was plotted at each detection wavelength. (In order to graph both experiments together, the results of the first experiment were scaled by multiplying the measured values (arbitrary units) by 500.) The X-axis value used for the first experiment was the center wavelength of the emission filter used for detection.

***Western blotting***

For quantifying protein levels, we picked L4 stage worms of each strain to three separate plates. After 12-14 hours at 25C, gravid young adults were collected from each plate. Three lysates were generated for each strain at a concentration of one worm per microliter (60 worms were picked into 45µl M9 Buffer and 15µl 4X Sample Buffer was added). Samples were frozen in liquid nitrogen and sonicated in boiling water for 10 minutes twice. Lysates were separated on 12% NuPAGE Novex Bis-Tris Protein Gels (Invitrogen) and transferred to an Immobilon PVDF-FL

membrane (Millipore) for immunoblotting. Fluorescent proteins expressed by transgenes were detected using a mouse anti-FLAG BioM2 (Sigma-Aldrich, catalog number F9291) antibody at 1:1000 dilution, and a rabbit anti-HCP-3 (Monen *et. al.,* 2005) was used at 1:1000 dilution as a loading control. The following fluorescent secondary antibodies were used (1µl per blot): AlexaFluor 680 goat anti-mouse and AlexaFluor 790 goat anti-rabbit (Invitrogen catalog numbers, A31562 and A11369, respectively). Three independent samples were collected and one blot from each biological replicate was performed. Blots were scanned using an Odyssey Infrared Imaging System (LI-COR Biosciences) and fluorescence intensity was quantified using ImageJ. A ratio of transgene protein intensity (~45kDa band in 680nm channel) to loading control intensity (~80KDa upper band in 790nm channel) was measured for each lane on a given blot. These measurements were normalized by dividing the ratio measured for each lane, by the total average ratio of all the lanes on a given blot. These normalized protein levels were plotted along with an average and 95%CIs using GraphPad Prism. Gel images were inverted and cropped slightly at the edges, and brightness and contrast were adjusted using ImageJ. Dashed line in Figure S1C indicates were blank lanes were cropped.

***Spectrum Viewer***

The fluorescence spectrum viewer was designed as a user-extensible collection of fluorescence spectra, dichroic filter spectra, and laser lines. Data were collected and digitized from a range of published fluorophore spectra using the WebPlotDigitizer software package (http://arohatgi.info/WebPlotDigitizer/). Digitized spectra were resampled at one nanometer wavelength increments and excitation

and emission spectra were each normalized to a maximum value of one relative fluorescent unit. Dichroic fluorescence filter data were similarly digitized from commercial plots. The spectrum viewer was implemented in Microsoft Excel using only worksheet range functions, avoiding the use of macro-language constructs. Up to four fluorophores, four fluorescent filters, and three laser lines may be selected and compared in an Excel chart through a simple graphical user interface. Possible spectral data listed in the user interface are populated from a “DataList” database worksheet, which in turn consists of spectrum names and accompanying worksheet ranges for stored spectral data. User selection of a spectrum to display populates a “Current” data worksheet via indirect references stored in the “DataList” database. The spectral chart is automatically updated to reflect changes in the “Current” data worksheet.

New fluorophore and fluorescent protein spectral data may be added to existing worksheets or as new worksheets. Indirect worksheet references must then be added to either the fluorophore or filter section of the “DataList” worksheet. The user interface is automatically repopulated with new choices. Simple, user-defined bandpass, shortpass, and longpass filter sets may also be defined on the “User Filters” worksheet for comparison to fluorophore spectra.

## 2.5 Chapter 2 Figures

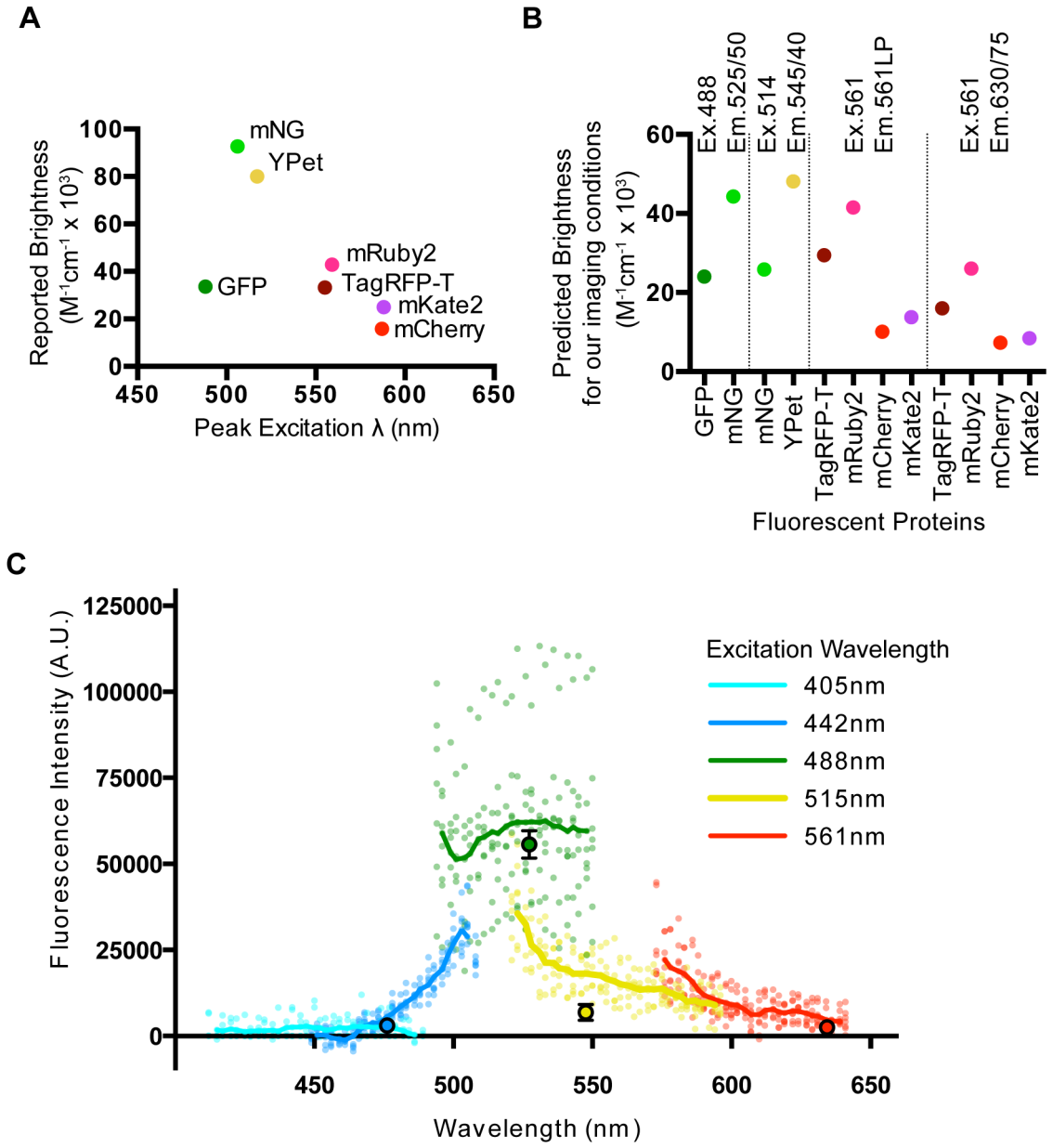


**Figure 2.1.** Predicted brightness of fluorescent proteins and embryo autofluorescence. A) Reported brightness for fluorescent proteins at peak excitation wavelengths. B) Predicted brightness of fluorescent protein comparisons performed in Figure 2. Excitation and emission wavelengths are at top. C) Embryo autofluorescence. Lines are averages of multiple embryos and small points are individual embryos acquired using a spectral detector. Large points represent spinning disk confocal autofluorescence data.

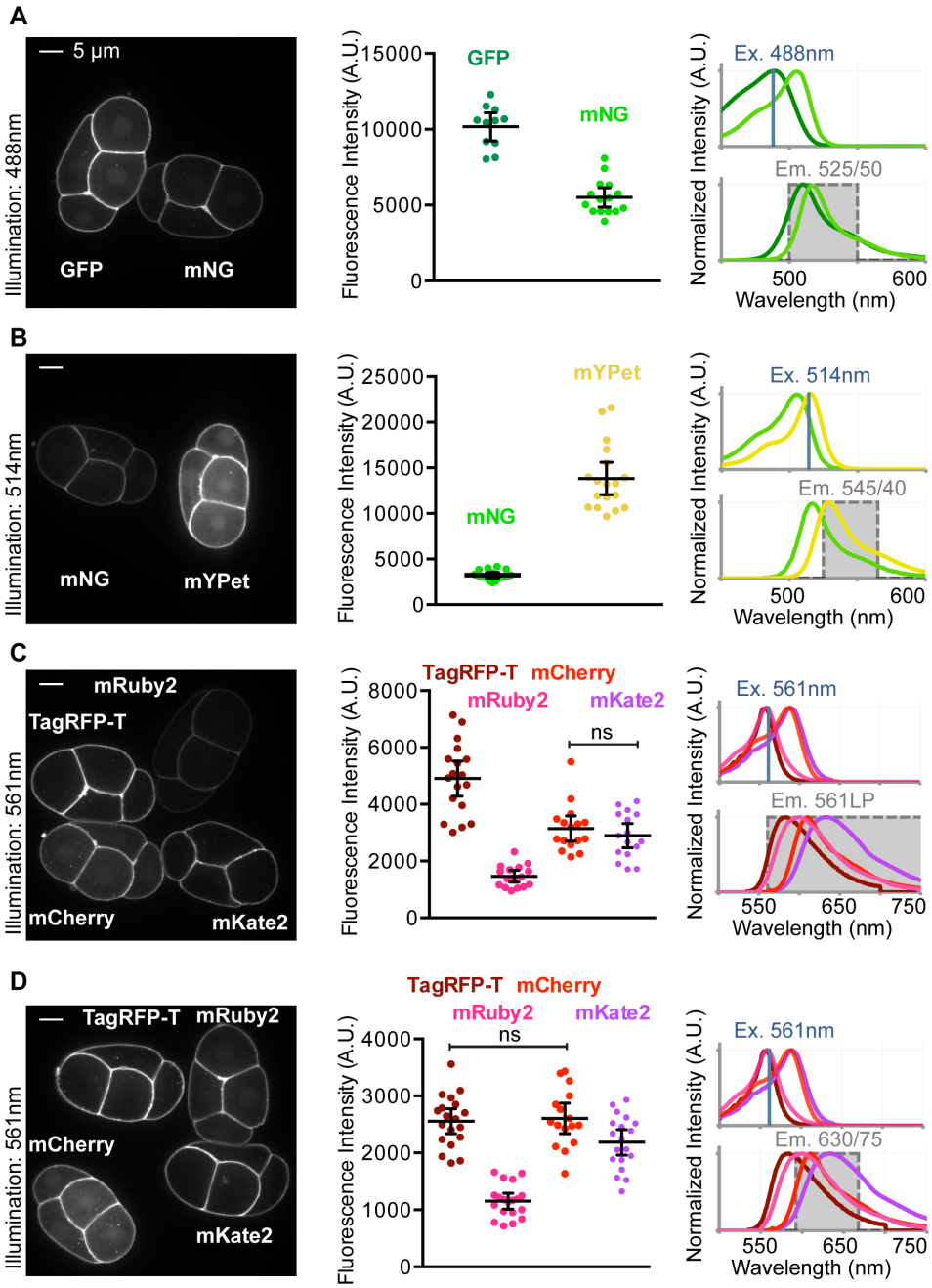


**Figure 2.2** *In vivo* fluorescent protein brightness. (A-D) Left column: Embryos mounted side-by-side and imaged under the same conditions used for quantification. Center column: Graphs show the quantification of each comparison. Each data point represents a single embryo. Black bars indicate the mean and 95% confidence intervals (CIs). Right column: Excitation (upper) and emission spectra (lower) of the compared fluorescent proteins. The illumination wavelength (Ex., blue line) and filter sets used for detection are indicated (Em., gray shading).

**A** ***C. elegans*** **strains used in this study**

| Strain Name | Genotype | Reference |
|---|---|---|
| N2 | wild type | |
| HT1593 | *unc-119(ed3)* III | Hochbaum *et. al.*, 2010 |
| LP306 | *cpIs53[Pmex-5::GFP-C1::PLCδ-PH::tbb-2 3'UTR + unc-119 (+)]* II; *unc-119(ed3)* III | This Study |
| LP274 | *cpIs45[Pmex-5::mNeonGreen::PLCδ-PH::tbb-2 3'UTR + unc-119(+)]* II; *unc-119(ed3)* III | This Study |
| LP402 | *cpIs64[Pmex-5::mYPet::PLCδ-PH::tbb-2 3'UTR + unc-119 (+)]* II; *unc-119(ed3)* III | This Study |
| LP193 | *cpIs56[Pmex-5::TagRFP-T::PLCδ-PH::tbb-2 3'UTR + unc-119 (+)]* II; *unc-119(ed3)* III | This Study |
| LP307 | *cpIs54[Pmex-5::mKate2::PLCδ-PH(A735T)::tbb-2 3'UTR + unc-119 (+)]* II; *unc-119(ed3)* III | This Study |
| LP308 | *cpIs55[Pmex-5::mCherry-C1::PLCδ-PH::tbb-2 3'UTR + unc-119 (+)]* II; *unc-119(ed3)* III | This Study |
| LP401 | *cpIs63[Pmex-5::mRuby2::PLCδ-PH::tbb-2 3'UTR + unc-119 (+)]* II; *unc-119(ed3)* III | This Study |
| LP403 | *cpIs65[Pmyo-2::GFP-C1::PLCδ-PH::tbb-2 3'UTR + unc-119 (+)]* II; *unc-119(ed3)* III | This Study |
| LP404 | *cpIs66[Pmyo-2::mNeonGreen::PLCδ-PH::tbb-2 3'UTR + unc-119 (+)]* II; *unc-119(ed3)* III | This Study |
| JA1610 | *weSi65[mtm-3 associated HOT core/his-58/GFP::tbb-2 3'UTR, unc-119(+)]* II; *unc-119(ed3)* III | Chen *et. al.*, 2014 |
| JA1699 | *weSi120[mtm-3 associated HOT core/his-58/mNeonGreen::tbb-2 3'UTR, unc-119(+)]* II; *unc-119(ed3)* III | This Study |
| LP362 | *gex-3(cp114[mNG^3xFlag::gex-3])* IV | Dickinson *et. al.*, 2015 |
| LP431 | *gex-3(cp114[GFP^3xFlag::gex-3])* IV | This Study |
| LP375 | *nmy-2(cp127[mNG-C1^3xFlag::nmy-2])* I | Dickinson *et. al.*, 2015 |
| LP572 | *nmy-2(cp278[GFP-C1^3xFlag::nmy-2])* I | This Study |
| LP395 | *rap-1(cp147[mNG-C1^3xFlag::rap-1])* IV | Dickinson *et. al.*, 2015 |
| LP574 | *rap-1(cp280[GFP-C1^3xFlag::rap-1])* IV | This Study |
| LP618 | *cpIs54[Pmex-5::mKate2::PLCδ-PH::tbb-2 3'UTR + unc-119 (+)]* II; *unc-119(ed3)* III | This Study |

**B PCR Genotyping confirming single-copy transgene knock-ins**

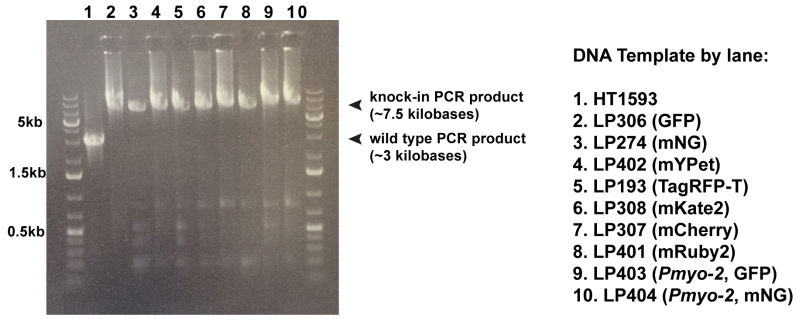


**C Fluorescent protein levels in sinlge-copy transgene knock-in strains**

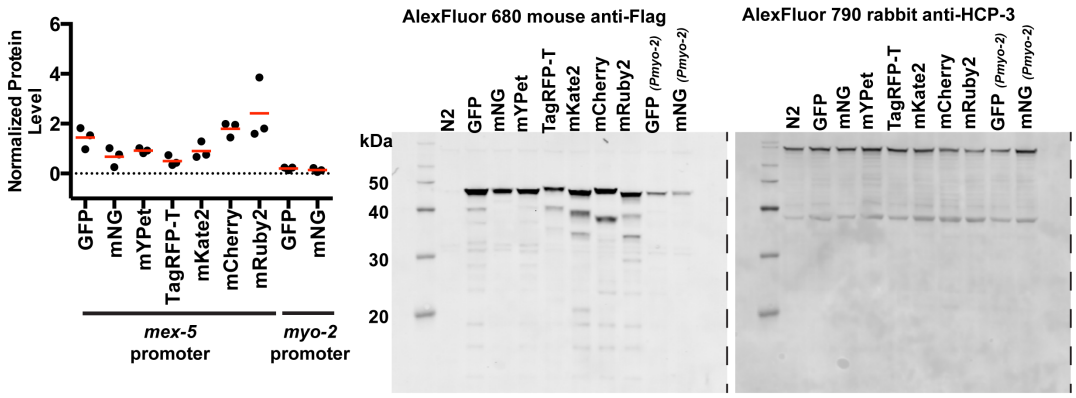


**Figure 2.3** A) *C. elegans strains* List of all the *C. elegans* strains used in this study. B) PCR genotyping confirming single-copy transgene knock-ins. PCR genotyping was performed using primers that flank the Cas9 target site on *C. elegans* chromosome II. The increased size (+4.5kb) of the PCR products in lanes 2-10 indicates a single-copy insertion. C) Fluorescent protein levels in single-copy transgene knock-ins. Lysates from worms expressing FP::PH::2XFlag driven by either the *mex-5* (embryos) or *myo-2* (pharynx) promoter were immunoblotted. Individual data points are normalized protein levels for each strain and black bars are a mean and 95% CIs.

**A Embryonic lethality observed in for single-copy knock-in strains at 25C**

| Strain Name | Total Counted (per plate) | Dead embryos | Percent dead embyos | Average percent dead embryos |
|---|---|---|---|---|
| **wild type** N2 | 311 | 6 | 1.9 | 0.9 |
| | 369 | 2 | 0.5 | |
| | 484 | 1 | 0.2 | |
| **LP306** GFP-C1::PLCδ-PH | 329 | 9 | 2.7 | 2.8 |
| | 294 | 8 | 2.7 | |
| | 105 | 3 | 2.9 | |
| **LP274** mNeonGreen::PLCδ-PH | 317 | 1 | 0.3 | 0.8 |
| | 369 | 3 | 0.8 | |
| | 341 | 4 | 1.2 | |
| **LP402** mYPet::PLCδ-PH | 233 | 10 | 4.3 | 4.7 |
| | 238 | 15 | 6.3 | |
| | 172 | 6 | 3.5 | |
| **LP193** TagRFP-T::PLCδ-PH | 334 | 15 | 4.5 | 3.9 |
| | 214 | 5 | 2.3 | |
| | 124 | 6 | 4.8 | |
| **LP307** mKate2::PLCδ-PH | 309 | 3 | 1 | 1.1 |
| | 499 | 11 | 2.2 | |
| | 126 | 0 | 0 | |
| **LP308** mCherry::PLCδ-PH | 140 | 6 | 4.3 | 3.4 |
| | 137 | 4 | 2.9 | |
| | 164 | 5 | 3 | |
| **LP401** mRuby2::PLCδ-PH | 172 | 8 | 4.7 | 2.6 |
| | 206 | 2 | 1 | |
| | 95 | 2 | 2.1 | |

**B Statistical analysis**

| **Figure** | **Strains Compared** | **Fluorescent Proteins** | **P-value** | **Significantly different? (p<0.05)** | **P-value** | **Significantly different? (p<0.05)** |
|---|---|---|---|---|---|---|
| 2A | LP306/LP274 | GFP vs. mNG | < 0.0001 | yes | | |
| 2B | LP274/LP402 | mNG vs. mYPet | < 0.0001 | yes | | |
| 2C | LP193/LP401 | TagRFP-T vs. mRuby2 | < 0.0001 | yes | | |
| 2C | LP193/LP308 | TagRFP-T vs. mCherry | < 0.0001 | yes | | |
| 2C | LP193/LP307 | TagRFP-T vs. mKate2 | < 0.0001 | yes | | |
| 2C | LP401/LP308 | mRuby2 vs. mCherry | < 0.0001 | yes | | |
| 2C | LP401/LP307 | mRuby2 vs. mKate2 | < 0.0001 | yes | | |
| 2C | LP308/LP307 | mCherry vs. mKate2 | 0.3908 | **ns** | | |
| 2D | LP193/LP401 | TagRFP-T vs. mRuby2 | < 0.0001 | yes | | |
| 2D | LP193/LP308 | TagRFP-T vs. mCherry | 0.7711 | **ns** | | |
| 2D | LP193/LP307 | TagRFP-T vs. mKate2 | 0.0174 | yes | | |
| 2D | LP401/LP308 | mRuby2 vs. mCherry | < 0.0001 | yes | | |
| 2D | LP401/LP307 | mRuby2 vs. mKate2 | < 0.0001 | yes | | |
| 2D | LP308/LP307 | mCherry vs. mKate2 | 0.0161 | yes | | |
| 3A | JA1610/JA1699 | GFP vs. mNG | 0.7799 | **ns** | | |
| 3B | LP403/LP404 | GFP vs. mNG | 0.2742 | **ns** | | |
| 3C | LP362/LP431 | GFP vs. mNG | 0.0012 | yes | | |
| 3D | LP395/LP574 | GFP vs. mNG | 0.116 | **ns** | | |
| 3E | LP375/LP572 | GFP vs. mNG | < 0.0001 | yes | | |
| | | | t 1/2 (seconds) | | Integrated intensity | |
| 4A | LP306/LP274 | GFP vs. mNG | 0.009 | yes | 0.0009 | yes |
| 4B | LP274/LP402 | mNG vs. mYPet | < 0.0001 | yes | 0.0001 | yes |
| 4C | LP193/LP401 | TagRFP-T vs. mRuby2 | < 0.0001 | yes | <0.0001 | yes |
| 4C | LP193/LP308 | TagRFP-T vs. mCherry | 0.1871 | **ns** | <0.0001 | yes |
| 4C | LP193/LP307 | TagRFP-T vs. mKate2 | < 0.0001 | yes | <0.0001 | yes |
| 4C | LP401/LP308 | mRuby2 vs. mCherry | < 0.0001 | yes | <0.0001 | yes |
| 4C | LP401/LP307 | mRuby2 vs. mKate2 | < 0.0001 | yes | <0.0001 | yes |
| 4C | LP308/LP307 | mCherry vs. mKate2 | 0.0043 | yes | 0.1016 | **ns** |

**Figure 2.4** A) Embryonic lethality B) Statistical analysis: Calculated P-values were judged as significantly different (p<0.05, yes) or not significantly different (p>0.05, ns). Non-significant results are labeled in the main text figures.

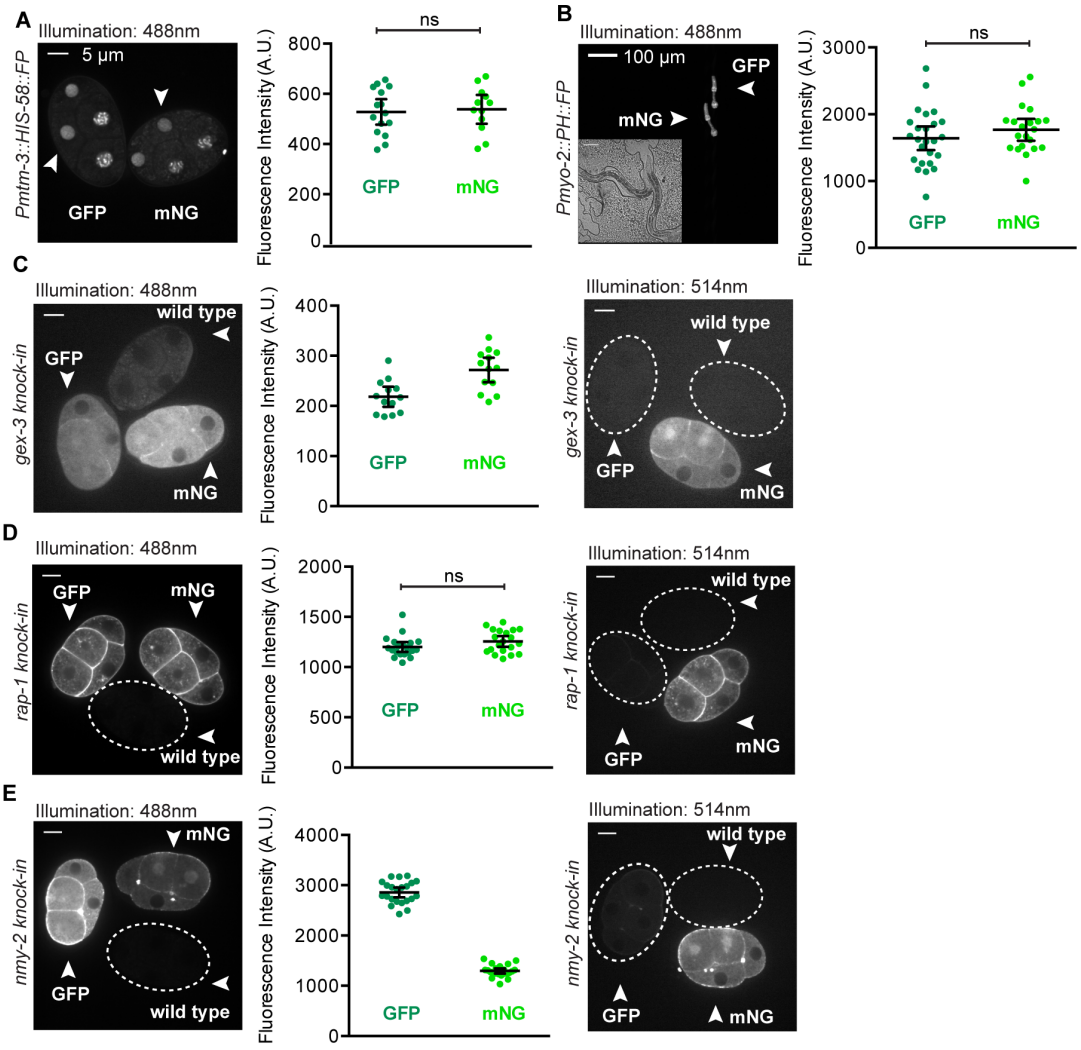


**Figure 2.5** Comparisons of GFP and mNeonGreen in single-copy transgenic strains and as knock-ins in endogenous genes. (A-C) Each data point represents a single embryo or animal, black bars represent the mean and 95% CIs. (A) Embryos expressing histone-fluorescent protein fusions. Fluorescence intensity of the EMS cell nucleus was measured (white arrowheads). (B) Young adult worms expressing membrane tag-fluorescent protein fusions in the pharynx (white arrowheads). The insert is a DIC image of the worms. (C) *gex-3* knock-in (D) *rap-1* knock-in (E) *nmy-2* knock-in and wild type embryos were imaged using 488nm illumination and 514nm illumination. Dotted lines outline embryos not visible under the given imaging conditions.

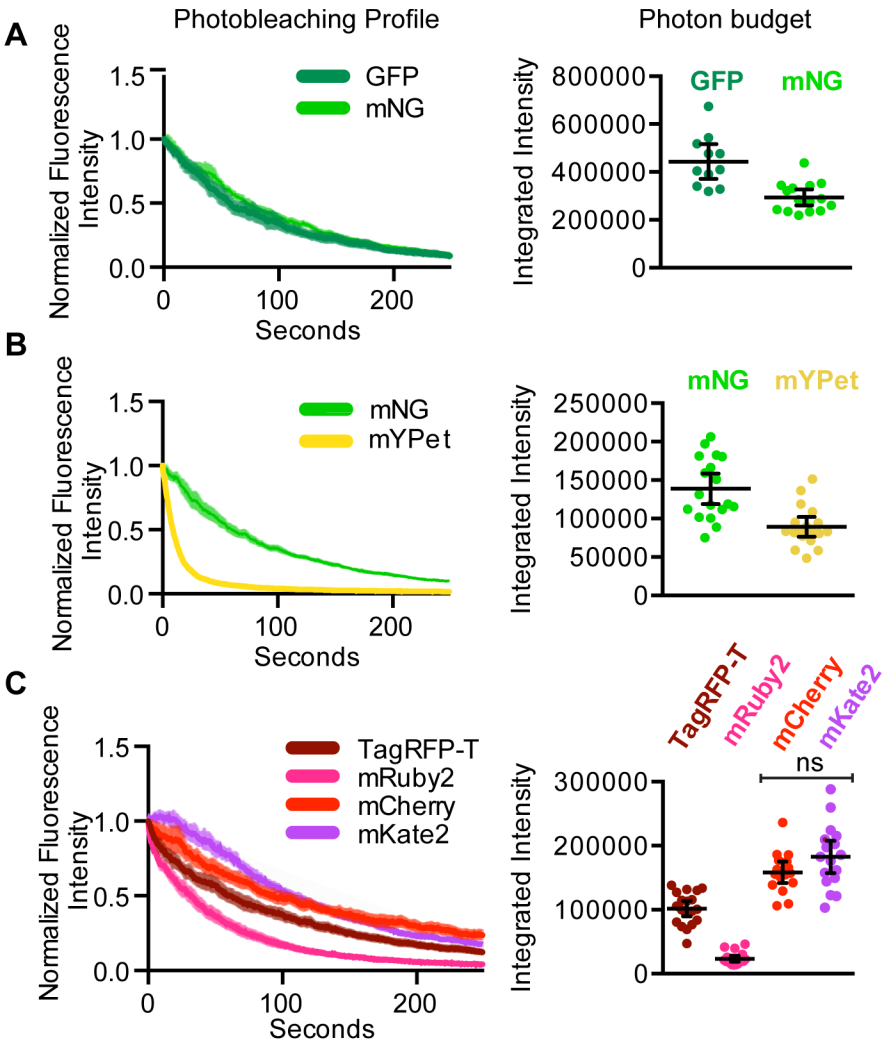


**Figure 2.6** *In vivo* fluorescent protein photostability. (A-C) Fluorescence intensity was measured in embryos over time. Photobleaching profile and photon budget were compared for membrane-associated fluorescent protein fusions. Each data point represents a single embryo, and the black bars represent the mean and 95% CIs.

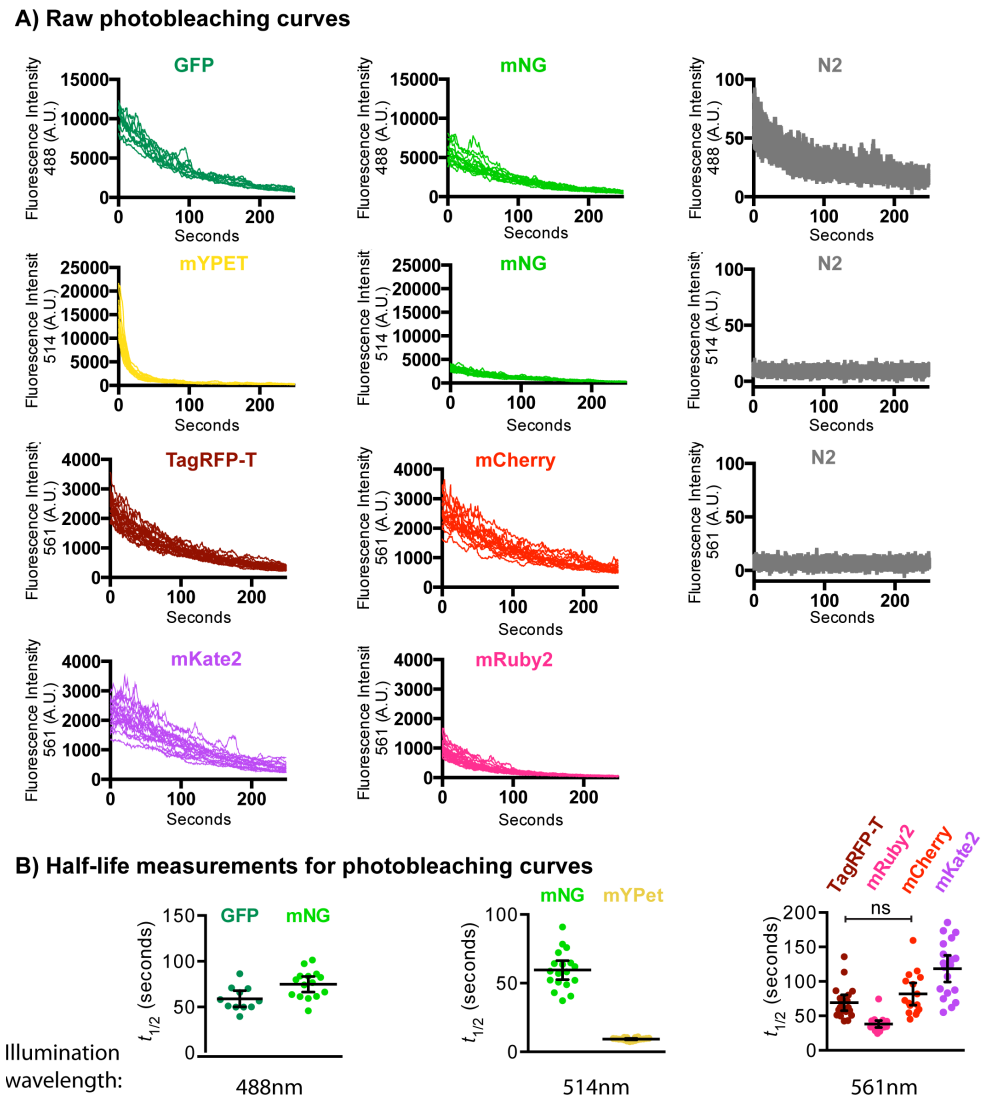


**Figure 2.7** A) Raw photobleaching curves B) Half-life measured from photobleaching curves**.** Half-life values measured from photobleaching curves in Figure 2.6A-C. C) Corrected mKate2::PH strain comparison

## REFERENCES


Aida, T., Chiyo, K., Usami, T., Ishikubo, H., Imahashi, R., Wada, Y., Tanaka, K. F., Sakuma, T., Yamamoto, T., and Tanaka, K. (2015). Cloning-free CRISPR/Cas system facilitates functional cassette knock-in in mice. Genome Biology 16, 87.

Audhya, A., Hyndman, F., McLeod, I. X., Maddox, A. S., Yates III, J. R., Desai, A., and Oegema, K. (2005). A complex containing the Sm protein CAR-1 and the RNA helicase CGH-1 is required for embryonic cytokinesis in Caenorhabditis elegans. The Journal of Cell Biology *171*, 267–279.

Auer, T. O., Duroure, K., De Cian, A., Concordet, J. P., and Del Bene, F. (2014). Highly efficient CRISPR/Cas9-mediated knock-in in zebrafish by homology-independent DNA repair. Genome Research *24*, 142–153.

Bassett, A. R., Tibbit, C., Ponting, C. P., and Liu, J. L. (2014). Mutagenesis and homologous recombination in Drosophila cell lines using CRISPR/Cas9. Biology Open *3*, 42–49.

Brenner, S. (1974). The Genetics of Caenorhabditis elegans. Genetics *77*, 71–94.

Chen, R. A. J., Stempor, P., Down, T. A., Zeiser, E., Feuer, S. K., and Ahringer, J. (2014). Extreme HOT regions are CpG-dense promoters in C. elegans and humans. Genome Research *24*, 1138–1146.

Corsi, A. K., Wightman, B., and Chalfie, M. (2015). A Transparent Window into Biology: A Primer on Caenorhabditis elegans. Genetics *200*, 387–407.

Davidson, M. W., and Campbell, R. E. (2009). Engineered fluorescent proteins: innovations and applications. Nature Methods *6*, 713–717.

Dickinson, D. J., Pani, A. M., Heppert, J. K., Higgins, C. D., and Goldstein, B. (2015). Streamlined Genome Engineering with a Self-Excising Drug Selection Cassette. Genetics *200*, 1035–1049.

Dickinson, D. J., Ward, J. D., Reiner, D. J., and Goldstein, B. (2013). Engineering the Caenorhabditis elegans genome using Cas9-triggered homologous recombination. Nature Methods *10*, 1028–1034.

Doudna, J. A., and Charpentier, E. (2014). The new frontier of genome engineering with CRISPR-Cas9. Science *346*, 1258096–1258096.

Doyon, J. B. *et al.* (2011). ncb2175. Nature Publishing Group *13*, 331–337.

Fire, A., Harrison, S. W., and Dixon, D. (1990) A modular set of lacZ fusion vectors for studying gene expression in Caenorhabditis elegans. Gene 93, 189-198

Frøkjær-Jensen, C., Wayne Davis, M., Hopkins, C. E., Newman, B. J., Thummel, J. M., Olesen, S.-P., Grunnet, M., and Jorgensen, E. M. (2008). Single-copy insertion of transgenes in Caenorhabditis elegans. Nat Genet *40*, 1375–1383.

Gilles, A. F., and Averof, M. (2014). Functional genetics for all: engineered nucleases, CRISPR and the gene editing revolution. EvoDevo *5*, 43.

Green, R. A., Audhya, A., Pozniakovsky, A., Dammermann, A., Pemble, H., Monen, J., Portier, N., Hyman, A. A., Desai, A., and Oegema, K. (2008). Expression and Imaging of Fluorescent Proteins in the C. elegans Gonad and Early Embryo. Methods in Cell Biology *85*, 179–218.

Harrison, M. M., Jenkins, B. V., O'Connor-Giles, K. M., and Wildonger, J. (2014). A CRISPR view of development. Genes & Development *28*, 1859–1872.

Hebisch, E., Knebel, J., Landsberg, J., Frey, E., and Leisner, M. (2013). High Variation of Fluorescence Protein Maturation Times in Closely Related Escherichia coli Strains. PLoS ONE *8*, e75991.

Heim, R., and Tsien, R. Y. (1996). Engineering green fluorescent protein for improved brightness, longer wavelengths and fluorescence resonance energy transfer. Current Biology *6*, 178–182.

Heppert J. K., Dickinson D. J., Pani A. M., Higgins C. D., Steward A., Ahringer J., Kuhn J. R., Goldstein B. (2016). Comparative assessment of fluorescent proteins for in vivo imaging in an animal model system. Molecular Biology of the Cell. *27*, 3385-3394.

Hochbaum, D., Ferguson, A. A., and Fisher, A. L. (2010). Generation of Transgenic C. elegans by Biolistic Transformation. JoVE.

Hsu, P. D., Lander, E. S., and Zhang, F. (2014). Development and Applications of CRISPR-Cas9 for Genome Engineering. Cell *157*, 1262–1278.

Huang, W.-Y., Aramburu, J., Douglas, P. S., and Izumo, S. (2000). Transgenic expression of green fluorescence protein can cause dilated cardiomyopathy. Nature Medicine *6*, 482–483.

Iizuka, R., Yamagishi-Shirasaki, M., and Funatsu, T. (2011). Kinetic study of de novo chromophore maturation of fluorescent proteins. Analytical Biochemistry *414*, 173–178.

Kim, E., Sun, L., Gabel, C. V., and Fang-Yen, C. (2013). Long-Term Imaging of Caenorhabditis elegans Using Nanoparticle-Mediated Immobilization. PLoS ONE *8*, e53419.

Krestel, H. E., Mihaljevic, A. L. A., Hoffman, D. A., and Schneider, A. (2004). Neuronal co-expression of EGFP and β-galactosidase in mice causes neuropathology and premature death. Neurobiology of Disease *17*, 310–318.

Lam, A. J. *et al.* (2012). Improving FRET dynamic range with bright green and red fluorescent proteins. Nature Methods *9*, 1005–1012.

Lee, S., Lim, W. A., and Thorn, K. S. (2013). Improved Blue, Green, and Red Fluorescent Protein Tagging Vectors for S. cerevisiae. PLoS ONE *8*, e67902.

Ma, Y., Ma, J., Zhang, X., Chen, W., Yu, L., Lu, Y., Bai, L., Shen, B., Huang, X., and Zhang, L. (2014). Generation of eGFPand Creknockin rats by CRISPR/Cas9. Febs J *281*, 3779–3790.

Matz, M. V., Fradkov, A. F., Labas, Y. A., Savitsky, A. P., Zaraisky, A. G., Markelov, M. L., and Lukyanov, S. (1999). Fluorescent proteins from nonbiouminescent Anthozoa species. Nature Biotechnology *17*, 969–973.

Monen, J., Maddox, P. S., Hyndman, F., Oegema, K., & Desai, A. (2005). Differential role of CENP-A in the segregation of holocentric C. elegans chromosomes during meiosis and mitosis. *Nat Cell Biol, 7*, 1248-55.

Nguyen, A. W., and Daugherty, P. S. (2005). Evolutionary optimization of fluorescent proteins for intracellular FRET. Nature Biotechnology *23*, 355–360.

Ohashi, T., Galiacy, S. D., Briscoe, G., and Erickson, H. P. (2007). An experimental study of GFP-based FRET, with application to intrinsically unstructured proteins. Protein Science *16*, 1429–1438.

Okkema, P. G., Harrison, S. W., Plunger, V., Aryana, A., and Fire, A. (1993). Sequence Requirements for Myosin Gene Expression adn Regulation in Ceanorhabditis elegans. Genetics *135*, 385–404.

Paix, A., Wang, Y., Smith, H. E., Lee, C.-Y., Calidas, D., Lu, T., Smith, J., Schmidt, H., Krause, M. W., and Seydoux, G. (2014). Scalable and Versatile Genome Editing Using Linear DNAs with Microhomology to Cas9 Sites in Caenorhabditis elegans. Genetics *198*, 1347–1356.

Peng, Y., Clark, K. J., Campbell, J. M., Panetta, M. R., Guo, Y., and Ekker, S. C. (2014). Making designer mutants in model organisms. Development *141*, 4042–4054.

Perry, K. J., and Henry, J. Q. (2015). CRISPR/Cas9-mediated genome modification in the mollusc, Crepidula fornicata. Genesis *53*, 237–244.

Ratz, M., Testa, I., Hell, S. W., and Jakobs, S. (2015). CRISPR/Cas9-mediated

endogenous protein tagging for RESOLFT super-resolution microscopy of living human cells. Sci. Rep. *5*, 9592.

Redemann, S., Schloissnig, S., Ernst, S., Pozniakowsky, A., Ayloo, S., Hyman, A. A., and Bringmann, H. (2011). Codon adaptation–based control of protein expression in C. elegans. Nature Methods *8*, 250–252.

Shaner, N. C. (2014). Fluorescent proteins for quantitative microscopy: Important properties and practical evaluation, Elsevier Inc.

Shaner, N. C. *et al.* (2013). A bright monomeric green fluorescent protein derived from Branchiostoma lanceolatum. Nature Methods *10*, 407–409.

Shaner, N. C., Campbell, R. E., Steinbach, P. A., Giepmans, B. N. G., Palmer, A. E., and Tsien, R. Y. (2004). Improved monomeric red, orange and yellow fluorescent proteins derived from Discosoma sp. red fluorescent protein. Nature Biotechnology *22*, 1567–1572.

Shaner, N. C., Lin, M. Z., McKeown, M. R., Steinbach, P. A., Hazelwood, K. L., Davidson, M. W., and Tsien, R. Y. (2008). Improving the photostability of bright monomeric orange and red fluorescent proteins. Nature Methods *5*, 545–551.

Shaner, N. C., Patterson, G. H., and Davidson, M. W. (2007). Advances in fluorescent protein technology. Journal of Cell Biology *120*, 4247–4260.

Shaner, N. C., Steinbach, P. A., and Tsien, R. Y. (2005). A guide to choosing fluorescent proteins. Nature Methods *2*, 905–909.

Shcherbo, D. *et al.* (2009). Far-red fluorescent tags for protein imaging in living tissues. Biochem. J. *418*, 567–574.

Shirayama, M., Seth, M., Lee, H.-C., Gu, W., Ishidate, T., Conte, D., Jr, and Mello, C. C. (2012). piRNAs Initiate an Epigenetic Memory of Nonself RNA in the *C. elegans* Germline. Cell *150*, 65–77.

Tsien, R. Y. (1998). The Green Fluorescent Protein. Annual Review of Biochemistry *67*, 509–544.

Wang, J. T., Smith, J., Chen, B.-C., Schmidt, H., Rasoloson, D., Paix, A., Lambrus, B. G., Calidas, D., Betzig, E., and Seydoux, G. (2014). Regulation of RNA granule dynamics by phosphorylation of serine-rich, intrinsically disordered proteins in C. elegans. Elife *3*.

Xue, Z., Ren, M., Wu, M., Dai, J., Rong, Y. S., and Guanjun, G. (2014). Efficient Gene Knock-out and Knock-in with Transgenic Cas9 in Drosophila. G3 *4*, 925–929.

Yang, T.-T., Cheng, L., and Kain, S. R. (1996). Optimized codon usage and

chromophore mutations provide enhanced sensitivity with the green fluorescent protein. Nuclaic Acids Research *24*, 4592–4593.

Zacharias, D. A., Violin, J. D., Newton, A. C., and Tsien, R. Y. (2002). Partitioning of Lipid-Modified Monomeric GFPs into Membrane Microdomains of Live Cells. Science *296*, 913–916.

Zeiser, E., Frøkjær-Jensen, C., Jorgensen, E., and Ahringer, J. (2011). MosSCI and Gateway Compatible Plasmid Toolkit for Constitutive and Inducible Expression of Transgenes in the C. elegans Germline. PLoS ONE *6*, e20082.

# CHAPTER 3: WNT SIGNALING POLARIZES APC AND DISHEVELLED, BUT NOT NUMA OR DYNEIN, DURING ASYMMETRIC CELL DIVISION IN EARLY *C. ELEGANS* EMBRYOS

## 3.1 Introduction

In both developing and established tissues, oriented cell divisions are essential for maintaining tissue architecture and generating cellular diversity (di Pietro *et al.*, 2016). Division orientation can be directed by extrinsic cues, and in some cases, those cues are signals from other cells (Gillies and Cabernard, 2011; Werts and Goldstein, 2011; Smith *et al.*, 2017). Evidence from a short, but growing list of systems gives some insight into how extracellular signaling directs mitotic spindle positioning (Le Grand *et al.*, 2009; Inaba *et al.*, 2010; Segalen *et al.*, 2010; Werts *et al.*, 2011; Yoshiura *et al.*, 2012; Habib *et al.*, 2013; Delaunay *et al.*, 2014; Xia *et al.*, 2015). Mis-regulation of cell division orientation is thought to contribute to diseases such as microcephaly and tumorigenesis (Pease and Tirnauer, 2011).

The position of the mitotic spindle within a dividing cell determines the plane or orientation of cell division (Rappaport, 1961). A conserved complex of proteins functions as a link between astral microtubule plus-ends and the cell cortex and plays an important role in positioning the mitotic spindle in many systems (reviewed (Kotak and Gönczy, 2013; Lu and Johnston, 2013)). This complex consists of the membrane-anchored protein Gαi (GOA-1 and GPA-16 in *C. elegans*), the GoLoco and TPR repeat domain containing protein LGN (GPR-1 and GPR-2 in *C. elegans*), and NuMA, (Nuclear Mitotic Apparatus protein, or LIN-5 in *C. elegans*), which is a

microtubule and microtubule-motor associated protein (Merdes *et al.*, 1996; Gotta and Ahringer, 2001; Couwenbergs *et al.*, 2007; Park and Rose, 2008; Yuzawa *et al.*, 2011). Through recruitment of the minus-end directed microtubule motor protein cytoplasmic dynein (the dynein heavy chain protein is DHC-1 in *C. elegans*), this complex generates pulling forces on astral microtubules to position the mitotic spindle within the cell (Grill *et al.*, 2003; Couwenbergs *et al.*, 2007; Nguyen-Ngoc *et al.*, 2007; Siller and Doe, 2008; Williams *et al.*, 2011). In response to both intrinsic and extrinsic polarity cues, members of this complex can be locally enriched to specific regions of the cell cortex in order to accurately, and sometimes asymmetrically, position the mitotic spindle (reviewed (di Pietro *et al.*, 2016)). In many known cases of oriented cell divisions, including *Drosophila* neuroblast cells and multiple mammalian epithelial tissues, LGN is the first member of this complex that is positioned asymmetrically (Siller *et al.*, 2006; Zheng *et al.*, 2010; Peyre *et al.*, 2011; Werts *et al.*, 2011; Williams *et al.*, 2011; Gloerich *et al.*, 2017). NuMA can also be cortically enriched to achieve mitotic spindle orientation, functioning in some contexts with diverse cortical adaptors, including Band 4.1 and Dishevelled, independent of LGN and Gαi (Segalen *et al.*, 2010; Kiyomitsu and Cheeseman, 2012; Seldin *et al.*, 2013). We would like to understand how proteins become enriched in discrete cortical domains to orient mitotic spindles.

In a few contexts, signaling between cells has been shown to regulate mitotic spindle positioning through the cortical enrichment of members of this complex (Bergstralh *et al.*, 2017). For example, in *Drosophila* sensory organ precursors, Planar Cell Polarity pathway members Frizzled and Dishevelled recruit NuMA to one

side of the precursor cell to orient the mitotic spindle in the along anterior-posterior axis (Segalen *et al.*, 2010). However, it is not clear whether this force-generating complex is a universal link between intercellular signaling pathways and the mitotic spindle, or whether there are alternative mechanisms by which intercellular signaling pathways can direct mitotic spindle positioning. In this work we set out to better understand mechanisms of mitotic spindle positioning directed by the Wnt signaling pathway in the early *C. elegans* embryo.

The early *C. elegans* embryo is an attractive model system for investigating mechanisms of mitotic spindle positioning by cell-cell interactions. The cell divisions in *C. elegans* embryos are highly stereotyped in both timing and orientation, and some oriented cell divisions are known to require cell-cell interactions (Goldstein, 1995b; Schlesinger *et al.*, 1999). At the four-cell stage, two neighboring cells, $P_2$ and EMS, use cell-cell signaling to orient their mitotic spindles toward their shared cell contact. In the germline precursor $P_2$ cell, signaling through the transmembrane receptor tyrosine kinase-like protein MES-1 serves as a spatial cue for LGN cortical enrichment within $P_2$ at the contact with EMS (Werts *et al.*, 2011). One pole of the $P_2$ spindle is pulled toward this domain of enriched LGN protein to position the spindle asymmetrically within the cell. However, in the neighboring EMS cell, LGN was not found to be enriched, suggesting that the mechanisms of signaling-induced oriented cell division may be different in EMS (Werts *et al.*, 2011).

When EMS divides, it gives rise to cells of the endodermal and mesodermal lineages. Contact with $P_2$ is required for endodermal fate specification and for EMS mitotic spindle orientation (Goldstein, 1992; 1993). Members of the highly conserved

Wnt signaling pathway and MES-1 are redundantly required for endodermal fate specification through β-catenin (WRM-1 and SYS-1 in *C. elegans*) dependent transcription of endodermal genes in the posterior daughter of EMS (Rocheleau and Priess, 1997; Thorpe *et al.*, 1997; Rocheleau *et al.*, 1999; Schlesinger *et al.*, 1999; Bei *et al.*, 2002; Liu *et al.*, 2008). Spindle orientation in EMS has been show to occur in the absence of new transcription, but also requires genes in Wnt and MES-1 signaling pathways (Schlesinger *et al.*, 1999, Bei *et al.,* 2002).

Experiments using isolated Wnt signaling cells and purified Wnt protein demonstrated that Wnts can act as extrinsic spatial cues to direct mitotic spindle positioning (Goldstein *et al.*, 2006; Habib *et al.*, 2013). $P_2$ signaling cells isolated from either Wnt (*mom-2* in *C. elegans*) mutant or *mes-1* mutant embryos and placed on naïve EMS cells revealed that neither signaling alone was sufficient for mitotic spindle positioning. But, if the two mutant signaling cells were placed on a single responding cell, the EMS spindle always rotated towards the *mes-1* mutant, Wnt signaling cell (Goldstein *et al.*, 2006). This experiment revealed that although MES-1 is required, its position does not matter. In contrast, a Wnt signaling cell can function as a positional cue for mitotic spindle positioning in this system. In a separate set of experiments, Habib et al. showed that a bead coated with purified Wnt3a can orient the cell divisions of isolated mouse embryonic stem cells (Habib *et al.*, 2013). How does the Wnt signaling pathway provide positional information to the rotating mitotic spindle? Does it require enrichment of conserved spindle orientation pathway proteins, or are there other proteins involved? If proteins are enriched asymmetrically, how does that enrichment occur? In this work we sought to address

these questions, and gain an increased mechanistic understanding Wnt signaling dependent mitotic spindle positioning.

Because of almost two decades of interest in this question, we have a sizable list of genes for which loss of function mutations, either alone, or in combination with the MES-1/Src pathway cause spindle orientation defects from genetic screens (Schlesinger *et al.*, 1999; Bei *et al.*, 2002; Tsou, 2003; Walston *et al.*, 2004; Zhang *et al.*, 2008; Liro and Rose, 2016). However, it is still not known which of these genes might encode proteins that provide positional information to the mitotic spindle; some proteins, for example proteins required for microtubule dynamics, may be required for the spindle to rotate, and may not have any involvement in serving as a positional cues. In fact, because we know that MES-1 acts as a permissive cue irrespective of its position on EMS, we might predict that its targets are among those proteins that are not likely serving as instructive cues, although they are required for the spindle to rotate. Our goal in this work was to identify proteins that provide positional information to the EMS mitotic spindle.

We hypothesized that proteins that serve as positional cues for spindle positioning would be cortically localized where they could respond to signaling inputs and contribute to force production on astral microtubules. We also hypothesized that they might be asymmetrically positioned along the ultimate axis of spindle positioning, the anterior-posterior axis of the embryo. Finally, we predicted these proteins would exhibit this asymmetric localization in the EMS cell during the period of spindle positioning. To test these hypotheses, we needed the ability to accurately visualize candidate proteins of interest over time, and the ability to make mosaic

embryos to determine which proteins were localized asymmetrically in EMS and not only nearby in neighboring cells. Although some tools such as antibodies and transgenic lines existed for some candidate proteins, they were not useful. Instead, we knock-ed in genes encoding fluorescent protein fusion tags into the endogenous genetic loci of proteins of interest, allowing us to confirm and extend previous observations and then to test our specific hypotheses (Dickinson *et al.*, 2013; Paix *et al.*, 2014; Dickinson *et al.*, 2015). We used these new strains to visualize the dynamic localizations of proteins of interest and to determine which are enriched at the EMS cortex specifically. Surprisingly, we found that members of the well-studied mitotic spindle positioning machinery NuMA and dynein were not asymmetric in EMS. However, members of the Wnt pathway, Dishevelled and APC, dynamically sorted to the anterior and posterior cortex of EMS respectively.

## 3.2 Results

### *Endogenous tags reveal localization and dynamics of candidate proteins at the four-cell stage*

To identify proteins that might act as positional cues for mitotic spindle orientation in EMS, we first generated a list of candidate proteins based on phenotypes in spindle rotation in EMS, microtubule-associated motor proteins, motor protein regulators, and signaling pathway members. To screen for candidates with cortical localization that might be asymmetrically localized during mitotic spindle rotation in EMS, we took advantage of new CRISPR-Cas9 mediated homologous recombination strategies to insert genes encoding fluorescent proteins at the endogenous loci encoding many of our candidate proteins (Figure 3.1) (Dickinson *et al.*, 2013; Paix *et al.*, 2014; Dickinson *et al.*, 2015).

Although tools such as antibodies and transgenes existed previously for some of our proteins of interest (Bei *et al.*, 2002; Srinivasan, 2003; Walston *et al.*, 2004; Gassmann *et al.*, 2008; Zhang *et al.*, 2008), we chose to insert tags into endogenous loci for two reasons. First, they allowed us to visualize protein localization and dynamics via live imaging throughout the cell cycle, and to directly compare protein dynamics in embryos under different treatment regimes. Second, endogenously tagged proteins are expressed at normal levels, using their native promoters and regulatory elements, and 100% of expressed protein is labeled (Dickinson *et al.*, 2013). This is critical as previous studies have revealed that overexpression of proteins involved in spindle orientation and signaling pathways can result in aberrant phenotypes (Werts *et al.*, 2011).

We isolated homozygous fluorescent protein knock-in strains for 23 of the 26 genes we targeted (Figure 3.1 and Figure 3.2). We observed significant embryonic lethality in the progeny of *klp-16* and *klp-18* candidate knock-ins and failed to isolate candidate knock-ins for *klp-3* for unknown reasons. Among the 23 genes tagged, we identified 14 genes with early embryonic protein products (Figure 3.2A). We expect the genes for which we did not detect protein products in the early embryo via fluorescence are either not expressed early in development, or are expressed too transiently or at such low levels as to be below our threshold of detection because in every case we could detect fluorescence if we looked at later stages (Figure 3.2B).

Cortical pulling forces often dominate mitotic spindle positioning, and eight of the protein products we observed appeared enriched at the cell cortex at the 4-cell stage (Figure 3.2 – top two rows). One of these proteins was cytoplasmic dynein

(DHC-1/Dynein heavy chain), and three were dynein-associated proteins, DNC-1/Dynactin p150, LIS-1/Lis1, and LIN-5/NuMA (Figure 3.2 – top row). The other four proteins were members of the Wnt signaling pathway known to regulate the EMS mitotic spindle (Figure 3.2 – second row) (Schlesinger *et al.*, 1999; Bei *et al.*, 2002; Sugioka *et al.*, 2011). The overall localization patterns of our endogenous tags matched previously reported localization patterns based on antibody staining and non-endogenously tagged transgenes (Srinivasan, 2003; Walston *et al.*, 2004; Zhang *et al.*, 2008; Sugioka *et al.*, 2011). We observed wild type development in our imaging experiments and measured no significant embryonic lethality, suggesting that the fusion proteins retained their function (Figure 3.9A).

We next imaged the 11 fusion proteins that were not detectable at the four-cell stage at later stages during development (Figure 3.2B). We found them to be expressed in a variety of tissue type at different developmental stages. Many of these expression patterns were consistent for known role of these proteins. For example, CAM-1 a Ror, receptor tyrosine kinase homolog, localized to the plasma membrane (Figure 3.2B – top row, second panel) (Green *et al.*, 2007). Interestingly, though KLP-17, has been shown to cause embryonic lethality at the one- and two-cell stage, we detected the KLP-17::mNG only in the sperm (Figure 3.2B – top row, far right) (Ali and Siddiqui, 2000). One advantage of our screening approach is the resulting collection of tagged strains (Figure 3.2). The tagged versions of these proteins are controlled by their endogenous regulatory elements, and therefore, should be expressed at each stage at which the endogenous functions. Although in

this work we are most interested in the four-cell stage, these strains can be used to study they dynamic properties of these proteins are other stages.

### *Live imaging of LIN-5 and DHC-1 reveals the dynamics of enrichment at the $P_2$:EMS contact*

To gain insight into the role these candidate proteins play in mitotic spindle positioning, we examined the localization of our mNeonGreen tagged fusion proteins throughout the EMS cell cycle using spinning disk confocal microscopy (Figure 3.3). Proteins that function as positional cues for mitotic spindle positioning often occupy a specific domain of the cell cortex towards which spindle poles are pulled (Lechler and Fuchs, 2005; Siller *et al.*, 2006; Zheng *et al.*, 2010; Peyre *et al.*, 2011; Werts *et al.*, 2011; Williams *et al.*, 2011; Gloerich *et al.*, 2017). Because we knew that a $P_2$ Wnt-signaling cell functions as a positional cue for EMS mitotic spindle positioning (Goldstein, 1995b), we hypothesized that force-generating complexes might be enriched in EMS where it contacts $P_2$. Therefore, to test whether our tagged proteins were enriched at the $P_2$:EMS contact, we compared the normalized mean fluorescence intensity at the $P_2$:EMS contact to the intensity at an EMS:AB cell contact during spindle rotation in EMS (Figure 3.3 B-E, 260 seconds prior to EMS cytokinesis during EMS spindle rotation).

Using this method, we first examined the localization of NuMA/LIN-5::mNG. NuMA, together with Gα and LGN, form a conserved protein complex that tethers the minus-end motor protein dynein to the cell cortex to regulate mitotic spindle positioning (Reviewed - Kotak and Gönczy, 2013). Previous experiments using a temperature sensitive allele of *lin-5* demonstrated that NuMA/LIN-5 function is required for proper spindle positioning in EMS (Liro and Rose, 2016). Consistent

with previous antibody staining for NuMA/LIN-5, NuMA/LIN-5::mNG was localized at cell contacts, centrosomes and decorated spindle microtubules in metaphase and anaphase ((Srinivasan, 2003), Figure 3.3B). NuMA/LIN-5::mNG was enriched at the $P_2$:EMS cell contact relative to an EMS:AB contact during EMS spindle rotation (Figure 3.3B). This enrichment continues during EMS spindle rotation and peaks after rotation is complete (Figure 3.3G).

We next examined cytoplasmic dynein heavy chain, DHC-1, the major subunit of the minus-end directed motor protein. Regulators of dynein, including the dynactin subunit, p150$^{glued}$/*dnc-1*, have been shown to be required for EMS spindle rotation (Zhang *et al.*, 2008). We observed that DHC-1::mNG is diffuse in the cytoplasm, decorates structures that look like microtubules and centrosomes, and is strongly enriched at the nuclear envelope and at kinetochores during metaphase (Figure 3.3C). These results are consistent with previous observations of DHC-1 immunohistochemistry and transgenic fluorescent protein fusions (Gonczy *et al.*, 1999; Malone *et al.*, 2003; Schmidt *et al.*, 2005; Gassmann *et al.*, 2008). Dynein/DHC-1::mNG was also enriched at the $P_2$:EMS cell contact during EMS spindle rotation (Figure 3.3C). Similar to LIN-5::mNG, this enrichment continued throughout EMS spindle rotation and peaked almost a minute after rotation was complete. Two regulators of dynein, DNC-1::mNG and LIS-1::mNG, also had some cortical localization at the four cell stage, consistent with previous reports (Cockell, 2004; Zhang *et al.*, 2008). However, we did not detect a significant difference in fluorescence intensity at the $P_2$:EMS cell contact versus the EMS:AB cell contact for either DNC-1::mNG or LIS-1::mNG (Figure 3.3 D and E). Taken together, these

results suggest that accumulation of an LIN-5, DHC-1 or both at the EMS cortex may be important for signaling-induced mitotic spindle positioning.

### *LIN-5/NuMA is enriched in $P_2$ and not asymmetric in EMS during spindle rotation*

It was previously shown via immunostaining that NuMA/LIN-5 enrichment at the $P_2$:EMS contact was not affected by loss of the wnt receptor *mom-5,* but was reduced in *mes-1* mutants (Srinivasan, 2003). We targeted the Wnt ligand *mom-2* by dsRNA injection, and confirmed that did not reduce the level of NuMA/LIN-5::mNG enrichment at the $P_2$:EMS cell contact (Figure 3.4A). We also confirmed that targeting of *mes-1* significantly reduced NuMA/LIN-5::mNG accumulation at the $P_2$:EMS contact (Figure 3.4B). These data are consistent with a previous report that LIN-5 enrichment at the $P_2$:EMS contact requires MES-1 signaling, but not Wnt signaling ((Srinivasan *et al.*, 2003) and Figure 3.4A and B).

We next sought to understand whether the source of the LIN-5::mNG protein enrichment at the $P_2$:EMS contact was contributed by $P_2$, EMS, or both cells. Signaling through MES-1 regulates spindle positioning in the $P_2$ cell through the enrichment of the NuMA binding partner LGN/GPR-1 at the $P_2$:EMS contact in the $P_2$ cell (Werts *et al.*, 2011). NuMA/LIN-5::mNG enrichment might follow this exact pattern, and become enriched only in $P_2$ and not EMS. Although most commonly associated with LGN/Gα, NuMA can also use other cortical adaptor proteins, and has been shown to direct mitotic spindle positioning through association with the Wnt pathway protein Dishevelled in *Drosophila* sensory organ precursor cells (Segalen *et al.*, 2010; Kiyomitsu and Cheeseman, 2013). This raises the possibility that NuMA/LIN-5 could be enriched in EMS by association with a cortical adaptor

other than LGN/GPR-1. To test whether NuMA is enriched in $P_2$, EMS or both cells, we made mosaic embryos by hand, placing NuMA/LIN-5::mNG $P_2$:EMS cell pairs and unlabeled $P_2$:EMS cell pairs in contact to create two new $P_2$:EMS contact sites (Figure 3.4C). This arrangement allows both $P_2$ and EMS enrichments to be compared in single experiments. We measured the fluorescence intensity at the labeled-unlabeled cell contacts during EMS spindle rotation, and we found an enrichment of protein in the $P_2$ cell, but not in the EMS cell (Figure 3.4C).

To rule out the possibility that an additional signaling cell contact might obscure detection of protein enrichment in EMS, we recombined labeled and unlabeled single cells and measured the maximum fluorescence intensity at the contacts. The results confirmed that there is a significant accumulation of LIN-5::mNG at the $P_2$:EMS contact in $P_2$, but not in EMS (Figure 3.4D). To determine whether the level of LIN-5::mNG enrichment in EMS is above that expected from a non-signaling cell, we placed a labeled LIN-5::mNG EMS cell in contact with a non-Wnt signaling, unlabeled AB cell (Figure 3.4D). We did not see a significant difference in the amount of LIN-5::mNG at the EMS cortex, whether EMS was in contact with a Wnt-signaling $P_2$ cell, or a non-signaling AB cell (Figure 3.4D). These results suggest that LIN-5::mNG is enriched at the $P_2$ cell cortex and not enriched in EMS. Because LIN-5::mNG not enriched at the EMS cortex during spindle rotation, LIN-5::mNG is unlikely to act as an asymmetrically-localized cue for mitotic spindle positioning in EMS.

### *DHC-1::mNG remains enriched at the $P_2$:EMS cell contact when mom-2/Wnt is depleted and is not enriched in EMS*

The dynein regulators we have examined to this point are not asymmetrically localized in EMS (Figure 3.3 and 3.4). However, it is possible that other unknown cortical adapters tether dynein at the $P_2$:EMS contact in response to Wnt signaling. Therefore, we next sought to test whether the enrichment of dynein/DHC-1::mNG we observed at the $P_2$:EMS cell contact was Wnt signaling dependent (Figure 3.3C). Targeting the Wnt signal *mom-2* by RNAi resulted in a slight change in the timing of enrichment, but no change in the maximum enrichment of DHC-1::mNG at the $P_2$:EMS contact (Figure 3.5A), suggesting that Wnt signaling is not required for DHC-1::mNG to accumulate at the $P_2$:EMS contact. Next, to test whether DHC-1::mNG is asymmetrically enriched within EMS, we recombined unlabeled $P_2$ cells with DHC-1::mNG-expressing EMS cells (Figure 3.5B). We did not see an enrichment of DHC-1::mNG at the $P_2$:EMS contact relative to a non-cell contacting region of the EMS cortex (Figure 3.5B). In fact the DHC-1::mNG signal appeared slightly reduced at the $P_2$:EMS contact compared to a non-contacting region of the cell. Because dynein/DHC-1::mNG is not enriched in EMS, these results suggest that dynein/DHC-1::mNG is unlikely to act as an asymmetrically localized cue for spindle positioning in EMS.

Taken together, our results for NuMA/LIN-5::mNG and dynein/DHC-1::mNG suggest that although members of the Gα/LGN/NuMA and dynein complex are functionally required for spindle rotation in EMS, they are not enriched in EMS cell cortex during spindle rotation (Figure 3.4 and 3.5) (Tsou, 2003; Zhang *et al.*, 2008; Liro and Rose, 2016). We conclude that this complex does not function to locally

recruit force-generating, DHC-1 containing complexes at the EMS cortex as happens in many other cases of oriented cell division. LGN/GPR-1 and NuMA/LIN-5 are instead asymmetrically enriched at the cortex of $P_2$ in response to MES-1 signaling, and likely function to locally tether dynein/DHC-1 to achieve spindle positioning in $P_2$.

### *Localization of endogenously tagged Wnt pathway components reveals timing of EMS polarization*

In our initial screen, we identified four additional candidate proteins as having some cortical localization at the four cell stage: Frizzled/MOM-5::YPET, Dishevelled/mNG::DSH-2, Dishevelled/mNG::MIG-5, and APC/mNG::APR-1 (Figure 4.2A – row2). Previous studies have demonstrated that *mom-5, dsh-2,* and *mig-5* loss of function or depletion results in defects in EMS spindle positioning, and that APR-1 contributes to astral microtubule asymmetry by stabilizing microtubules in the anterior of EMS (Walston 2004, Sugioka2011). To determine whether these proteins might be acting as asymmetrically localized cues for EMS spindle positioning, we examined the dynamics of their localization during the EMS cell cycle (Figure 3.6).

To our knowledge, the localization of the Wnt receptor Frizzled/MOM-5 was previously unknown at the *C. elegans* four cell stage. We found Frizzled/MOM-5::YPET to be distributed at the plasma membrane of all four cells, and most enriched at cell-cell contacts (Figure 3.6A). Additionally, MOM-5::YPET labeled a significant pool of dynamically moving internal cell membranes, including the internalizing midbody in the anterior of the EMS cell (Figure 3.6A, arrow, ref midbody). We did not detect statically significant enrichment at the $P_2$:EMS contact over EMS:AB cell contacts during spindle rotation (Figure 3.6A).

Dishevelled is a component of the Wnt signaling pathway that binds the intercellular domain of Frizzled when Frizzled is activated by a Wnt ligand (Wong *et al.*, 2003). It was previously reported, via antibody staining, that Dishevelled/DSH-2 is enriched at the $P_2$:EMS contact, and that its cortical localization is dependent on *frizzled/mom-5* (Walston *et al.*, 2004; Hawkins, 2005). Our observations of mNG::DSH-2 are consistent with the previously reported cortical localization and enrichment at the $P_2$:EMS contact (Figure 3.6B). We do not see a significant difference in intensity between the $P_2$:EMS and EMS:AB contacts during mitotic spindle rotation. However, the level of mNG::DSH-2 continues to rise and peak ~120 seconds before EMS cytokinesis (Figure 3.6E). Another tagged Dishevelled homolog, mNG::MIG-5 was more pronounced at all cell contacts than mNG::DSH-2 (Figure 3.6C). mNG::MIG-5 was enriched at the $P_2$:EMS contact during EMS spindle rotation (Figure 3.6C). Taken together these results suggest that the two major Dishevelleds implicated in spindle rotation in EMS, are polarized to the posterior cortex of EMS.

Adenomatus polyposis coli, or APC, is a key component of the β-catenin destruction complex. APC/APR-1 has been previously shown to be enriched in the anterior of EMS, and to regulate mitotic spindle asymmetry and microtubule stability (Sugioka *et al.*, 2011). The implications of this localization were principally shown to affect the distribution of fate determinants in the EMS daughter cells, and the possible contribution of APR-1/APC to mitotic spindle rotation remains unknown. We examined APC/mNG::APR-1 localization throughout the EMS cell cycle and found that APC is enriched in the anterior of EMS and largely excluded from the $P_2$:EMS cell contact (Figure 3.6D). This asymmetry is apparent earlier (before 480 seconds

prior to EMS division) than other asymmetry we have observed so far, and is consistent with previous reports of APC/APR-1 localization (Sugioka *et al.*, 2011). From these experiments we conclude that Dishevelled and APC are asymmetrically localized on opposite sides of the EMS cell during spindle positioning.

***mom-2/Wnt is a necessary spatial cue for polarization of APR-1 and DSH-2***

We noticed that in the latter half of the EMS cell cycle, Dishevelled and APC appear to be occupying distinct cortical domains in the EMS cortex. Because these proteins are downstream members of the Wnt pathway, we hypothesized that robust Wnt signaling would be important for these polarized localization patterns. To test this hypothesis, we injected RNAi targeting the Wnt ligand *mom-2*. For each experiment, we determined that 100% of the *mom-2* RNAi treated embryos failed to hatch, consistent with the maternal effect embryonic lethal phenotype of *mom-2* null mutants (Thorpe *et al.*, 1997). We found that mNG::DSH-2 fails to become enriched at the $P_2$:EMS contact in *mom-2* RNAi treated embryos (Figure 3.7A). When we compared control and *mom-2* RNAi treated embryos for APC/mNG::APR-1, we observed that APC/mNG::APR-1 was no longer restricted to the anterior of EMS (Figure 3.7B). We observed that APC/mNG::APR-1 cortical domain expanded to the $P_2$:EMS contact, although we did not find a statistical difference in levels between control and *mom-2* RNAi embryos at the time of EMS spindle rotation (Figure 3.7B). These results suggest that Wnt-dependent recruitment of Dishevelled at the $P_2$:EMS contact may function to exclude APC from the posterior cortex of EMS.

To investigate the dynamics of these proteins simultaneously in the same embryos, we generated a dual labeled strain with both Dishevelled/mNG::DSH-2

and APC/mScarlet::APR-1. We observed that the two proteins' localization patterns begin to polarize during spindle rotation (~240 seconds), and remain in distinct cortical domains through EMS division (Figure 3.7C). In these embryos (n=5) we noticed APC/APR-1 enriched in the anterior of EMS prior to Dishevelled/mNG::DSH-2 enrichment in the posterior (Figure 3.7C). To observe polarization within the EMS cell, we recombined unlabeled $P_2$ signaling cells and labeled EMS cells. Similar to our experiments in embryos, we observed that mScarlet::APR-1 was enriched on the anterior cortex of EMS and that mNG::DSH-2 became enriched at the $P_2$:EMS contact (Figure 3.7D). In both cases we observed polarization of APC/APR-1 prior to DSH-2 enrichment. This could be because mNG::APR-1 becomes is excluded from the $P_2$:EMS contact before DSH-2 arrives, or because the initial recruitment of DSH-2 is too dim to detect.

***Dishevelled is required for APR-1/APC polarization***

How do these proteins become polarized to different domains at the cell cortex? We next sought to test whether Dishevelled and APC affect one another's localization in EMS. We first examined the localization of Dishevelled/mNG::DSH-2 when we targeted APC/APR-1, and found no change in the fluorescence intensity of Dishevelled/mNG::DSH-2 (Figure 3.8A). However, when we targeted the two major Dishevelled proteins involved in EMS spindle rotation, DSH-2 and MIG-5, the cortical domain of APC/mNG::APR-1 expanded, and we detected APC/mNG::APR-1 at the $P_2$:EMS contact where it is normally excluded (Figure 8B). This confirms that Dishevelleds are important for native APR-1 (when tagged) to become localized to the anterior of EMS, consistent with results seen previously with a tagged transgene

expressed at undetermined levels alongside wild type protein (Sugioka *et al.*, 2011). These results suggest that robust cortical Dishevelled is important for excluding APC/mNG::APR-1 from a domain of the posterior cortex of EMS, but that Dishevelled occupies a polarized cortical domain at the $P_2$:EMS even when APC is reduced.

### 3.3 Discussion

Cell-cell signaling results in oriented cell divisions both during development and for populations of cells that continue to divide in adult tissues, such as stem cells. However, our mechanistic knowledge of this process is limited to a handful of systems (Inaba *et al.*, 2010; Segalen *et al.*, 2010; Werts *et al.*, 2011; Werts and Goldstein, 2011). Here, we explored how Wnt signaling orients the mitotic spindle using the well-characterized EMS cell division of early *C. elegans* embryo. Using novel fluorescent protein fusions that we generated via Cas9-triggered homologous recombination, we screened for cortically localized proteins and imaged the dynamics of those eight proteins throughout the EMS cell cycle (Figure 3.3 and Figure 3.6). Although NuMA and dynein were enriched at the $P_2$:EMS contact in intact embryos, surprisingly, we found that neither protein was enriched in the EMS cell (Figure 3.4C and D, Figure 3.5B). We found instead that NuMA is enriched in $P_2$ at the contact with EMS (Figure 3.4C and D), similar to LGN, which functions as an upstream binding partner of NuMA in many systems (Werts *et al.*, 2011). We speculate that NuMA is enriched at the $P_2$ cortex and functions in $P_2$ spindle orientation downstream of MES-1 and LGN. We analyzed other candidate proteins in the Wnt pathway for potential asymmetry during spindle rotation and found that

Dishevelled and APC were enriched in the posterior and anterior of EMS respectively (Figure 3.7). The asymmetric localization of these cortical cues was dependent on *mom-2*/Wnt signaling, and targeting of Dishevelled by RNAi resulted in ectopic APC localization at the $P_2$:EMS contact (Figure 3.8). These results suggest that if asymmetric protein localization is important for mitotic spindle positioning in EMS, NuMA and Dynein do not play this role, but instead components of the Wnt signaling pathway, Dishevelled and APC might serve as asymmetric cortical cues.

***Creating fluorescent protein fusions***

We took an unusual approach to test our hypothesis that Wnt signaling directs mitotic spindle positioning by locally recruiting force-generating complexes to the EMS cortex. A "parts-list" existed of gene products required for spindle rotation in EMS from genetic experiments (Schlesinger *et al.*, 1999; Bei *et al.*, 2002; Tsou, 2003; Walston *et al.*, 2004; Zhang *et al.*, 2008; Liro and Rose, 2016), but tagged versions of these proteins were needed to follow live protein dynamics and determine which are asymmetrically localized in the EMS cell. Therefore, we decided to develop the tools to address this problem using CRISPR-Cas9 triggered homologous recombination to insert genes encoding fluorescent proteins at the endogenous genetic loci of many of our genes of interest. Although the labor involved in making these tagged strains prevented us from taking an exhaustive, non-biased approach, the approach resulted in a number of valuable strains to investigate our hypotheses (Figure 3.2). Our data eliminate specific hypotheses that we had previously considered likely; such as NuMA being asymmetrically localized

in EMS by Dishevelled, as is the case in *Drosophila* sensory organ precursor oriented cell division (Segalen *et al.*, 2010).

***Asymmetric localization vs. asymmetric activation***

The majority of cases of oriented cell division that have been well characterized involve the asymmetric localization of proteins to a specific site at the cell cortex towards which the mitotic spindle is pulled (Kotak and Gönczy, 2013; di Pietro *et al.*, 2016; Bergstralh *et al.*, 2017). These asymmetric protein complexes typically contain LGN and/or NuMA, and are thought to generate force on mitotic spindles through recruitment of the dynein motor protein and its interaction with astral microtubules. Together with previous studies, our results suggest that this is not the mechanism of mitotic spindle positioning in EMS (Werts *et al.*, 2011, Figure 3.4 and 3.5). However, it is possible that members of these canonical complexes are not asymmetrically localized, but instead are asymmetrically activated to generate localized pulling forces. In fact, recent studies in the one-cell stage *C. elegans* embryo suggest that phosphorylation of NuMA is important for its ability to bind dynein and induce asymmetric spindle positioning (Portegijs *et al.*, 2016). However, these sites of phospho-regulation did not appear to impact NuMA's function in EMS spindle positioning (Portegijs *et al.*, 2016). This suggests either a different mechanism for NuMA activation is important in EMS, or that spindle positioning in EMS does not require differential activation of NuMA. The idea that dynein or one of its regulators might be locally activated is, unfortunately, a difficult one to test given the number of possible regulators and the difficulty of isolating sufficient stage-specific material to do phosphoproteomics. Loss-of-function temperature sensitive

mutants in *gpa-16* (Gα), *lin-5* (NuMA) and the dynein regulator *dnc-1* (p150, dynactin) impair EMS spindle rotation (Tsou, 2003; Zhang *et al.*, 2008; Liro and Rose, 2016). Together with our results, this suggests that symmetrically distributed Gα/LGN/NuMA complexes are likely important for allowing normal spindle movement, despite not serving as positional cues. If the dynamics of microtubules at the cortex differ across the cell, this could affect frequency, duration, or productivity of interaction with symmetrically distributed force-generating complexes in distinct cortical domains.

### *How might members of the Wnt pathway, Dishevelled and APC, act as positional cues for mitotic spindle positioning?*

We showed that by the end of mitotic spindle rotation, Dishevelled and APC occupy distinct domains of the EMS cortex, polarized along the anterior-posterior axis (Figure 3.7). This reciprocal localization pattern is highly reminiscent of the Par protein polarity in the one-cell stage embryo (Cuenca *et al.*, 2003). Like Par protein complexes, it is possible that APC and Dishevelled have downstream effectors that regulate mitotic spindle positioning, and that their cortical asymmetry serves as a spatial cue for mitotic spindle positioning (Grill *et al.*, 2001). At this point it is unknown if one or both proteins might serve as a sufficient spatial cue for orienting the mitotic spindle. It is possible that one protein plays this role and the other protein functions solely to restrict its localization to one side of EMS. Although we observed polarized localization of APC first, well before EMS spindle rotation, reduction of APC levels (via RNAi) did not decrease Dishevelled enrichment at the $P_2$:EMS contact (Figure 3.6E, Figure 3.8A). However, when we reduced levels of Dishevelled (DSH-2 and MIG-5) by RNAi, APC was no longer restricted to the anterior cortex of

EMS (Figure 3.8B), suggesting that Dishevelled enrichment on the posterior cortex of EMS is “upstream” of APC localization. One possible explanation for this discrepancy is that Dishevelled is polarizing prior to APC, but that we did not detect Dishevelled localization earlier due to the low expression level of DSH-2.

Neither APC nor Dishevelled contain catalytic domains, therefore it is unlikely that these molecules generate force on astral microtubules directly, the way a motor protein might. More likely, they either directly regulate microtubule dynamics, or indirectly regulate or activate force-generating complexes within their respective cortical domains. Homologs of *C. elegans* APC are known to interact and stabilize microtubules through the microtubule plus-end binding protein EB1 (Su *et al.*, 1995) In mitotic spindle positioning in budding yeast, Kar9 (APC) and Bim1 (EB1) serve as a link between astral microtubules and myosin motor proteins at the cell cortex (Lee, 2000; Yeh *et al.*, 2000). APC has also been shown to play a role in centrosome anchoring during spindle orientation in *Drosophila* germline stem cells (Yamashita, 2003).

There is some evidence in *C. elegans* that APR-1 regulates microtubule plus-end dynamics. Microtubule dwell times are longer at the anterior cortex than in the posterior cortex of EMS during telophase, and this difference is lost when APR-1 is reduced (Sugioka *et al.*, 2011). This activity of APR-1 is also thought to cause asymmetry in the number of spindle microtubules in the anterior vs. posterior late in the EMS cell cycle, and this asymmetry is important for nuclear asymmetry and fate in the resulting EMS daughter cells through differential trafficking of proteins between the nucleus and the cell cortex (Sugioka *et al.*, 2011). Because we observe

APR-1 polarization prior to and during EMS spindle rotation (Figure 3.6E and Figure 3.7C and D), it is possible that APR-1 plays a role in mitotic spindle positioning through the direct regulation of microtubules, similar to its role late in the EMS cell cycle. Reduction of APR-1 by RNAi was previously shown to have no effect on spindle orientation in EMS (Bei *et al.*, 2002), but knock-down or loss of APR-1 is the opposite of what happens in the absence of Wnt signaling, which is that the domain of APR-1 expands to the posterior cortex of EMS ((Sugioka *et al.*, 2011), Figure 3.7). It is possible that when Wnt signaling is reduced, microtubules are inappropriately stabilized by APR-1 on both sides of EMS, preventing the proper spatial positioning that is possible when APR-1 is polarized in the anterior of EMS.

APC or Dishevelled might serve as positional cues for mitotic spindle positioning by recruiting activators or inhibitors of motor proteins. LET-99 is a DEP domain containing protein, and an antagonist of the Gα/LGN/NuMA force-generating complex in the one-cell stage *C. elegans* embryo (Tsou, 2003). LET-99 is required for spindle positioning in EMS (Liro and Rose, 2016). In intact four-cell stage embryos, LET-99 is localized cortically and is reduced at the $P_2$:EMS contact in a similar pattern to APR-1 (Tsou, 2003; Werts *et al.*, 2011). It is possible that APR-1 regulates LET-99 to tune pulling forces on one side of the EMS cortex. Dishevelled might also recruit proteins that modulate motor activity. Hypotheses about how Dishevelled and APC might act as positional cues for mitotic spindle positioning would be greatly informed by knowledge of the direction of force imbalances generated on the mitotic to facilitate positioning within EMS.

APC and Dishevelled are both well known scaffolding proteins and their role in astral microtubule regulation could be indirect, and regulated through a binding partner or complex member. WRM-1/β-catenin cortical association has also been hypothesized to be important for spindle positioning in EMS (Kim *et al.*, 2013). Although we did not examine WRM-1 localization in the study, our data are consistent with the possibility that Wnt pathway proteins, and potentially WRM-1 containing protein complexes, are polarized in EMS and likely to serve as spatial cues for mitotic spindle positioning. Wnt pathway signaling mutants expand the WRM-1 cortical domain into the posterior of EMS (Kim *et al.*, 2013), similar to what we and others have observed for APR-1 ((Sugioka *et al.*, 2011), Figure 3.7). It is possible that WRM-1 and APR-1 are co-regulated as a part of a common complex at the anterior cortex of EMS, and that they act together in spindle positioning in EMS. Wnt pathway kinases have also been implicated in spindle rotation in EMS (Schlesinger *et al.*, 1999; Bei *et al.*, 2002; Walston *et al.*, 2004) and might be asymmetrically activated at the EMS cortex in association with either Dishevelled or APC.

In conclusion, we found Dishevelled and APC, but not NuMA and dynein to be asymmetrically localized at the EMS cortex. It will be interesting to explore a possible mechanism for mitotic spindle positioning that does not appear to rely on the asymmetric localization of the conserved Gα/LGN/NuMA protein complex. We speculate that there may be more cases where signaling pathway proteins serve as spatial cues for mitotic spindle positioning independent of Gα/LGN/NuMA localization.

## 3.4 Materials and Methods

### *C. elegans strains*

*Caenorhabditis elegans* animals were cultured on Normal Growth Media (NGM) plates, fed *E. coli* (OP50 strain), and grown at 20C for experiments. Worms were moved to 25C for incubation during strain construction. A list of strains generated for this work is available in Figure 3.1. Additional strains used are as followed: Bristol N2 (wild type); DP38 (unc-119(ed3) III).

### *Repair template construction and gene tagging*

Strains were generated using methods from Dickinson et al. 2013, Paix et al. 2014, and Dickinson et al. 2015 (protocol used to create each strain is designated in Figure 3.1). The presence of multiple isoforms, the locations of catalytic or protein-protein interaction domains, as well as information about the functionality of previous tags, were used to determine fluorescent protein fusion site for a given protein (N- or C-terminus). Repair templates were constructed by inserting homology arm PCR products amplified from worm genomic DNA, into vectors containing a fluorescent protein and a selection cassette via Gibson Assembly (New England Biolabs) as described in detail in Dickinson et al. 2013, and Dickinson et al. 2015. Cas9 targeting sequences for each gene were selected using the CRISPR Design tool (crispr.mit.edu). These sequences were cloned into the Cas9-sgRNA expression vector DD162 (Dickinson *et al.*, 2013), and co-injected into adult germlines with repair templates and array markers (Figure 3.9B).

Candidate knock-ins were selected by drug treatment and phenotypic identification (rol) as described in Dickinson et al. 2015 (except where indicated in

Figure 3.1), and singled to new plates to establish independent lines. Candidate knock-ins with 100% roller (rol) progeny were identified as putative homozygous insertions (C-terminal tags or non-essential genes); heterozygous insertions were isolated in the remaining cases (N-terminal tags of essential genes). To excise selectable elements, Cre was expressed in the candidate knock-ins, either by injection of a Cre containing expression plasmid into the germline (Dickinson *et al.*, 2013), or by heatshock expression of Cre from the Self Excising Cassette (Dickinson *et al.*, 2015). Candidate knock-ins were checked for expression of inserted tags using a dissecting microscope (Leica M165FC) equipped with fluorescence (89 North PhotoFluor LM-75). Although in some cases, no fluorescence was detected using this method due to low gene expression levels. PCR genotyping was used to confirm homozygous insertion and removal of selectable makers in all isolated strains (see below). Embryonic lethality was quantified and negligible for all strains used for further experiments in this work (Figure 3.9A)

***Genomic DNA isolation and genotyping***

Genomic DNA was isolated from plates of worms using standard phenol-chloroform nucleic acid extraction and ethanol precipitation. Genomic DNA from candidate knock-in strains and N2 unmodified worms were used as template for genotyping PCR reactions with LongAmp Taq DNA polymerase (New England Biolabs).

***Microscopy***

Embryos were dissected from gravid adults in Egg Buffer and mounted at the 2-4 cell stage on poly-L-lysine coated coverslips, with 2.5% agarose pads. Cells

isolated from embryos were mounted in Shelton's Media using clay feet as spacers between the slide and coverslip. Both embryos and cells were imaged using a spinning disk confocal microscope with a Nikon TiE stand and a 60X 1.4NA Plan Apo immersion oil objective (Nikon), CSUXI spinning disk head (Yokogawa), and an ImagEM EMCCD (Hamamatsu). mNG strains were excited using 514nm solid state lasers with a 545/40 YFP emission filter set and were imaged in 690MHz non-EM mode with varying exposure times. Single channel embryo and isolation samples were filmed at 20-second intervals. To prepare figures, images were cropped and rotated, and brightness and contrast were adjusted using FIJI.

***RNAi***

Adult animals were injected with dsRNAs targeting specific gene products according to standard procedures (Dudley, 2002). The concentrations of dsRNAs injected are available in Figure 3.9C. Embryos were dissected from injected adults and imaged 18-28 hours post injection. At least 3 samples per experiment were prepared by mounting control embryos (from uninjected worms) side by side with RNAi treated embryos for direct comparison and quantification. Additional samples were mounted in groups of treated or untreated embryos and imaged under identical conditions as the paired embryos.

***Cell isolations***

Cells were isolated from embryos and cultured as described by Edgar and Goldstein 2012 (Edgar and Goldstein, 2012). Chitinase from *Streptomyces griseus* was used at a concentration of 20U/ml dissolved in Egg Buffer to remove eggshells (Sigma - C6137). To isolate $P_2$:EMS cell pairs, eggshells were removed at the 2-cell

stage, the P1 and AB cells were separated, and the division timing of the P1 cell was tracked. Recombinations of $P_2$:EMS cell pairs, or individual EMS cells were preformed within 4min P1 cell division and EMS birth (Goldstein, 1995a). Cells were cultured in Shelton's Media and mounted on glass slides with coverslips for imaging (Werts *et al.*, 2011).

***Quantification and statistical analysis***

A 5 pixel-wide line was drawn through the contacts of interest, the cytoplasm, and off embryo. A kymograph was generated using the 5-pixel average. From that kymograph, the maximum intensity for each contact was recorded and the average intensity of the cytoplasm and off embryo background was recorded for each time point. Fluorescence intensity was calculated by subtracting off embryo background from the values for the contact and cytoplasm. Fluorescence intensity measured at the contacts was normalized by dividing by average intensity of the cytoplasm. Measurements over time are expressed as seconds until the onset of EMS cytokinesis was observed. FIJI and Metamorph Software (Molecular Devices) software were used to quantify fluorescence intensity from micrographs. Unpaired t-tests with Welch's correction was used to compare means and were performed using GraphPad Prism 7 Software (GraphPad Software, Inc.). p-values and n values for each experiment are reported in figures, figure legends, or text.

## 3.5 Chapter 3 Figures

**Strain List**

| Mammalian gene name | *C. elegans* gene name | Tag location | Strain Name | Genotype | Method | References for genes that affect spindel rotation in EMS |
|---|---|---|---|---|---|---|
| Wnt | *mom-2* | 3'end | LP559 | mom-2(cp267[mom-2::mNG-C1^3xFlag]) V | 2 | Schlesinger et al., Bei et al. |
| Frizzled | *mom-5* | 3'end | LP697 | mom-5(cp367[mom-5::mNG-C1^3xFlag]) I | 3 | Schlesinger et al., Bei et al. |
| Frizzled | *mom-5* | 3'end | LP184 | mom-5(cp31[mom-5::YPET + LoxP]) I | 1 | Schlesinger et al., Bei et al. |
| Gsk3 | *gsk-3* | 3'end | LP538 | gsk-3(cp251[gsk-3::mNG-C1^3xFlag]) | 3 | Schlesinger et al., Bei et al. |
| Dishevelled | *dsh-2* | 5'end | LP228 | dsh-2(cp51[mNeonGreen::dsh-2]) II | 1 | Bei et al., Walston et al. |
| Dishevelled | *mig-5* | 5'end | LP728 | mig-5(cp385[mNG-GLO^AID::mig-5]) II | 3 | Bei et al., Walston et al. |
| Dishevelled | *dsh-1* | internal | LP705 | dsh-1(cp375[dsh-1DIX::mNG-C1^3xFlag::PDZ,DEP]) II | 3 | Bei et al., Walston et al. |
| APC | *apr-1* | 5'end | LP435 | apr-1(cp166[mNG-C1^3xFlag::apr-1]) I | 3 | Schlesinger et al. |
| Axin | *pry-1* | 3'end | LP713 | pry-1(cp383[pry-1::mNG-C1^3xFlag]) I | 3 | |
| ROR | *cam-1* | 3'end | LP530 | cam-1(cp243[cam-1::mNG-C1^3xFlag]) | 3 | |
| — | *mes-1* | 3'end | LP527 | mes-1(cp240[mes-1::mNG-C1^3xFlag] | 3 | Bei et al. |
| p150 Dynactin | *dnc-1* | 3'end | LP563 | dnc-1(cp271[dnc::mNG-C1^3xFlag]) IV | 3 | Zhang et al. |
| NuMA | *lin-5* | 3'end | LP585 | lin-5(cp288[lin-5::mNG-C1^3xFlag]) II | 3 | Liro et al. |
| Dynein | *dhc-1* | 3'end | LP560 | dhc-1(cp268[dhc::mNG-C1^3xFlag]) I | 3 | |
| NudE | *nud-2* | 3'end | LP439 | nud-2(cp170[nud-2::mNG-C1^3xFlag]) I | 3 | |
| BicaudalD | *bicd-1* | 5'end | LP451 | bicd-1(cp180[mNG-C1^3xFlag::bicd-1]) IV | 3 | |
| Lis1 | *lis-1* | 3'end | LP591 | lis-1(cp294[lis-1::mNG-C1^3xFlag]) III | 3 | |
| Discs large | *dlg-1* | 3'end | LP598 | dlg-1(cp301[dlg-1::mNG-C1^3xFlag]) X | 3 | |
| MCAK | *klp-7* | 3'end | LP447 | klp-7(cp178[klp-7::mNG-C1^3xFlag]) III | 3 | |
| Kinesin | *klp-17* | 3'end | LP443 | klp-17(cp174[klp-17::mNG-C1^3xFlag]) II | 3 | |
| Kinesin | *klp-12* | 3'end | LP521 | klp-12(cp234[klp-12::mNG-C1^3xFlag]) | 3 | |
| Kinesin | *klp-20* | 3'end | LP608 | klp-20(cp311[klp-20::mNG-C1^3xFlag]) III | 3 | |
| Kinesin | *klp-4* | 3'end | LP600 | klp-4(cp303[klp-4::mNG-C1^3xFlag]) X | 3 | |
| Kinesin | *klp-8* | 3'end | LP604 | klp-8(cp307[klp-8::mNG-C1^3xFlag]) X | 3 | |

**Figure 3.1 List of *C. elegans* strains generated.** Method refers to the method used to generate the knock-ins 1 = Dickinson et al., 2103, 2 = Paix et al., 2014, 3 = Dickinson et al., 2015. References are works that report EMS spindle rotation defects for the given genes,

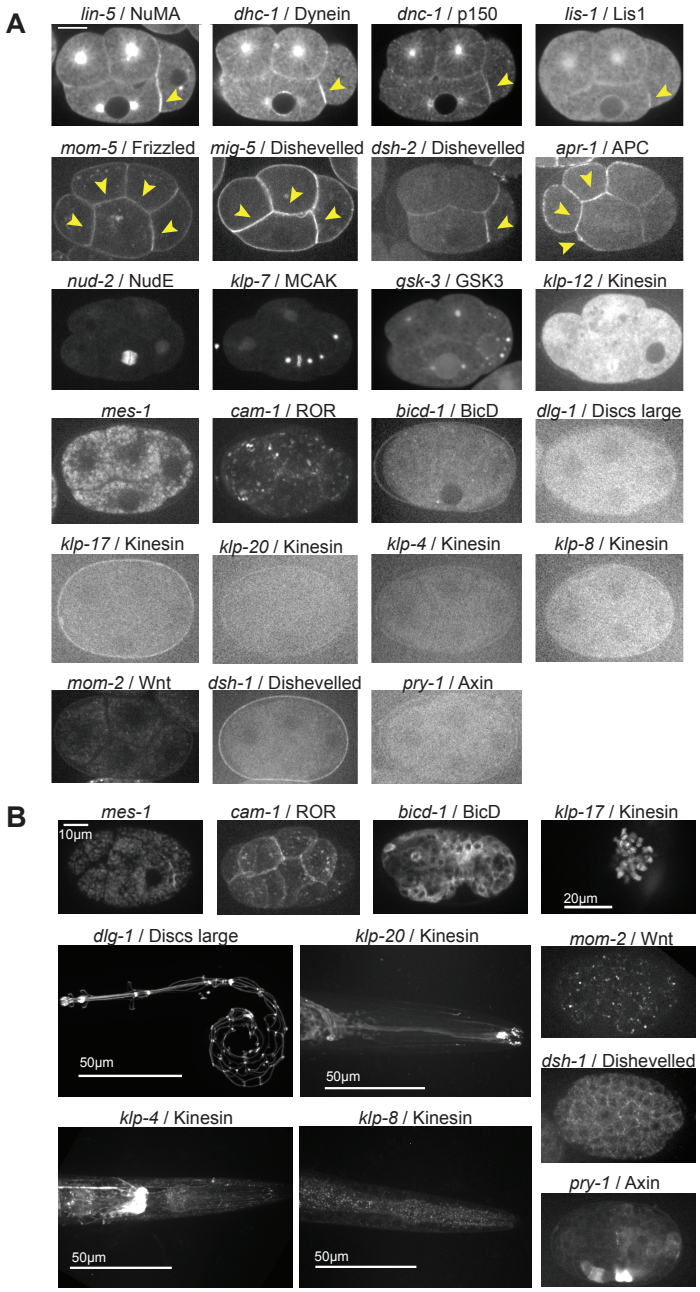


**Figure 3.2 Localization of endogenously tagged candidate proteins**

A) Four-cell stage embryos from each strain generated. Images are a single Z-slice through a center plane of the embryo, except for *cam-1,* which is a maximum projection. Scale bar, 10µm. B) Later stage embryos and animals for strains with no detectable fluorescent signal at the four-cell stage. *mes-1, cam-1, bicd-1, mom-2, ds-1, pry-1*: multi-cell stage embryos. *klp-17*: sperm. *dlg-1*: whole larva. *klp-20, klp-4, klp-8:* pharyngeal region. Images are maximum intensity projection of multiple Z planes. Scale bar lengths are indicated on panels.

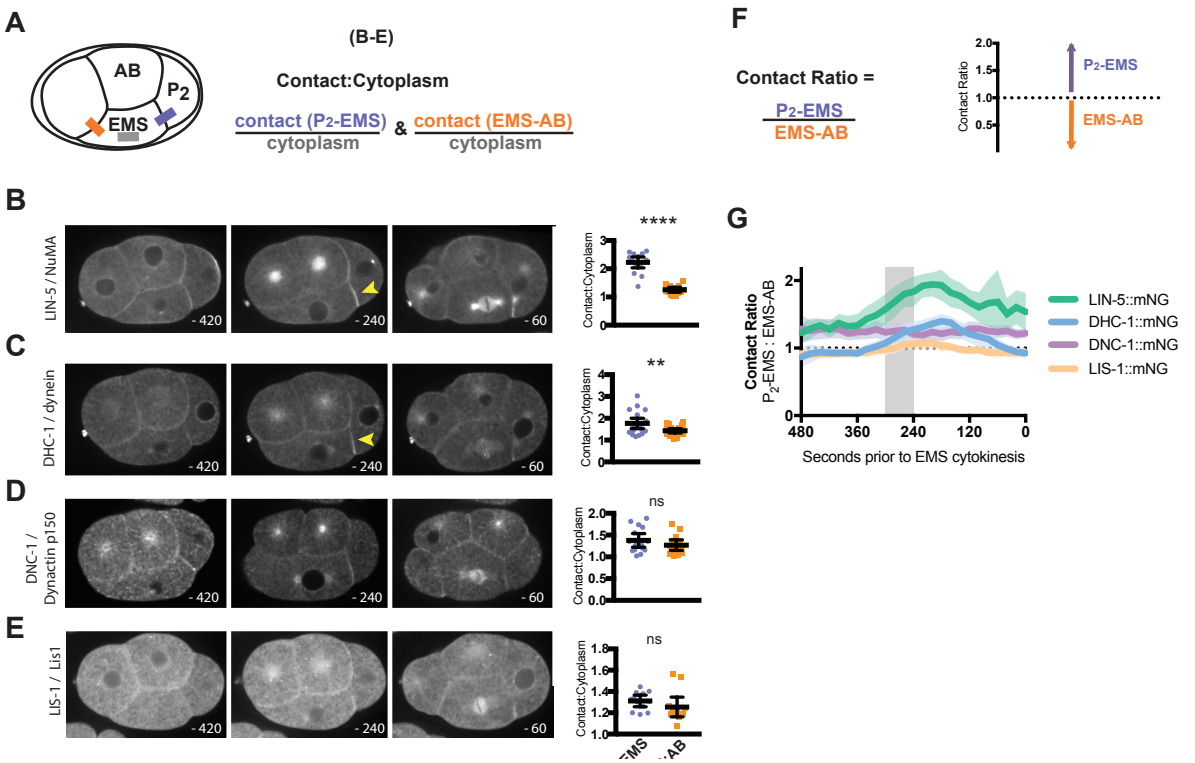


**Figure 3.3 Localization of NuMA, dynein, dynactin p150, and Lis1 during the EMS cell cycle.**

A) Schematic describing the strategy for quantification of fluorescence at the cell-cell contacts during spindle rotation ($P_2$:EMS = purple, EMS:AB = orange, cytoplasm = gray). B-E) Localization of tagged proteins at three different times during the EMS cell cycle. Images are single Z-planes. Quantification was performed during spindle rotation at -260 seconds prior to EMS division. Seconds before EMS division are indicated at the bottom right of each panel. NuMA n=16, p=<0.0001; Dynein Heavy Chain n=21, p=0.0096; Dynactin p150 n=16, p=0.2516; Lis1 n=12, p=0.2592. Statistical test used was an unpaired t-test. Black lines represent means and 95% confidence intervals. Gray bar is the period during which the EMS spindle rotates. F) Schematic describing the strategy for quantification of fluorescence at the cell-cell contacts over time, expressed as a ratio. G) Ratio of intensity at the $P_2$:EMS contact and EMS:AB contact over time for each stain B-E. Colored lines represent means, and error bars are 95% confidence intervals.

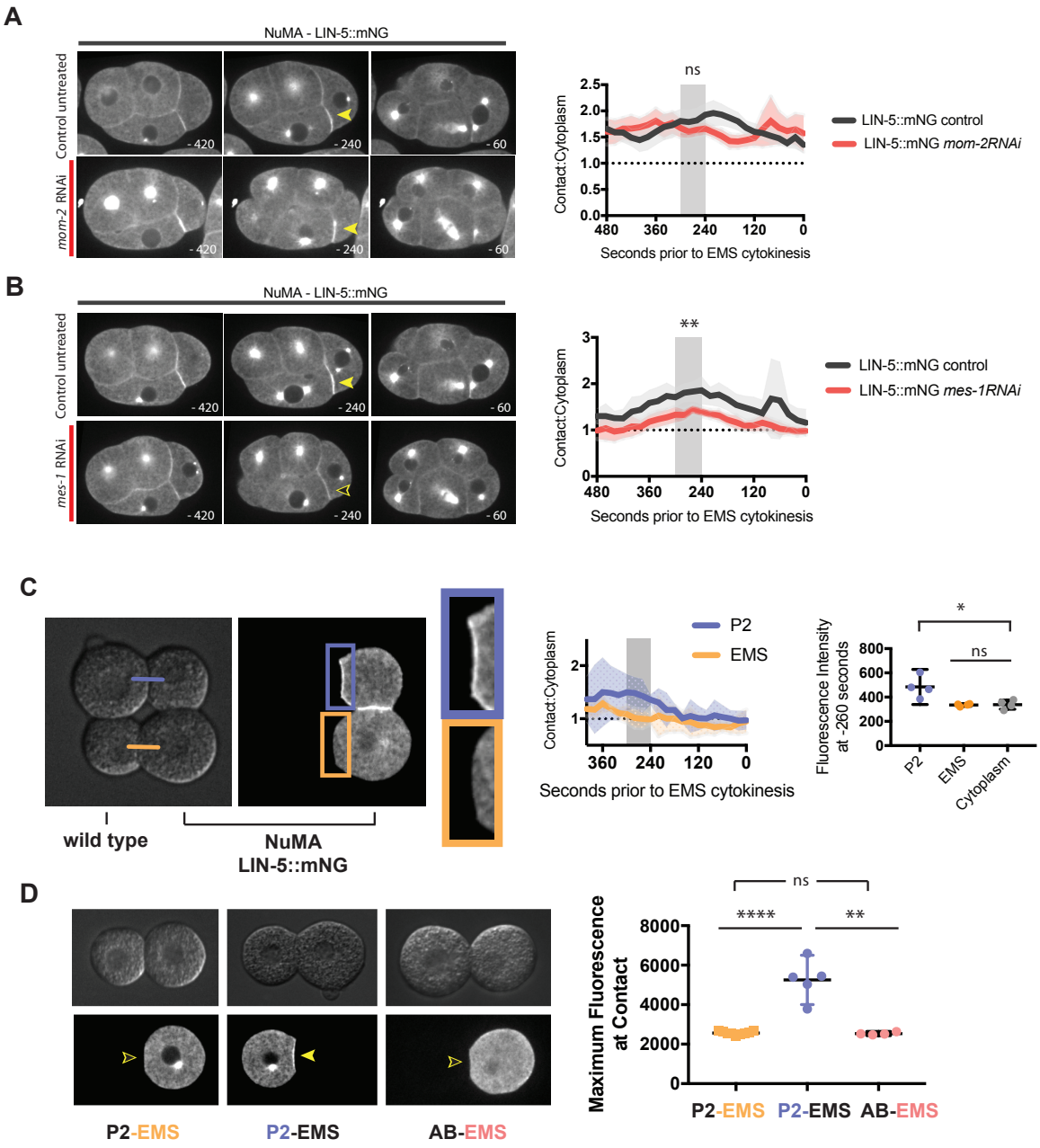


**Figure 3.4 NuMA is enriched in the $P_2$ cell at the contact with EMS**

A) Live imaging of embryos expressing LIN-5::mNG in control and *mom-2* RNAi treated conditions. Arrowheads point to enrichment of LIN-5::mNG at $P_2$:EMS contact site. Control n =17; *mom-2* RNAi n =20. Statistical test performed during spindle rotation (-260 seconds) p =0.1537. B) Embryos expressing LIN-5::mNG in control and *mes-1* RNAi treated conditions. control n =7; *mes-1* RNAi n =7. Statistical test performed during spindle rotation (-260 seconds) p =0.0014. Black lines are control untreated embryos and red lines are RNAi conditions. C) Partial embryos made by direct manipulation of unlabled and LIN-5::mNG labeled $P_2$ and EMS cell pairs. $P_2$ cells are the smaller cells. Purple and orange lines represent new

contacts where fluorescent protein levels were quantified. n=4. Plot compares fluorescence intensity at the contacts to the cytoplasmic fluorescence intensity. $P_2$ contact vs. cytoplasm p=0.0252; EMS contact vs. cytoplasm p=0.8722. D) Recombined LIN-5::mNG and unlabeled cells. Arrowheads point to cell contacts. Plot is the maximum fluorescence reached during the EMS cell cycle. $P_2$:EMS n=9; $P_2$:EMS n=5; AB:EMS n=4. ns p=0.5913; ** p=0.0011; **** p=<0.0001. Solid lines indicate means with 95% confidence intervals.

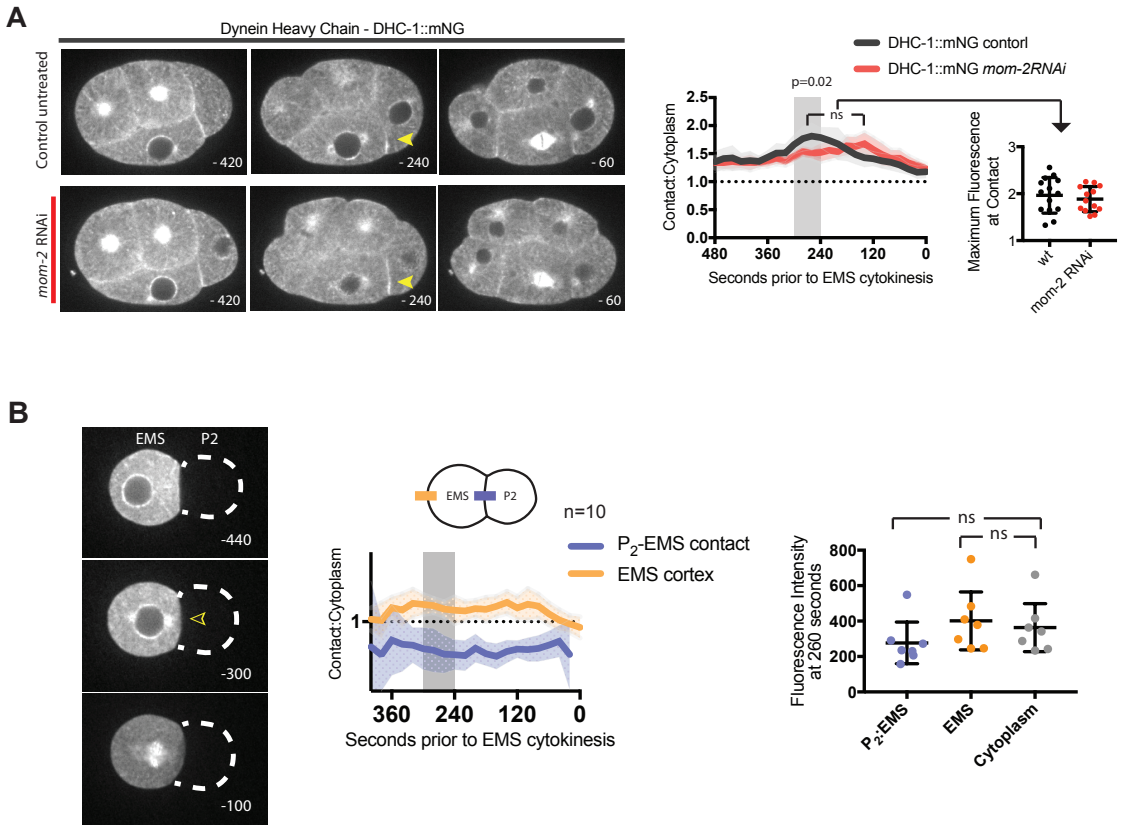


**Figure 3.5 Dynein is not enriched in EMS at the $P_2$:EMS contact**

A) Live imaging of embryos expressing DHC-1::mNG in control and *mom-2* RNAi treated conditions. Arrowheads point to enrichment of DHC-1::mNG at $P_2$:EMS contact site. control n =13; *mom-2* RNAi n =12. Statistical test performed during spindle rotation (-260 seconds); p =0.0206. The maximum intensity at the $P_2$:EMS contact compared in control vs. *mom-2* RNAi ns: p=0.5293. B) Recombined DHC-1::mNG and unlabeled cells. Arrowheads point to cell contacts. n=10; $P_2$:EMS vs. cytoplasm ns, p=0.2627; EMS cortex vs. cytoplasm ns, p=0.6707. Diagram depicts linescan used for quantification.

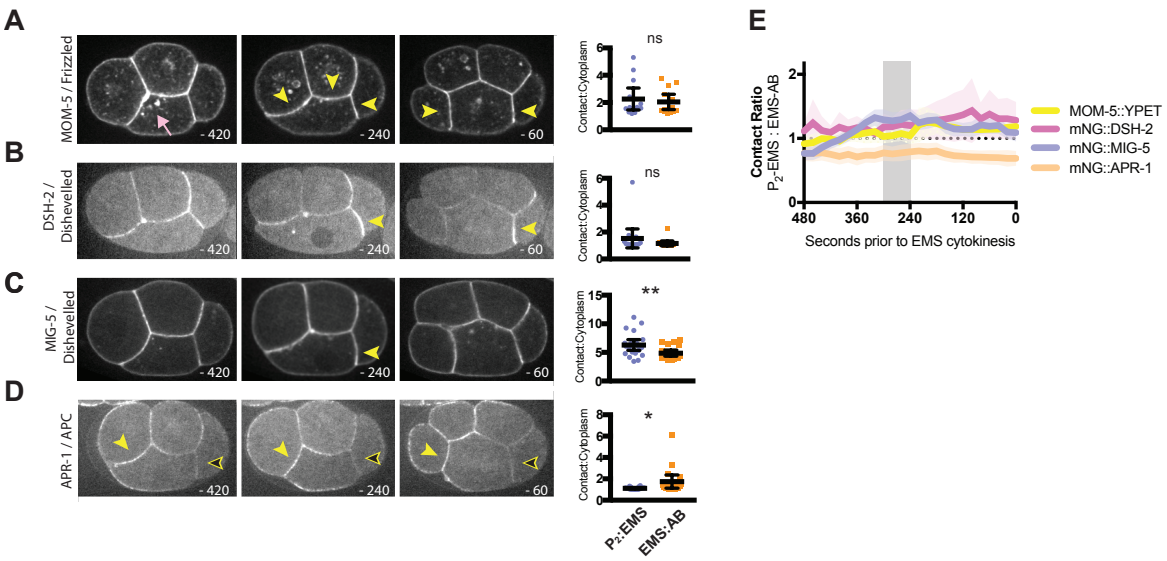


**Figure 3.6 Localization of Frizzled, Dishevelled, and APC during the EMS cell cycle**

A-D) Localization of tagged proteins at three different times during the EMS cell cycle. Images are single Z planes. Quantification was performed during spindle rotation at -260 seconds prior to EMS division. Seconds before EMS division are indicated at the bottom right of each panel. MOM-5 n=13, p=0.6423; DSH-2 n=15, p=0.2827; MIG-5 n=22, p=0.0089; APC n=18, p=0.0401. Black lines represent means and 95% confidence intervals. Gray bar is the period during which the EMS spindle rotates. E) Ratio of intensity at the $P_2$:EMS contact and EMS:AB contact over time for each stain A-D. Colored lines represent means, and error bars are 95% confidence intervals.

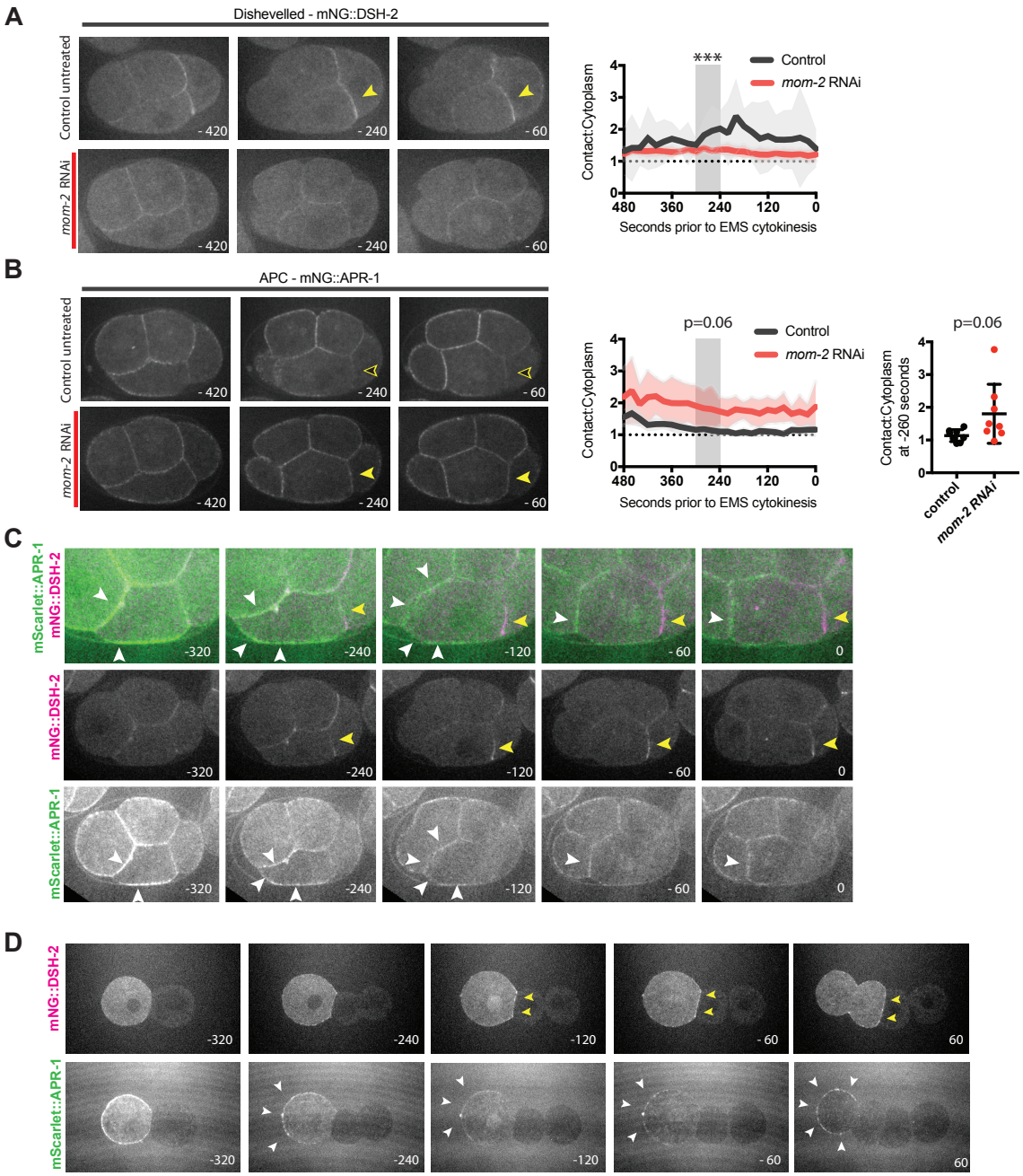


**Figure 3.7 Dishevelled and APC are enriched on opposite sides of EMS**

A) Live imaging of embryos expressing mNG::DSH-2 in control and *mom-2* RNAi treated conditions. Arrowheads point to enrichment of mNG::DSH-2 at $P_2$:EMS contact site. Control n =3; *mom-2* RNAi n =11. Statistical test performed during spindle rotation (-260 seconds) p =0.0002. B) Embryos expressing mNG::APR-1 in control and *mom-2* RNAi treated conditions. Control n =8; *mom-2* RNAi n =8. Statistical test performed during spindle rotation (-260 seconds) p =0.0608. Black lines are control untreated embryos and red lines are RNAi conditions. C)

mNG::DSH-2 and mScarlet::APR-1 dual-labeled embryos. Top row is a merge of the EMS cell and bottom two rows are single channel embryos from the corresponding time-points. n= 5 D) Recombined cell pair of unlabeled $P_2$ cells and dual-labeled mNG::DSH-2 and mScarlet::APR-1 expressing EMS cells. Panels are the individual channels (mNG::DSH-2 - green; mScarlet::APR-1 - red). Arrowheads point to enrichments on either side of EMS. n= 6.

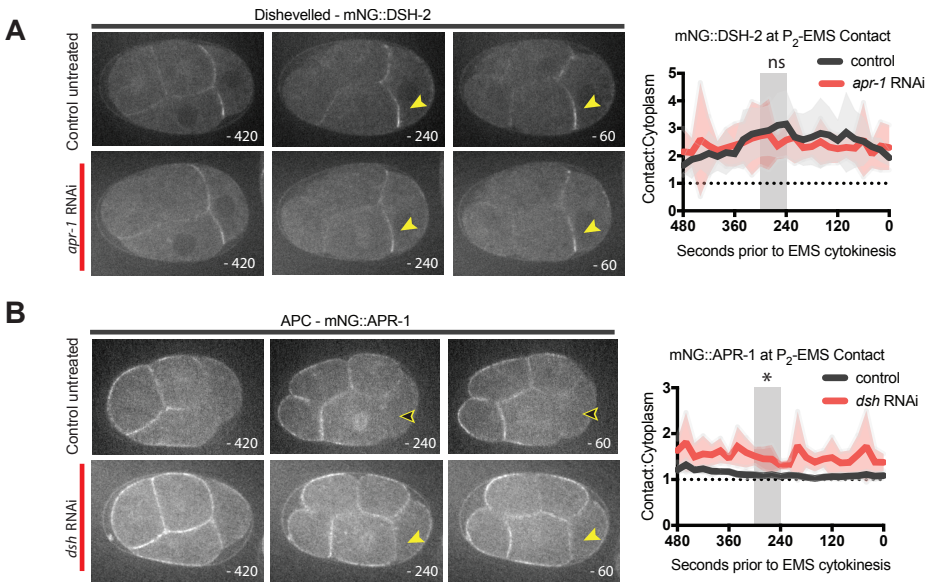


**Figure 3.8 Dishevelled is required for APC localization in EMS**

A) Live imaging of embryos expressing mNG::DSH-2 in control and *apr-1* RNAi treated conditions. Arrowheads point to enrichment of mNG::DSH-2 at $P_2$:EMS contact site. control n =7; *apr-1* RNAi n =7. Statistical test performed during spindle rotation (-260 seconds) p =0.1759. B) Embryos expressing mNG::APR-1 in control and *dsh* RNAi treated conditions. control n =8; *dsh* RNAi n =8. Statistical test performed during spindle rotation (-260 seconds) p =0.0227. Black lines are control untreated embryos and red lines are RNAi conditions. Arrowheads point to enrichments on either side of EMS.

**A**

| | Strain | Avg. % lethality |
|---|---|---|
| wild type | N2 | 0.8926 |
| *mom-5* 3'end | LP184 | 0.2710 |
| *dsh-2* 5'end | LP228 | 0.2931 |
| *mig-5* 5'end | LP728 | 0.1235 |
| *apr-1* 5'end | LP435 | 0.3112 |
| *lin-5* 3'end | LP585 | 0.2826 |
| *dhc-1* 3'end | LP560 | 0.8103 |
| *dnc-1* 3'end | LP563 | 0.8012 |
| *lis-1* 3'end | LP591 | 0.2623 |

**B**

| **Target** | **sgRNA primer sequence** |
|---|---|
| *mom-2* 3'end | ACATACATTGGGCCCAATAT GTTTTAGAGCTAGAAATAGCAAGT |
| *mom-5* 3'end | TGACCTCGAAGAGAGTGCC GTTTTAGAGCTAGAAATAGCAAGT |
| *mom-5* 3'end | TGTACCTGCTCATGTTGATC GTTTTAGAGCTAGAAATAGCAAGT |
| *gsk-3* 3'end | CGGTGATGTGGCTGGCCCAT GTTTTAGAGCTAGAAATAGCAAGT |
| *dsh-2* 5'end | CGTCAAATGATGAATCAAT GTTTTAGAGCTAGAAATAGCAAGT |
| *mig-5* 5'end | CTGCAGTCTGATGTGCATGGGTTTTAGAGCTAGAAATAGCAAGT |
| *dsh-1* internal | TCAAGGCTCATAGAGGACTC GTTTTAGAGCTAGAAATAGCAAGT |
| *apr-1* 5'end | TGAGTAGATTCCACTTCCAC GTTTTAGAGCTAGAAATAGCAAGT |
| *pry-1* 3'end | ATAATCCCACTATCGGAGCT GTTTTAGAGCTAGAAATAGCAAGT |
| *cam-1* 3'end | AGAGGATGGTGATTCTGATT GTTTTAGAGCTAGAAATAGCAAGT |
| *mes-1* 3'end | GGGTGTATTCATCTAAACCG GTTTTAGAGCTAGAAATAGCAAGT |
| *dnc-1* 3'end | CTACCACACGATTCCCCACT GTTTTAGAGCTAGAAATAGCAAGT |
| *lin-5* 3'end | GTCCAAGAAAAAGAACCGTC GTTTTAGAGCTAGAAATAGCAAGT |
| *dhc-1* 3'end | AGACGATTAGAGAGTTGAGTGTTTTAGAGCTAGAAATAGCAAGT |
| *nud-2* 3'end | CCGTGTCGTTGTAAGATGAC GTTTTAGAGCTAGAAATAGCAAGT |
| *bicd-1* 5'end | CAATTCTGATTCAGCCATTG GTTTTAGAGCTAGAAATAGCAAGT |
| *lis-1* 3'end | ATGGAGAATATTTCGGTCAA GTTTTAGAGCTAGAAATAGCAAGT |
| *dlg-1* 3'end | TAATGACGTGGCACCCAAAT GTTTTAGAGCTAGAAATAGCAAGT |
| *klp-7* 3'end | AGACGTTTTCCACGGCGACA GTTTTAGAGCTAGAAATAGCAAGT |
| *klp-17* 3'end | GGAAAAGCAGTTGTTCAAAC GTTTTAGAGCTAGAAATAGCAAGT |
| *klp-12* 3'end | GAGATTCGACAGTCGGATTC GTTTTAGAGCTAGAAATAGCAAGT |
| *klp-20* 3'end | ATTGCTCACATAACTGGTAC GTTTTAGAGCTAGAAATAGCAAGT |
| *klp-4* 3'end | ATCCACCAGGTCTCCTGAAA GTTTTAGAGCTAGAAATAGCAAGT |
| *klp-8* 3'end | CAGCGTGCTTAAAGTTCCCA GTTTTAGAGCTAGAAATAGCAAGT |

**C**

| **gene dsRNA targeting** | **Concentration (ng/ul)** |
|---|---|
| mom-2 | 499 |
| mes-1 | 441 |
| apr-1 | 698 |
| mig-5 | 840 |
| dsh2 | 259 |

**Figure 3.9** A) Average percent lethality for each strain used in Figures 3.3 on. B) sgRNA primers used generate the Cas9 vector and sgRNA to target each site for gene-specific knock-in. C) Concentrations of double stranded RNAs injected as measured using a nano-drop.

## REFERENCES


Ali, M. Y., and Siddiqui, S. S. (2000). cDNA Cloning and Expression of a C-Terminus Motor Kinesin-like Protein KLP-17, Involved in Chromosomal Movement in Caenorhabditis elegans. Biochemical and Biophysical Research Communications *267*, 643–650.

Bei, Y., Hogan, J., Berkowitz, L. A., Soto, M. C., Rocheleau, C. E., Collins, J., and Mello, C. C. (2002). SRC-1 and Wnt Signaling Act Together to Specify Endoderm and to Control Cleavage Orientation in Early *C. elegans* Embryos. Developmental Cell *3*, 113–125.

Bergstralh, D. T., Dawney, N. S., and St Johnston, D. (2017). Spindle orientation: a question of complex positioning. Development *144*, 1137–1145.

Cockell, M. M., Baumer, K., and Gönczy, P. (2004). lis-1 is required for dynein-dependent cell division processes in C. elegans embryos. Journal of Cell Biology *117*, 4571–4582.

Couwenbergs, C., Labbe, J. C., Goulding, M., Marty, T., Bowerman, B., and Gotta, M. (2007). Heterotrimeric G protein signaling functions with dynein to promote spindle positioning in C. elegans. The Journal of Cell Biology *179*, 15–22.

Cuenca, A. A., Schetter, A., Aceto, D., Kemphues, K., and Seydoux, G. (2003). Polarization of the C. elegans zygote proceeds via distinct establishment and maintenance phases. Development *130*, 1255–1265.

Delaunay, D., Cortay, V., Patti, D., Knoblauch, K., and Dehay, C. (2014). Mitotic spindle asymmetry: a Wnt/PCP-regulated mechanism generating asymmetrical division in cortical precursors. CellReports *6*, 400–414.

di Pietro, F., Echard, A., and Morin, X. (2016). Regulation of mitotic spindle orientation: an integrated view. EMBO Reports *17*, 1106–1130.

Dickinson, D. J., Pani, A. M., Heppert, J. K., Higgins, C. D., and Goldstein, B. (2015). Streamlined Genome Engineering with a Self-Excising Drug Selection Cassette. Genetics *200*, 1035–1049.

Dickinson, D. J., Ward, J. D., Reiner, D. J., and Goldstein, B. (2013). Engineering the Caenorhabditis elegans genome using Cas9-triggered homologous recombination. Nature Methods *10*, 1028–1034.

Edgar, L. G., and Goldstein, B. (2012). Culture and Manipulation of Embryonic Cells. In: Methods in Cell Biology, Elsevier, 151–175.

Gassmann, R. *et al.* (2008). A new mechanism controlling kinetochore-microtubule

interactions revealed by comparison of two dynein-targeting components: SPDL-1 and the Rod/Zwilch/Zw10 complex. Genes & Development *22*, 2385–2399.

Gillies, T. E., and Cabernard, C. (2011). Cell Division Orientation in Animals. Current Biology *21*, R599–R609.

Gloerich, M., Bianchini, J. M., Siemers, K. A., Cohen, D. J., and Nelson, W. J. (2017). Cell division orientation is coupled to cell-cell adhesion by the E-cadherin/LGN complex. Nature Communications *8*, 13996.

Goldstein, B. (1992). Induction of Gut in *Caenorhabditis Elegans* Embryos. Nature, 255–257.

Goldstein, B. (1993). Establishment of gut fate in the E lineage of C. elegans: the roles of lineage-dependent mechanisms and cell interactions. Development *118*, 1267–1277.

Goldstein, B. (1995a). An analysis of the response to gut induction in the C. elegans embryo. Development *121*, 1227–1236.

Goldstein, B. (1995b). Cell Contacts Orient Some Cell Division Axes in the C. elegans Embryo. The Journal of Cell Biology *129*, 1071–1080.

Goldstein, B., Takeshita, H., Mizumoto, K., and Sawa, H. (2006). Wnt Signals Can Function as Positional Cues in Establishing Cell Polarity. Developmental Cell *10*, 391–396.

Gonczy, P., Pichler, S., Kirkham, M., and A, H. A. (1999). Cytoplasmic dynein is required for distinct aspects of MTOC positioning, including centrosome separation, in the one cell stage Caenorhabditis elegans embryo. The Journal of Cell Biology *147*, 135–150.

Gotta, M., and Ahringer, J. (2001). Distinct roles for Galpha and Gbetagamma in regulating spindle position and orientation in Caenorhabditis elegans embryos. Nature Cell Biology *3*, 297–300.

Green, J. L., Inoue, T., and Sternberg, P. W. (2007). The C. elegans ROR receptor tyrosine kinase, CAM-1, non-autonomously inhibits the Wnt pathway. Development *134*, 4053–4062.

Grill, S. W., Gonczy, P., Stelzer, E. H. K., and Hyman, A. A. (2001). Polarity controls forces governing asymmetric spindle positioning in the Caenorhabditis elegans embryo. Nature *409*, 630–633.

Grill, S. W., Howard, J., Schäffer, E., Stelzer, E. H. K., and Hyman, A. A. (2003). The distribution of active force generators controls mitotic spindle position. Science *301*, 518–521.

Habib, S. J., Chen, B. C., Tsai, F. C., Anastassiadis, K., Meyer, T., Betzig, E., and Nusse, R. (2013). A Localized Wnt Signal Orients Asymmetric Stem Cell Division in Vitro. Science *339*, 1445–1448.

Hawkins, N. C., Ellis, G. C., Bowerman, B., and Garriga, G. (2005). MOM-5 frizzled regulates the distribution of DSH-2 to control C. elegans asymmetric neuroblast divisions. Developmental Biology *284*, 246–259.

Inaba, M., Yuan, H., Salzmann, V., Fuller, M. T., and Yamashita, Y. M. (2010). E-Cadherin Is Required for Centrosome and Spindle Orientation in Drosophila Male Germline Stem Cells. PLoS ONE *5*, e12473.

Kim, S., Ishidate, T., Sharma, R., Soto, M. C., Conte, D., Mello, C. C., and Shirayama, M. (2013). Wnt and CDK-1 regulate cortical release of WRM-1/ -catenin to control cell division orientation in early Caenorhabditis elegans embryos. Proceedings of the National Academy of Sciences *110*, E918–E927.

Kiyomitsu, T., and Cheeseman, I. M. (2012). Chromosome- and spindle-pole-derived signals generate an intrinsic code for spindle position and orientation. Nature Cell Biology *14*, 311–317.

Kiyomitsu, T., and Cheeseman, I. M. (2013). Cortical Dynein and Asymmetric Membrane Elongation Coordinately Position the Spindle in Anaphase. Cell *154*, 391–402.

Kotak, S., and Gönczy, P. (2013). Mechanisms of spindle positioning: cortical force generators in the limelight. Current Opinion in Cell Biology *25*, 741–748.

Le Grand, F., Jones, A. E., Seale, V., Scimè, A., and Rudnicki, M. A. (2009). Wnt7a activates the planar cell polarity pathway to drive the symmetric expansion of satellite stem cells. Cell Stem Cell *4*, 535–547.

Lechler, T., and Fuchs, E. (2005). Asymmetric cell divisions promote stratification and differentiation of mammalian skin. Nature *437*, 275–280.

Lee, L., Tirnauer, J. S., Li, J., Schuyler, S. C., Liu, J. Y., and Pellman, D. (2000). Positioning of the mitotic spindle by a cortical-microtubule capture mechanism. Science *287*, 2260–2262.

Liro, M. J., and Rose, L. S. (2016). Mitotic Spindle Positioning in the EMS Cell of Caenorhabditis elegans Requires LET-99 and LIN-5/NuMA. Genetics *204*, 1177–1189.

Liu, J., Phillips, B. T., Amaya, M. F., Kimble, J., and Xu, W. (2008). The C. elegans SYS-1 protein is a bona fide beta-catenin. Developmental Cell *14*, 751–761.

Lu, M. S., and Johnston, C. A. (2013). Molecular pathways regulating mitotic spindle

orientation in animal cells. Development *140*, 1843–1856.

Malone, C. J., Misner, L., Le Bot, M., Tsai, M.-C., Campbell, J. M., Ahringer, J., and White, J. G. (2003). The *C. Elegans* Hook Protein, ZYG-12, Mediates the Essential Attachment Between the Centrosome and Nucleus. 1–12.

Merdes, A., Ramyar, K., Vechio, J. D., and Cleveland, D. W. (1996). A complex of NuMA and cytoplasmic dynein is essential for mitotic spindle assembly. Cell *87*, 447–458.

Nguyen-Ngoc, T., Afshar, K., and Gönczy, P. (2007). Coupling of cortical dynein and Gα proteins mediates spindle positioning in Caenorhabditis elegans. Nature Publishing Group *9*, 1294–1302.

Paix, A., Wang, Y., Smith, H. E., Lee, C.-Y., Calidas, D., Lu, T., Smith, J., Schmidt, H., Krause, M. W., and Seydoux, G. (2014). Scalable and Versatile Genome Editing Using Linear DNAs with Microhomology to Cas9 Sites in Caenorhabditis elegans. Genetics *198*, 1347–1356.

Park, D. H., and Rose, L. S. (2008). Dynamic localization of LIN-5 and GPR-1/2 to cortical force generation domains during spindle positioning. Developmental Biology *315*, 42–54.

Pease, J. C., and Tirnauer, J. S. (2011). Mitotic spindle misorientation in cancer--out of alignment and into the fire. Journal of Cell Biology *124*, 1007–1016.

Peyre, E., Jaouen, F., Saadaoui, M., Haren, L., Merdes, A., Durbec, P., and Morin, X. (2011). A lateral belt of cortical LGN and NuMA guides mitotic spindle movements and planar division in neuroepithelial cells. The Journal of Cell Biology *193*, 141–154.

Portegijs, V., Fielmich, L.-E., Galli, M., Schmidt, R., Muñoz, J., van Mourik, T., Akhmanova, A., Heck, A. J. R., Boxem, M., and van den Heuvel, S. (2016). Multisite Phosphorylation of NuMA-Related LIN-5 Controls Mitotic Spindle Positioning in C. elegans. PLoS Genet *12*, e1006291.

Rappaport, R. (1961). Experiments concerning the cleavage stimulus in sand dollar eggs. The Journal of Experimental Zoology *148*, 81–89.

Rocheleau, C. E., and Priess, J. R. (1997). Wnt Signaling and an APC-Related Gene Specify Endoderm in Early C. Elegans Embryos. 1–10.

Rocheleau, C. E., Yasuda, J., Shin, T. H., Lin, R., Sawa, H., Okano, H., Priess, J. R., Davis, R. J., and Mello, C. C. (1999). WRM-1 activates the LIT-1 protein kinase to transduce anterior/posterior polarity signals in C. elegans. Cell *97*, 717–726.

Schlesinger, A., Shelton, C. A., Maloof, J. N., Meneghini, M., and Bowerman, B.

(1999). Wnt pathway components orient a mitotic spindle in the early Caenorhabditis elegans embryo without requiring gene transcription in the responding cell. Genes & Development *13*, 2028–2038.

Schmidt, D. J., Rose, D. J., Saxton, W. M., and Strome, S. (2005). Functional Analysis of Cytoplasmic Dynein Heavy Chain in *Caenorhabditis elegans* with Fast-acting Temperature- sensitive Mutations. Molecular Biology of the Cell *16*, 1200–1212.

Segalen, M., Johnston, C. A., Martin, C. A., Dumortier, J. G., Prehoda, K. E., David, N. B., Doe, C. Q., and Bellaïche, Y. (2010). The Fz-Dsh Planar Cell Polarity Pathway Induces Oriented Cell Division via Mud/NuMA in Drosophila and Zebrafish. Developmental Cell *19*, 740–752.

Seldin, L., Poulson, N. D., Foote, H. P., and Lechler, T. (2013). NuMA localization, stability, and function in spindle orientation involve 4.1 and Cdk1 interactions. Molecular Biology of the Cell *24*, 3651–3662.

Siller, K. H., and Doe, C. Q. (2008). Lis1/dynactin regulates metaphase spindle orientation in Drosophila neuroblasts. Developmental Biology *319*, 1–9.

Siller, K. H., Cabernard, C., and Doe, C. Q. (2006). The NuMA-related Mud protein binds Pins and regulates spindle orientation in Drosophila neuroblasts. Nature Publishing Group *8*, 594–600.

Smith, P., Azzam, M., and Hinck, L. (2017). Extracellular Regulation of the Mitotic Spindle and Fate Determinants Driving Asymmetric Cell Division. In: Results and Problems in Cell Differentiation, Cham: Springer International Publishing, 351–373.

Srinivasan, D. G., Fisk, R. M., Xu, H., and van den Heuvel, S. (2003). A complex of LIN-5 and GPR proteins regulates G protein signaling and spindle function in C elegans. Genes & Development *17*, 1225–1239.

Su, L. K., Burrell, M., Hill, D. E., Gyuris, J., Brent, R., Wiltshire, R., Trent, J., Vogelstein, B., and Kinzler, K. W. (1995). APC binds to the novel protein EB1. Cancer Res. *55*, 2972–2977.

Sugioka, K., Mizumoto, K., and Sawa, H. (2011). Wnt Regulates Spindle Asymmetry to Generate Asymmetric Nuclear β-Catenin in C. elegans. Cell *146*, 942–954.

Thorpe, C. J., Schlesinger, A., Carter, J. C., and Bowerman, B. (1997). Wnt Signaling Polarizes an Early C. Elegans Blastomere to Distinguish Endoderm From Mesoderm. 1–11.

Tsou, M. F. B. (2003). LET-99 opposes G /GPR signaling to generate asymmetry for spindle positioning in response to PAR and MES-1/SRC-1 signaling. Development

*130*, 5717–5730.

Walston, T., Tuskey, C., Edgar, L., Hawkins, N., Ellis, G., Bowerman, B., Wood, W., and Hardin, J. (2004). Multiple Wnt Signaling Pathways Converge to Orient the Mitotic Spindle in Early C. elegans Embryos. Developmental Cell *7*, 831–841.

Werts, A. D., and Goldstein, B. (2011). How signaling between cells can orient a mitotic spindle. Seminars in Cell & Developmental Biology *22*, 842–849.

Werts, A. D., Roh-Johnson, M., and Goldstein, B. (2011). Dynamic localization of C. elegans TPR-GoLoco proteins mediates mitotic spindle orientation by extrinsic signaling. Development *138*, 4411–4422.

Williams, S. E., Beronja, S., Pasolli, H. A., and Fuchs, E. (2011). nature09793. Nature *470*, 353–358.

Wong, H.-C., Bourdelas, A., Krauss, A., Lee, H.-J., Shao, Y., Wu, D., Mlodzik, M., Shi, D.-L., and Zheng, J. (2003). Direct binding of the PDZ domain of Dishevelled to a conserved internal sequence in the C-terminal region of Frizzled. Molecular Cell *12*, 1251–1260.

Xia, J. *et al.* (2015). Semaphorin-Plexin Signaling Controls Mitotic Spindle Orientation during Epithelial Morphogenesis and Repair. Developmental Cell *33*, 299–313.

Yamashita, Y. M., Jones, D. L., and Fuller, M. T. (2003). Orientation of asymmetric stem cell division by the APC tumor suppressor and centrosome. Science *301*, 1547–1550.

Yeh, E., Yang, C., Chin, E., Maddox, P., Salmon, E. D., Lew, D. J., and Bloom, K. (2000). Dynamic positioning of mitotic spindles in yeast: role of microtubule motors and cortical determinants. Molecular Biology of the Cell *11*, 3949–3961.

Yoshiura, S., Ohta, N., and Matsuzaki, F. (2012). Tre1 GPCR Signaling Orients Stem Cell Divisions in the Drosophila Central Nervous System. Developmental Cell *22*, 79–91.

Yuzawa, S., Kamakura, S., Iwakiri, Y., Hayase, J., and Sumimoto, H. (2011). Structural basis for interaction between the conserved cell polarity proteins Inscuteable and Leu-Gly-Asn repeat-enriched protein (LGN). Proceedings of the National Academy of Sciences *108*, 19210–19215.

Zhang, H., Skop, A. R., and White, J. G. (2008). Src and Wnt signaling regulate dynactin accumulation to the P2-EMS cell border in C. elegans embryos. Journal of Cell Biology *121*, 155–161.

Zheng, Z., Zhu, H., Wan, Q., Liu, J., Xiao, Z., Siderovski, D. P., and Du, Q. (2010).

LGN regulates mitotic spindle orientation during epithelial morphogenesis. The Journal of Cell Biology *189*, 275–288.

# CHAPTER 4: DISCUSSION

The major contributions of the work in this dissertation include a technical advance quantitatively comparing fluorescent proteins *in vivo*, and discoveries related to how mitotic spindles are positioned within cells via cell-cell interactions.

Much of the work in this thesis was facilitated by the advent of CRISPR-Cas9 mediated genome editing strategies in 2012 (Jinek *et al.*, 2012). My labmate, Dan Dickinson adapted this system to enable targeted gene insertion in *C. elegans* beginning in 2013 (Dickinson *et al.*, 2013; 2015). By making a precise break in the DNA using the RNA guided Cas9 enzyme, and introducing a repair template with sequence homology to the *C. elegans* genome, it became possible to introduce genetically encoded fluorescent proteins at specific endogenous loci. This technology was especially important for tagging genes expressed in the early *C. elegans* embryo, as germline silencing of transgenes had prevented the live imaging of some proteins and complicated the imaging of others. In many cases, germline silencing can be overcome using CRISPR to tag the endogenous copy of important genes. Tagging genes at their endogenous loci also ensures that proteins are expressed as close as possible to endogenous levels, and that 100% of the protein is labeled (Dickinson *et al.*, 2013). Expression level is critical for the function of many proteins, but especially for those that function in force generation, as overexpression can result in deleterious phenotypes (Werts *et al.*, 2011). Although inserting

transgenes into a common locus in the genome was possible before the invention of CRISPR-Cas9 genome editing, via transposon based insertion (MosSCI), CRISPR increased the rapidity and efficiency with which we were able to make the strains used in fluorescent protein comparisons (Figure 2.2 and 2.3) (Frøkjær-Jensen *et al.*, 2008). CRISPR also made comparisons of fluorescent proteins knocked into endogenous loci possible, as prior to these advances, we could not target specific genetic loci. Utilizing these new techniques, I was able to generate tools to increase our understanding of which fluorescent proteins perform best *in vivio* in an animal model, and how mitotic spindles are become oriented in response to Wnt signaling.

**4.1 Comparison of fluorescent proteins in an in vivo animal model system**

Our study comparing fluorescent proteins *in vivo* was the first to systematically examine the performance of fluorescent proteins in a multicellular animal. We believed this question to be worthy of investigation because we were always asking ourselves which fluorescent proteins would be best for our experiments. Before this work, we used the available data from the literature, usually collected *in vitro* using purified proteins, or anecdotal reports from our lab or others about which fluorescent proteins would be the brightest and most photostable (Figure 2.1). Our efforts revealed that if we had chosen fluorescent proteins based only on the data available in the literature, our choices would not have been optimal for our model system (Figure 2.2 and 2.5).

*Future Directions*

One limitation of our study was that we did not investigate why the brightness of the fluorescent proteins we tested *in vivo* differed from predictions based on the

their measured brightness *in vitro* (Figure 2.1 and 2.2). This is a difficult question to address because of the diversity of variables, both biological and technical that can affect the observed brightness of fluorescent proteins *in vivo.* One of the goals of our experiments was to control for as many of these variables as possible. While we established controlled conditions for many of the technical variables, such as illumination, detector sensitivity and filter sets, the biological variables of a multicellular animal were more difficult to control. Some biological variables that could have resulted in differences from the previous observations include: expression level, translational and folding efficiency, stability, pH, temperature, protein tagged, and monomeric character of the fluorescent protein. We were able to carefully control for expression conditions (promoter and regulatory elements), temperature, pH and the protein tagged between comparisons, thus establishing clear conditions and standards for our work and for future comparisons.

Our results suggest that in some cases, different fluorescent tags may result in differing amounts of protein observed, even under identical expression conditions (Figure2.3). Thus, differences in observed brightness may not be due entirely to the inherent brightness of a given fluorescent protein. Instead, inherent brightness plus the cellular environment of a given experimental system govern fluorescent protein performance *in vivo*. Differences in protein levels could be caused by differential regulation of mRNA transcripts, translational and folding efficiency between fluorescent proteins or differential protein stability. Potential differences in transcriptional and translational efficiency could be tested using promoters that turn fluorescent protein fusions on and off at different times during development. Using

the timing of appearance and disappearance of fluorescent proteins, the rates of protein synthesis and degradation could be quantified.

Though we controlled for codon bias in our fluorescent protein sequences using a *C. elegans*-specific algorithm to standardize codon usage and eliminate rare codons from our sequences (Redemann *et al.*, 2011), it is also possible that differences in protein levels are due to sequence-specific, differential germline silencing of transcripts. Germline silencing has been anecdotally reported to have a greater effect on more highly expressed genes. We observed a correlation between mNeonGreen performance and gene expression levels for our genes tagged at their endogenous loci (Figure 2.5): the more highly a gene was expressed, the greater the difference between mNeonGreen performance and expectation compared to GFP. One way to test this hypothesis would be to test different sequence variants of fluorescent proteins and observe brightness and protein levels. These experiments may be worth pursuing, as they would shed light on whether a C. elegans-specific process such as germline silencing largely responsible for our findings, or whether more universally relevant mechanisms of regulation may be at play.

The other major result from this work that I have found most critical is the quantitative difference in background fluorescence when exciting early *C. elegans* embryos with different wavelengths of light (Figure 2.1). We knew anecdotally from imaging transgenic strains that there is more background fluorescence using 488nm illumination. However, we did not know the extent of the difference between the 488nm and 514nm wavelengths (Figure 2.1). It turns out that this background fluorescence makes all the difference when trying to tag lowly expressed genes that

result in dim signal and near the limit of detection. Some of the proteins I analyzed for my work investigating Wnt signaling and mitotic spindle orientation probably would not have been visible at the four-cell stage using GFP and 488nm illumination.

One additional contribution of this work is that it provides a platform for testing new fluorescent proteins as they are developed. In fact recently, a new, reportedly bright, red monomeric fluorescent protein, mScarlet has been developed (Bindels *et al.*, 2017). In a matter of weeks, our lab has been able to efficiently compare this fluorescent protein to the ones we currently use by creating a matched strain to compare with the strains I created as benchmarks (Figure 2.2 and Mark Slabodnick, unpublished). Overall this technical undertaking has benefitted my own research tremendously, and provided valuable information for our lab and the field for choosing fluorescent proteins to use *in vivo*.

### 4.2 Wnt signaling polarizes APC and Dishevelled, but not NuMA or Dynein, to achieve asymmetric cell division in early C. elegans embryos

Over a decade of genetic studies provided us with a robust list of proteins involved in spindle positioning at the four-cell stage in the *C. elegans* embryo (Thorpe *et al.*, 1997; Schlesinger *et al.*, 1999; Bei *et al.*, 2002; Tsou, 2003; Walston *et al.*, 2004; Zhang *et al.*, 2008). Importantly however, this list did not enable us to distinguish between proteins required for mitotic spindle functions that indirectly affect rotation, and proteins that provide positional information for mitotic spindle positioning. We would expect that depleting or disabling any protein required for spindle microtubules to form normally for example, might result in spindle rotation defects due to the fact that the mitotic apparatus is functionally compromised. These phenotypes would be indistinguishable from those expected from a spindle that

lacks positional information. To resolve this issue, I took an unusual approach to specifically identify the proteins that provide spatial information to the EMS mitotic spindle. Using CRISPR-Cas9 mediated homologous recombination, I fluorescently labeled the gene products of over twenty proteins of interest and observing their localization during mitotic spindle positioning in EMS (Figure 3.2).

Many asymmetric spindle-positioning mechanisms we know of to date function through the local enrichment of a member of the Gα/LGN/NuMA cortical adaptor complex to one side of a cell. Therefore, we began with the hypothesis that dynein, or a regulator of dynein such as Gα, LGN, or NuMA, would be localized to the $P_2$:EMS contact site. Work by Adam Werts in 2011 had determined that GPR-1/LGN, though enriched at the $P_2$:EMS contact, was in fact enriched in $P_2$ and not in the EMS cell (Werts *et al.*, 2011). Our results revealed that our tagged version LIN-5/NuMA, though enriched at the $P_2$:EMS contact, was also enriched on the side of the $P_2$ signaling cell, and not in EMS (Figure 3.4). This suggested to us that the mechanism of spindle positioning in EMS does not appear to require local enrichment of either LGN or NuMA. Further, our work suggested that dynein, the most downstream member of this complex, is not asymmetric in EMS (Figure 3.5). Because Gα, LGN, and NuMA are required for spindle rotation in EMS, we concluded that although this complex of proteins is required for spindle rotation, it does not provide positional information through its asymmetric localization. Our observation that APR-1/APC and DSH-2/Dishevelled localize to opposing domains during EMS spindle rotation and their roles regulating the EMS mitotic spindle (Figure 3.6), leads us to believe that one or both of these molecules may provide

positional information to the mitotic spindle. How these proteins interact with the mitotic spindle to achieve spindle positioning is not yet clear. However, there are plausible hypotheses based on what is known about Dishevelled and APC function in the EMS cell and other systems.

***How might Dishevelled and/or APC regulate mitotic spindle positioning?***

Neither Dishevelled nor APC have catalytic domains, so it is unlikely that these molecules generate force on microtubules through rounds of conformational changes, as do motors such as dynein. However, they may function to localize other force generating motor proteins, such as kinesins. Although we tagged multiple kinesins, none localized to the P2:EMS contact. It is possible that Wnt pathway components could locally recruit one of the kinesin motor proteins that we did not look at to the EMS cortex.

Another possibility is that these proteins recruit activators or inhibitors of motor proteins. Although we did not observe dynein localization to be asymmetric in EMS (Figure 3.5), it is possible that APC or Dishevelled modulate the activity of dynein on one side of EMS by recruiting a motor activator or inhibitor. LET-99 is an antagonist of LGN/GPR-1/2, is required for EMS spindle rotation, and has a similar localization to APR-1 in EMS (Park and Rose, 2008; Werts *et al.*, 2011). It is possible that APR-1 regulates LET-99 to tune pulling forces on one side of the EMS cortex. To test this hypothesis, one could deplete *mom-2* or *apr-1* and look for changes in LET-99 localization. Although we did not find DNC-1/p150 glued to be asymmetrically localized at the P2:EMS contact, a different member of the eleven

protein complex may be asymmetrically localized through Wnt signaling to modulate dynein activity (Zhang *et al.*, 2008).

APC and/or Dishevelled could interact directly or indirectly with astral microtubules at the cell cortex. Both Dishevelled and APC have been reported to interact with and stabilize microtubules in other contexts. Dishevelled has been shown to stabilize microtubules in axons by inhibiting GSK3β in a mechanism independent of transcriptional activity, and the Dishevelled DEP domain is required for this activity (Krylova *et al.*, 2000; Ciani, 2004; Salinas, 2007). APC has well characterized interactions with the microtubule cytoskeleton. The mammalian version of the protein has a C-terminal microtubule-binding domain and binds to the microtubule plus-end binding protein EB1 (Su *et al.*, 1995). Although the *C. elegans* APC homolog, APR-1, is highly divergent, APR-1/APC has been implicated in the regulation of astral microtubules in EMS. APR-1 was shown to affect mitotic spindle asymmetry by stabilizing microtubules at the anterior cortex of EMS (Sugioka *et al.*, 2011). This function of APC may be important for mitotic spindle positioning in EMS. In the absence of Wnt, APC is no longer restricted to the anterior. Therefore, it might stabilize microtubules evenly across the EMS cell cortex causing defects in rotation due to this loss of asymmetry and positional information.

Modulating the stability of cortical microtubules could have a variety of possible outcomes, and could interfere with their interactions with cortical dyneins. One possibility is that an increase in microtubule stability on one side of the cell might promote interactions with dynein complexes at the cortex. This would result in an increase in pulling forces on one side of the cell even in the absence of cortical

dynein enrichment. Microtubule depolymerization promotes force generation (Inoué and Salmon, 1995; Grishchuk *et al.*, 2005), and it is also possible that either APC or Dishevelled complexes could increase the depolymerization rate of microtubules. If microtubules are interacting with dyneins evenly on the cortex, but depolymerizing more on one side of the cell versus the other, this could generate greater force on one side of the cell to position the mitotic spindle.

Because APC and Dishevelled are both well known scaffolding proteins, their role in astral microtubule regulation could be indirect, and regulated through a binding partner or complex member. GSK3β and β-catenin would be good candidates for this regulation. GSK3β can regulate microtubule stability through regulation of CLASP binding to the microtubule lattice (Wittmann and Waterman-Storer, 2005). Although GSK3β/GSK-3 did not exhibit asymmetric localization in EMS (Figure 3.2 – third row), GSK-3 could be asymmetrically active, and as a member of the destruction complex, is known to associate with APC. β-catenin has also been implicated in spindle postioning in EMS (Kim *et al.*, 2013). The phosphorylation state and localization of β-catenin at the EMS cortex may rely on APC and Dishevelled localization. The presence or phosphorylation state of β-catenin in APC complexes may affect APC localization and how these complexes interact with astral microtubules at the cell cortex.

***Future directions: Is a cortical domain of APC or Dishevelled sufficient for mitotic spindle positioning in the early C. elegans embryo?***

Answering this question is highly likely to increase our understanding of how the polarity axis established by these two proteins in EMS interfaces with the mitotic apparatus. I have attempted two types of approaches to answer this question. The

first approach was the development of a LOV-domain based light inducible dimer system (iLID) (Guntas *et al.*, 2015; Zimmerman *et al.*, 2016). The idea behind this approach is to use light to induce the recruitment of a target protein (Dishevelled or APC) to the plasma membrane. I was able to generate a membrane-tethered version of the iLID switch and a cytoplasmic version of the binding protein that is recruited by activation of the switch. I could recruit the cytoplasmic protein to the membrane using light. However, the recruitment to the plasma membrane was ubiquitous and never in a specific region of the cell cortex. It is possible that the sensitivity of switch I used (the micro affinity version) was not properly tuned to our system, and a next step might be to test a different affinity version of this switch (the milli version).

The second approach I attempted was based on the fly S2 cell induced polarity system (Johnston *et al.*, 2009). This system takes advantage of the fly transmembrane protein Echinoid to create protein domains at cell-cell interfaces. When two Echinoid expressing cells contact one another, Echinoid induces adhesion and efficiently localizes at the cortex only to the site of cell-cell contact. This way, domains of proteins of interest can be formed by fusing the proteins of interest to the intercellular domain of Echinoid. The original authors of this technique have used it to great effect to study proteins involved in spindle orientation in different contexts in Drosophila (Johnston *et al.*, 2009; Segalen *et al.*, 2010; Johnston *et al.*, 2013). I created and expressed a control Echinoid transgene using an inducible heat shock promoter in a subset of cells in the early embryo using a cell lineage-specific 3'UTR. I created versions of this construct fused to APC and

Dishevelled, but these transgenes did not express well. Both approaches reached the point of a technical hurdle that I could not overcome within the span of my work on this project. However, each remains a viable option, and the tools I have made provide a starting point for attempting this critical experiment.

***Other Future Directions***

Our study raises questions about how members of the Wnt signaling pathway achieve oriented cell division along the polarity axis they establish. Members of the Wnt pathway have been shown to interact with microtubules in diverse contexts (Salinas, 2007). One possibility is that a member or members of the Wnt pathway stabilize astral microtubules directly. This possibility could be explored by imaging astral microtubules at the cortex along with labeled members of the Wnt pathway.

It is also possible that members of the Wnt pathway regulate mitotic spindle positioning through the recruitment of an unknown cofactor. A traditional biochemical approach to identifying such candidates would be to pull down the relevant Wnt pathway proteins and perform mass spectrometry to identify associated peptides. Our tags would facilitate such an experiment, however it would be difficult to get enough stage-specific material to identify protein interactions specific to mitotic spindle rotation at the four-cell stage. However, putative interactions could be validated and characterized by stage-specific, single molecule pull down (Jain *et al.*, 2012)(Dickinson unpublished).

Another unbiased approach to identifying unknown potential Wnt pathway integrators would be a genetic screen. The two partially redundant signals, Wnt and MES-1, suggest a sensitized screen for new players is possible: in mom-2/Wnt-

mutants, about 20% of embryos form endoderm, while in mes-1 mutants about 100% of embryos form endoderm (Thorpe *et al.*, 1997; Bei *et al.*, 2002). However, in mom-2;mes-1 double mutant embryos 0% form endoderm (Bei *et al.*, 2002). Therefore RNAi feeding of candidates that enhance lethality in MES-1, may lead to previously unknown members of the pathway. A candidate screen is currently being carried out in collaboration with Dr. Jenny Tenlen and undergraduate genetics students at Seattle Pacific University.

It is also possible that activation of the Wnt pathway and cell polarization leads to mitotic spindle positioning through the asymmetric activation of genes involved in mitotic spindle positioning. For example LGN and NuMA are regulated by phosphorylation (Johnston *et al.*, 2009; Galli *et al.*, 2011; Kotak *et al.*, 2013; Portegijs *et al.*, 2016). Local activation of Wnt pathway kinases such as GSK3, Casein Kinase at the cell cortex in response to Wnt might result in asymmetric changes in the activity of motor proteins such as dynein, or other microtubule regulators. Phosphorylation states would be difficult to probe biochemically in this system due to the limitations previously described. However, CRISPR would allow for the targeted mutation of candidate phosphorylation sites in target proteins.

These results expand our understanding of how oriented cell divisions are achieved in response to cell-cell signaling. We propose that the orientation of a Wnt-dependent cell division in the *C. elegans* embryo relies not on asymmetric localization of NuMA or dynein, but instead, is either directly or indirectly mediated by members of Wnt pathway: APC and/or Dishevelled.

## REFERENCES


Bei, Y., Hogan, J., Berkowitz, L. A., Soto, M. C., Rocheleau, C. E., Collins, J., and Mello, C. C. (2002). SRC-1 and Wnt Signaling Act Together to Specify Endoderm and to Control Cleavage Orientation in Early *C. elegans* Embryos. Developmental Cell *3*, 113–125.

Bindels, D. S. *et al.* (2017). mScarlet: a bright monomeric red fluorescent protein for cellular imaging. Nature Methods *14*, 53–56.

Ciani, L., Krylova, O., Smalley, M. J., Dale, T. C., and Salinas, P. C. (2004). A divergent canonical WNT-signaling pathway regulates microtubule dynamics: dishevelled signals locally to stabilize microtubules. The Journal of Cell Biology *164*, 243–253.

Dickinson, D. J., Pani, A. M., Heppert, J. K., Higgins, C. D., and Goldstein, B. (2015). Streamlined Genome Engineering with a Self-Excising Drug Selection Cassette. Genetics *200*, 1035–1049.

Dickinson, D. J., Ward, J. D., Reiner, D. J., and Goldstein, B. (2013). Engineering the Caenorhabditis elegans genome using Cas9-triggered homologous recombination. Nature Methods *10*, 1028–1034.

Frøkjær-Jensen, C., Wayne Davis, M., Hopkins, C. E., Newman, B. J., Thummel, J. M., Olesen, S.-P., Grunnet, M., and Jorgensen, E. M. (2008). Single-copy insertion of transgenes in Caenorhabditis elegans. Nat Genet *40*, 1375–1383.

Galli, M., Muñoz, J., Portegijs, V., Boxem, M., Grill, S. W., Heck, A. J. R., and van den Heuvel, S. (2011). aPKC phosphorylates NuMA-related LIN-5 to position the mitotic spindle during asymmetric division. Nature Publishing Group *13*, 1132–1138.

Grishchuk, E. L., Molodtsov, M. I., Ataullakhanov, F. I., and McIntosh, J. R. (2005). Force production by disassembling microtubules. Nature *438*, 384–388.

Guntas, G., Hallett, R. A., Zimmerman, S. P., Williams, T., Yumerefendi, H., Bear, J. E., and Kuhlman, B. (2015). Engineering an improved light-induced dimer (iLID) for controlling the localization and activity of signaling proteins. Proceedings of the National Academy of Sciences *112*, 112–117.

Inoué, S., and Salmon, E. D. (1995). Force generation by microtubule assembly/disassembly in mitosis and related movements. Molecular Biology of the Cell *6*, 1619–1640.

Jain, A., Liu, R., Xiang, Y. K., and Ha, T. (2012). Single-molecule pull-down for studying protein interactions. Nature Protocols *7*, 445–452.

Jinek, M., Chylinski, K., Fonfara, I., Hauer, M., Doudna, J. A., and Charpentier, E. (2012). A programmable dual-RNA-guided DNA endonuclease in adaptive bacterial immunity. Science *337*, 816–821.

Johnston, C. A., Hirono, K., Prehoda, K. E., and Doe, C. Q. (2009). Identification of an Aurora-A/PinsLINKER/ Dlg Spindle Orientation Pathway using Induced Cell Polarity in S2 Cells. Cell *138*, 1150–1163.

Johnston, C. A., Manning, L., Lu, M. S., Golub, O., doe, C. Q., and Prehoda, K. E. (2013). Formin-mediated actin polymerization cooperates with Mushroom body defect (Mud)-Dynein during Frizzled-Dishevelled spindle orientation. Journal of Cell Biology *126*, 4436–4444.

Kim, S., Ishidate, T., Sharma, R., Soto, M. C., Conte, D., Mello, C. C., and Shirayama, M. (2013). Wnt and CDK-1 regulate cortical release of WRM-1/ -catenin to control cell division orientation in early Caenorhabditis elegans embryos. Proceedings of the National Academy of Sciences *110*, E918–E927.

Kotak, S., Busso, C., and nczy, P. G. O. (2013). 2517.full. The EMBO Journal *32*, 2517–2529.

Krylova, O., Messenger, M. J., and Salinas, P. C. (2000). Dishevelled-1 regulates microtubule stability: a new function mediated by glycogen synthase kinase-3beta. The Journal of Cell Biology *151*, 83–94.

Park, D. H., and Rose, L. S. (2008). Dynamic localization of LIN-5 and GPR-1/2 to cortical force generation domains during spindle positioning. Developmental Biology *315*, 42–54.

Portegijs, V., Fielmich, L.-E., Galli, M., Schmidt, R., Muñoz, J., van Mourik, T., Akhmanova, A., Heck, A. J. R., Boxem, M., and van den Heuvel, S. (2016). Multisite Phosphorylation of NuMA-Related LIN-5 Controls Mitotic Spindle Positioning in C. elegans. PLoS Genet *12*, e1006291.

Redemann, S., Schloissnig, S., Ernst, S., Pozniakowsky, A., Ayloo, S., Hyman, A. A., and Bringmann, H. (2011). Codon adaptation–based control of protein expression in C. elegans. Nature Methods *8*, 250–252.

Salinas, P. C. (2007). Modulation of the microtubule cytoskeleton: a role for a divergent canonical Wnt pathway. Trends in Cell Biology *17*, 333–342.

Schlesinger, A., Shelton, C. A., Maloof, J. N., Meneghini, M., and Bowerman, B. (1999). Wnt pathway components orient a mitotic spindle in the early Caenorhabditis elegans embryo without requiring gene transcription in the responding cell. Genes & Development *13*, 2028–2038.

Segalen, M., Johnston, C. A., Martin, C. A., Dumortier, J. G., Prehoda, K. E., David, N. B., Doe, C. Q., and Bellaïche, Y. (2010). The Fz-Dsh Planar Cell Polarity Pathway Induces Oriented Cell Division via Mud/NuMA in Drosophila and Zebrafish. Developmental Cell *19*, 740–752.

Su, L. K., Burrell, M., Hill, D. E., Gyuris, J., Brent, R., Wiltshire, R., Trent, J., Vogelstein, B., and Kinzler, K. W. (1995). APC binds to the novel protein EB1. Cancer Res. *55*, 2972–2977.

Sugioka, K., Mizumoto, K., and Sawa, H. (2011). Wnt Regulates Spindle Asymmetry to Generate Asymmetric Nuclear β-Catenin in C. elegans. Cell *146*, 942–954.

Thorpe, C. J., Schlesinger, A., Carter, J. C., and Bowerman, B. (1997). Wnt Signaling Polarizes an Early C. Elegans Blastomere to Distinguish Endoderm From Mesoderm. 1–11.

Tsou, M. F. B. (2003). LET-99 opposes G /GPR signaling to generate asymmetry for spindle positioning in response to PAR and MES-1/SRC-1 signaling. Development *130*, 5717–5730.

Walston, T., Tuskey, C., Edgar, L., Hawkins, N., Ellis, G., Bowerman, B., Wood, W., and Hardin, J. (2004). Multiple Wnt Signaling Pathways Converge to Orient the Mitotic Spindle in Early C. elegans Embryos. Developmental Cell *7*, 831–841.

Werts, A. D., Roh-Johnson, M., and Goldstein, B. (2011). Dynamic localization of C. elegans TPR-GoLoco proteins mediates mitotic spindle orientation by extrinsic signaling. Development *138*, 4411–4422.

Wittmann, T., and Waterman-Storer, C. M. (2005). Spatial regulation of CLASP affinity for microtubules by Rac1 and GSK3beta in migrating epithelial cells. The Journal of Cell Biology *169*, 929–939.

Zhang, H., Skop, A. R., and White, J. G. (2008). Src and Wnt signaling regulate dynactin accumulation to the P2-EMS cell border in C. elegans embryos. Journal of Cell Biology *121*, 155–161.

Zimmerman, S. P., Hallett, R. A., Bourke, A. M., Bear, J. E., Kennedy, M. J., and Kuhlman, B. (2016). Tuning the Binding Affinities and Reversion Kinetics of a Light Inducible Dimer Allows Control of Transmembrane Protein Localization. Biochemistry *55*, 5264–5271.